SELENIUM DOPED CALCIUM PHOSPHATE BIOMIMETIC COATING ON Ti6Al4V ORTHOPEDIC IMPLANT MATERIAL FOR ANTI-CANCER AND ANTI-BACTERIAL PURPOSES

A THESIS SUBMITTED TO
THE GRADUATE SCHOOL OF NATURAL AND APPLIED SCIENCES
OF
MIDDLE EAST TECHNICAL UNIVERSITY

BY
BENGİ YILMAZ

IN PARTIAL FULFILLMENT OF THE REQUIREMENTS
FOR
THE DEGREE OF DOCTOR OF PHILOSOPHY
IN
BIOMEDICAL ENGINEERING

DECEMBER 2014

Approval of the thesis:

SELENIUM DOPED CALCIUM PHOSPHATE BIOMIMETIC COATING ON Ti6Al4V ORTHOPEDIC IMPLANT MATERIAL FOR ANTI-CANCER AND ANTI-BACTERIAL PURPOSES

submitted by **BENGİ YILMAZ** in partial fulfillment of the requirements for the degree of **Doctor of Philosophy in Biomedical Engineering Department, Middle East Technical University** by,

Prof. Dr. Gülbin Dural Ünver _____
Dean, Graduate School of **Natural and Applied Sciences**

Prof. Dr. Vasıf Hasırcı _____
Head of Department, **Biomedical Engineering**

Assoc. Prof. Dr. Zafer Evis _____
Supervisor, **Engineering Sciences Dept., METU**

Assoc. Prof. Dr. Sreeparna Banerjee _____
Co-Supervisor, **Biology Dept., METU**

Examining Committee Members:

Prof. Dr. Ahmet Nedim Eraslan _____
Engineering Sciences Dept., METU

Assoc. Prof. Dr. Zafer Evis _____
Engineering Sciences Dept., METU

Assoc. Prof. Dr. Ayşen Tezcaner _____
Engineering Sciences Dept., METU

Assoc. Prof. Dr. Volkan Şahin _____
Prosthodontics Dept., Kırıkkale University

Assist. Prof. Dr. Mustafa Tolga Yılmaz _____
Engineering Sciences Dept., METU

Date: 19.12.2014

I hereby declare that all information in this document has been obtained and presented in accordance with academic rules and ethical conduct. I also declare that, as required by these rules and conduct, I have fully cited and referenced all material and results that are not original to this work.

Name, Last name: Bengi Yılmaz

Signature:

ABSTRACT

SELENIUM DOPED CALCIUM PHOSPHATE BIOMIMETIC COATING ON Ti6Al4V ORTHOPEDIC IMPLANT MATERIAL FOR ANTI-CANCER AND ANTI-BACTERIAL PURPOSES

Yılmaz, Bengi
Ph.D., Department of Biomedical Engineering
Supervisor : Assoc. Prof. Dr. Zafer Evis
Co-Supervisor: Assoc. Prof. Dr. Sreeparna Banerjee

December 2014, 115 pages

In order to prevent recurrent osteosarcoma in patients undergone surgical resection for implant insertion and infection around implant site, which is a very common complication after surgery, it is very important to functionalize the surface. In this study, to combine the effective antioxidant and potential anti-cancer and anti-bacterial properties of selenium with the high biocompatibility and bioactivity of hydroxyapatite, selenium was added to the structure of hydroxyapatite via biomimetic method and coated on Ti6Al4V plates.

Firstly, 1.5×SBF (solution with ion concentrations at 1.5 times that of normal simulated body fluid, SBF) and selenate (SeO_4^{2-}) ion added 1.5×SBF solutions were prepared. The pretreated Ti6Al4V plates were coated with pure or selenium added hydroxyapatite by immersing them into these solutions. The surface and micro-structure of the resulting coatings were characterized by SEM, EDS, XRD, ICP-MS, FTIR and Raman spectroscopy. From SEM micrographs, it was observed that the nucleation had already started on the 4^{th} day of immersion, the precipitation continued around the nucleation sites with increasing immersion time and the

calcium phosphate precipitate grew in the form of half-spheres in both of the solutions. Selenium-containing coatings, similar to the coatings obtained from the normal 1.5×SBF, exhibited the standard hydroxyapatite XRD peaks. There were no significant differences observed in the FTIR spectra. However, there was an extra band at 764 cm^{-1} in the Raman spectrum of the selenate added coating that demonstrates the successful incorporation of selenium into the structure of hydroxyapatite. Additionally, selenium was detected in all of the coatings obtained from selenate added 1.5×SBF with different immersion times ranging from 4 to 21 days via ICP-MS method. According to the scratch test results, the critical lateral forces of the coatings varied between 60 and 80 mN.

In addition, cell viability tests were performed by using normal human osteoblasts (hFOB 1.19) and osteosarcoma cells (Saos-2). It was determined that adding 100µl solution, which contains 5×10^{-8} g selenium, into 1ml of the cell culture media provided the optimum concentration of selenium in terms of inhibiting the growth of Saos-2 cells while promoting the growth of hFOB 1.19 cells. However, the cell viability of both of the cell types, which were seeded directly on the pure or selenium containing coatings, was less than that of the control group, which was seeded on tissue culture plastic. In order to evaluate the anti-bacterial property of the coatings, the adhesion and proliferation behavior of *S. epidermidis* bacteria was studied. It was shown that the number of bacteria was decreased in the supernatant media of the coating which is obtained from the selenate added 1.5×SBF at 14^{th} day of immersion with respect to pure HA coating and control.

Keywords: Selenium, Hydroxyapatite, Biomimetic Coating, Ion Doping

ÖZ

Ti6Al4V ORTOPEDİK İMPLANT MALZEMESİ ÜZERİNE ANTİ-KANSER VE ANTİ-BAKTERİYEL AMAÇLI SELENYUM EKLENMİŞ KALSİYUM FOSFAT BİYOMİMETİK KAPLAMA

Yılmaz, Bengi

Doktora, Biyomedikal Mühendisliği Bölümü

Tez Yöneticisi : Doç. Dr. Zafer Evis

Ortak Tez Yöneticisi : Doç. Dr. Sreeparna Banerjee

Aralık 2014, 115 sayfa

Cerrahi müdahale ile hastalıklı doku alınarak implant yerleştirilmiş kemik kanserli hastalarda kanserin tekrar oluşumunu ve implant yerleştirme ameliyatları sonrasında sıklıkla görülen enfeksiyonun önlenmesi için implant yüzeylerinin fonksiyonelleştirilmesi önem taşımaktadır. Bu çalışmada, selenyumun etkili bir antioksidan, potansiyel bir anti-kanser ve anti-bakteriyel ajan olma özelliklerini, hidroksiapatitin yüksek biyouyumluluk ve biyoaktivitesi ile birleştirmek amacıyla, biyomimetik yöntem ile yapısına selenyum eklenmiş hidroksiapatit Ti6Al4V plakalar üzerine kaplanmıştır.

İlk olarak, 1.5×SBF (iyon derişimi normalden 1,5 kat daha yoğun yapay vücut sıvısı, SBF) ile içerisine selenat (SeO_4^{-2}) iyonu eklenmiş 1.5×SBF çözeltileri üretilmiştir. Ön-işlem görmüş Ti6Al4V plakalar, bu çözeltilerde bekletilerek saf halde veya yapısına selenyum eklenmiş hidroksiapatitle kaplanmıştır. Elde edilen kaplamaların yüzey ve mikro yapıları SEM, EDS, XRD, ICP-MS, FTIR ve Raman spektroskopisi ile incelenmiştir.

SEM görüntülerinden, her iki çözeltide kaplanan yüzeylerde 4. günde çekirdeklenmenin başlamış olduğu, çözeltide bekleme süresi arttıkça çekirdeklerin etrafında çökelmenin devam ettiği ve oluşan kalsiyum fosfat yapının küçük yarım kürecikler halinde büyüdüğü görülmüştür. Selenyum içeren kaplamaların, normal kompozisyondaki 1.5xSBF'den elde edilen kaplamalarda olduğu gibi, standart hidroksiapatit XRD pikleri verdiği saptanmıştır. FTIR spektrumlarında önemli bir farka rastlanmamıştır. Ancak selenyum eklenen kaplamanın Raman spektrumunda, selenyumunun hidroksiapatit yapısına girdiğini gösteren ekstra 764 cm^{-1} bandı görülmüştür. Ayrıca, selenat eklenmiş 1.5xSBF'de bekletilme süreleri 4 ile 21 gün arasında değişen kaplamaların tamamında ICP-MS yöntemiyle selenyum tespit edilmiştir. Çizik testi sonuçlarına göre, kaplamaların kritik yanal kuvvetlerinin 60-80 mN arasında farklı değerler aldığı görülmüştür.

Ayrıca, sağlıklı insan kemik hücreleri (hFOB 1.19) ve osteosarkom hücreleri (Saos-2) ile hücre canlılık testleri yapılmıştır. Saos-2 hücrelerinin çoğalmasının baskılanması ve hFOB 1.19 hücre canlılığında artış görülmesi açısından, 1ml hücre kültür ortamına 5×10^{-8}g selenyum içeren 100 µl çözelti eklemenin optimum selenyum derişimini sağladığı gösterilmiştir. Ancak saf veya selenyum içeren kaplamalar üzerine doğrudan ekilen iki farklı hücre tipi için de canlılığın, hücre kültür plastiği üzerine ekilen kontrol grubundan düşük olduğu tespit edilmiştir. Kaplamaların anti-bakteriyel özelliklerini araştırmak için *S. epidermidis* bakterisinin implant yüzeyi üzerindeki tutunma ve çoğalma davranışı tespit edilmiştir. Selenat eklenmiş 1.5×SBF'de 14. günde elde edilen kaplamanın bulunduğu ortamda bakteri sayısının saf HA kaplama ve kontrole göre azaldığı gözlemlenmiştir.

Anahtar Kelimeler: Selenyum, Hidroksiapatit, Biyomimetik Kaplama, İyon Ekleme

To My Dear Father Tahsin and
Three generations of wonderful women of my family,
Gülver, Bilge, Gözde…

ACKNOWLEDGMENTS

First and foremost, I am deeply indebted to my advisor, Assoc. Prof. Dr. Zafer Evis for his precious guidance, consistent support and numerous opportunities that he has provided me over the years. This thesis would not be possible without his endless patience and encouragement. I am also grateful for his invaluable contributions to my professional development by training me on the path towards to an academic career.

I owe a great debt of gratitude to my co-advisor Assoc. Prof. Dr. Sreeparna Banerjee not only for kindly opening her laboratory to me, but for patiently advising me on my experiments and giving substantive feedbacks whenever I need.

I would sincerely express my profound gratitude to Assoc. Prof. Dr. Ayşen Tezcaner for her insightful discussion, valuable advices and support during the whole period of the study.

I would like to extend my special thanks to Prof. Dr. İrem Dikmen Toker, Assistant to the Rector, for always being kind, understanding and supportive throughout this process. I am very much indebted to the past and present members of METU Research Coordination Office; Gözde Emen, Tuğba Gürçel, Begüm Öngel, Işık Tekin, Semih Gökatalay and all of my colleagues with whom I have been working for many years in a lovely and joyful environment.

Both my friends and labmates deserve my hearty thanks for their constant support and encouragement. In particular, I am thankful to Merve Güldiken, Ayşegül Kavas and Özge Erdemli for their help in my experiments. I also owe a lot to Sibel Ataol, Deniz Atila, Hazal Aydoğdu, Alişan Kayabölen, Ömer Aktürk, Nil Göl Berker, Zeynep Gürtürk, Ali Deniz Dalgıç, Engin Pazarçeviren and Aydın Tahmasebifar for sharing moments of happiness with me.

I also would like to thank The Scientific and Technological Research Council of Turkey (TÜBİTAK). This study was supported by TÜBİTAK under the project No: 111M262.

I would express a deep sense of gratitude to my family, especially to my dearest parents, for their constant love, encouragement, moral support and blessings. A final heart full word of acknowledgment is addressed to the lovely memory of Serdar Kömürcü who was not just a cousin but closer than a brother to me.

TABLE OF CONTENTS

LIST OF TABLES

TABLES

LIST OF FIGURES

FIGURES

LIST OF ABBREVIATIONS

α –TCP	α -Tricalcium phosphate
β –TCP	β -Tricalcium phosphate
ACP	Amorphous calcium phosphate
ASTM	American Society for Testing and Materials
ATCC	American type culture collection
A-W	Apatite-wollastonite
BMSC	Bone marrow mesenchymal stem cell
CaP	Calcium phosphate
CDHA	Calcium-deficient hydroxyapatite
c-HA	Carbonated hydroxyapatite
c-SBF	Conventional simulated body fluid
DCPA	Dicalcium phosphate anhydrous
DCPD	Dicalcium phosphate dihydrate
DMEM	Dulbecco's Modified Eagle's medium
DNA	Deoxyribonucleic acid
EDS	Energy dispersive X-ray spectroscopy
EDTA	Ethylenediaminetetraacetic acid
ELI	Extra-low interstitial variant
FA	Fluorapatite
FBS	Fetal bovine serum
FE-SEM	Field emission scanning electron microscopy
FITC	Fluorescein isothiocyanate
FTIR	Fourier transform infrared spectroscopy
G418	Geneticin® reagent
GAGs	Glycosaminoglycans
HA	Hydroxyapatite
HEPES	4-(2-Hydroxyethyl)piperazine-1-ethanesulfonic acid
h-FOB 1.19	Human fetal osteoblast cell line
HMDSO	Hexamethyldisiloxane

ICDD	International Centre for Diffraction Data
ICP-MS	Inductively coupled plasma-mass spectrophotometry
IR	Infrared
i-SBF	Ionized simulated body fluid
IUD	Intrauterine device
K	Equilibrium constant
K_{1c}	Fracture toughness
LB	Luria-Bertani medium
MCPA	Monocalcium phosphate anhydrous
MCPM	Monocalcium phosphate monohydrate
MG63	Human osteosarcoma cell line
MIR	Mid-infrared
m-SBF	Modified simulated body fluid
NCPs	Non-collagenous proteins
NHOst	Normal human osteoblasts
n-SBF	Newly improved simulated body fluid
OBM	Osteoblast basal medium
OCP	Octacalcium phosphate
OGM	Osteoblast growth medium
PBS	Phosphate buffered saline
PI	Propidium iodide
PET	Poly(ethylene terephthalate)
PLA	Poly(lactic acid)
PMMA	Poly(methyl methacrylate)
PLD	Pulsed laser deposition
PTFE	Poly(tetrafluoro ethylene)
r-SBF	Revised simulated body fluid
RT	Room temperature
Saos-2	Human osteosarcoma cell line
SBF	Simulated body fluid
SEM	Scanning electron microscopy
SiC	Silicon carbide

SSC	Saline-sodium citrate solution
SV40	Simian vacuolating virus 40 or Simian virus 40
TEM	Transmission electron microscopy
THR	Total hip replacement
TRIS	Tris(hydroxymethyl)aminomethane
TTCP	Tetracalcium phosphate
USA	United States of America
XRD	X-ray diffraction
YSZ	Yttrium-stabilized zirconia

CHAPTER 1

INTRODUCTION

Biomaterials engineering is an interdisciplinary research field whose outcomes significantly affect the human health and also have an impact on economy and other scientific fields. The use of biomaterials, such as prosthetic limbs, dates back to ancient times; however, accelerating increments in the number of scientific breakthroughs have happened in the last century. The very first generation of biomaterials was intended to perform the functions of damaged tissues but now they can be designed to support and stimulate the regeneration of the patient's own tissue. A wide range of materials can now be used in biomaterials including polymers, metals, ceramics, composites and even biological materials.

1.1. Biomaterials

A definition of biomaterial given by a consensus of experts in 1986 is as follows: "A biomaterial is a nonviable material used in a medical device, intended to interact with biological systems." [1]. Later, the definition was revised many times within the concept of evolving biomaterials science and its applications. In a leading opinion paper, the biomaterial was redefined as: "A biomaterial is a substance that has been engineered to take a form which, alone or as part of a complex system, is used to direct the course of any therapeutic or diagnostic procedure by controlling the interactions with components of living systems, in human or veterinary medicine." [2]. The scope of the biomaterials term can change from one perspective to another or from one field of application to another. As an example, the emphasis on non-viability may or may not be included in the definition considering the development of materials containing living cells.

An important term for understanding the desired characteristics of biomaterials is biocompatibility. Biocompatibility is defined as the ability of a material to perform with an appropriate host response in a specific application [3]. Appropriate host response refers to a normal healing process without complications such as thrombogenesis, mutagenesis and carcinogenesis. Any material implanted in an organism would generate a tissue reaction but in different ways and grades. The types of reactions between the material and the tissue in contact with it are defined by the terms: bioinertness, bioactivity and bioresorbability (see Table 1). Biotoxicity, which causes a pathological change or rejection of the material by the organism, is another possible reaction but omitted here due to being an unacceptable property for a biomaterial.

Table 1 Types of biomaterials according to their reaction with surrounding living tissues [4].

Biomaterial type	**Reaction of organism**	**Material**
Bioinert (to various degrees)	Coexistence with the material without noticeable change, separation from the material by a layer of fibrous tissue of various thickness	Tantalum, titanium, aluminum and zirconium oxides
Bioactive	Formation of direct biochemical bonds with the surface of the material and free growth	High density hydroxyapatite and tricalcium phosphate, certain bioglasses
Bioresorbable	Gradual dissolution of the material by the biosystem of the organism, replacement without toxicity and rejection	Tricalcium phosphate, porous hydroxyapatite, calcium phosphate salts, certain bioglasses, polyurethane

In general, materials can be classified according to their micro and macro structures, atomic bonding and origin, as shown in Figure 1. The same classifications apply to biomaterials. However, the most common way of classifying biomaterials is based on the bonding as metals, ceramics and polymers. When any two or more of these come together, they form composites.

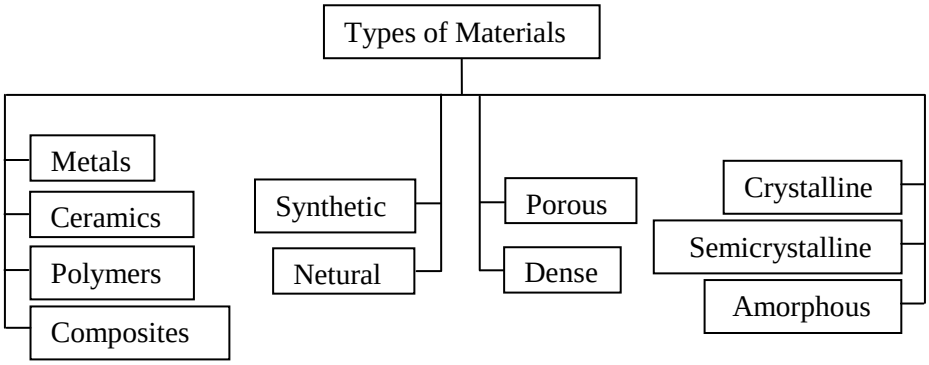

Figure 1 Different types of materials [5].

All three types of materials, their composites and coatings find use in the biomaterials field. Applications of common types of biomaterials are listed in Table 2. The structural features of these materials determine the application areas. For example, in both dental and bone implants metals and alloys are preferred while ceramics with good osteoconductivity are more suitable for bone tissue engineering. Generally, metals are not biodegradable (except Mg) and ceramics are difficult to be processed into highly porous structures due to their brittleness. Therefore, polymers are dominant materials used for scaffolding in tissue engineering applications [6].

The most diverse class of materials in medicine is the polymers (both natural and synthetic). They can exhibit a large variety of functions. Owing to the modifiability of their chemistry, polymers offer great diversity in physical and mechanical properties. According to the desired biomaterial characteristics such as mechanical strength, biodegradability, permeability and transparency, the appropriate one can be chosen from a variety of polymers. The actual property that makes the polymers attractive biomaterials is their degradability; meaning that they are able to be broken down and excreted or resorbed without removal or surgical revision [7]. Some examples of natural polymers used as biomaterials are: (1) collagen in absorbable sutures, sponge wound dressing, drug delivery microspheres, (2) chitosan and its derivatives in controlled-delivery systems, (3) poly(amino acids), such as poly(α,L-lysine), poly(α,L-glutamic acid), poly(aspartic acid) in oligomeric drug carriers, (4) hyaluronic acid in lubricants.

Some of the synthetic polymeric biomaterials in addition to those listed in Table 2 are: (1) poly(lactic acid), poly(glycolic acid) and their co-polymers in drug-delivery systems and tissue engineering, (2) poly(hydroxy butyrate), poly(ε-caprolactone) and copolymers, poly(alkylene succinates) used as a matrix for drug-delivery systems and cell microencapsulation, (3) poly(cyano acrylates) in surgical adhesives and glues, (4) polyphosphazenes as films and hydrogels and (5) poly(ethylene oxide) in a variety of biomedical applications [8]. Polymeric biomaterials are not limited to these examples and new ones can be synthesized for specialized uses in time.

Table 2 Applications of selected polymers, metals and ceramics in medicine [3].

Application	**Biomaterials Used**
Skeletal system	
Joint replacements (hip, knee, shoulder)	Titanium, stainless steel, polyethylene
Bone fixation plates and screws	Metals, poly(lactic acid) (PLA)
Bone cement	Poly(methyl methacrylate) (PMMA)
Bone defect repair	Calcium phosphates
Artificial tendon and ligament	Poly(tetrafluoro ethylene) (PTFE), poly(ethylene terephthalate) (PET)
Dental implant-tooth fixation	Titanium
Cardiovascular system	
Blood vessel prosthesis	PET, expanded PTFE
Heart valve	PET, carbon, metal, treaded natural tissue
Pacemaker, Implantable defibrillator	Titanium, polyurethane
Stent	Stainless steel, other metals, PLA
Catheter	PTFE, silicone, polyurethane
Organs	
Hearth assist device	Polyurethane, titanium, stainless steel
Hemodialysis	Polysulfone, silicone
Blood oxygenerator	Silicone
Skin substitute	Collagen, cadaver skin, nylon, silicon
Ophthalmologic	
Contact lens	Acrylate/metacrylate/silicone polymers
Intraocular lens	Acrylate/metacrylate polymers
Corneal bandage lens	Hydrogel
Glaucoma drain	Silicone, polypropylene

Table 2 Cont'd.

Application	Biomaterials Used
Other	
Cochlear prosthesis	Platinum, platinum-iridium, silicone
Breast Implant	Silicone
Hernia mesh	Silicone, polypropylene, PTFE
Sutures	PLA, polydioxanone, polypropylene, stainless steel
Blood Bags	Poly(vinyl chloride)
Ear tubes (tympanostomy)	Silicone, PTFE
Intrauterine device (IUD)	Silicone, copper

Other major groups of biomaterials are metals and ceramics. They will be described in the following sections for their therapeutic uses in hard tissue replacement.

1.2. Metallic Biomaterials

In the treatment of trauma, disease or malfunction of organs, if loading is involved; the use of the metallic biomaterials is the first choice [9]. They are generally used to construct medical devices in the fields of orthopedic surgery, dentistry and blood circulatory system. About 70% of the materials used to produce implants are found to be metallic materials [10]. In the load bearing applications, polymers are often excluded because of their low Young's modulus and viscoelastic nature. Similarly, inherent brittleness of ceramics limits their applications where the loads are predominantly compressive [11].

If only bone tissue-related implants are considered, metallic biomaterials are used in many devices for load-bearing parts, such as artificial joints, osteosynthesis devices and spinal fixation devices. They have a wide range of applications as dental restorations, artificial teeth roots, denture bases, orthodontic wires, prosthetic valves, electrodes, clips, etc. [12]. Figure 2 shows the types and *in vivo* application sites of metallic implant materials.

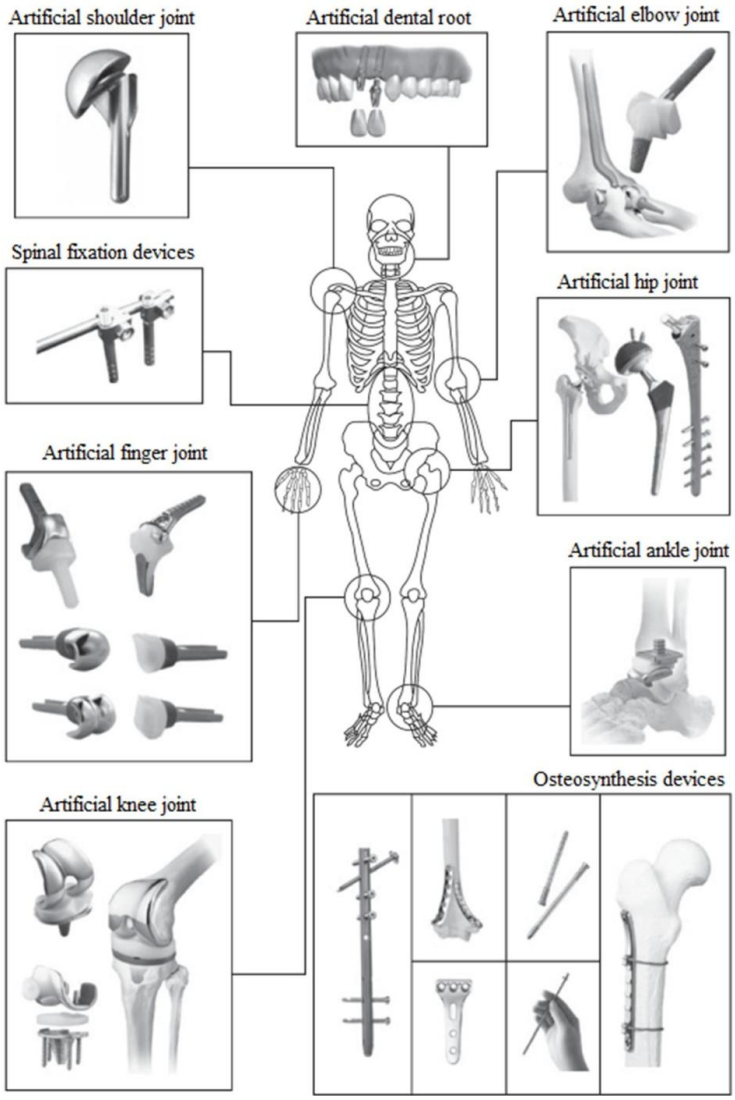

Figure 2 Various bone-related implants that are used *in vivo* for orthopedic surgery and dentistry [12].

The metals that can be tolerated in the body in minute amounts (e.g., Fe, Cr, Co, Ni, Ti, Ta, Mo, and W) are used in manufacturing of implants [13]. Common metallic biomaterials are stainless steels, cobalt based alloys and titanium based alloys. The main advantages, disadvantages, and primary uses of these materials are listed in Table 3 [11].

Stainless steel is an iron-based alloy, which contains over 12–13 wt% chromium (Cr) and some other elements, provided that the content of iron (Fe) is not over 50 wt% [14]. The most widely used stainless steel in implants is austenitic stainless steel, especially type 316L.

Table 3 Common metallic implant materials and their characteristics [11].

Material	Advantages	Disadvantages	Primary uses
Stainless steels	Low cost; availability of processing	High modulus	Temporary devices (plates, screws) and hip stems
Co-based alloys	Wear resistance; corrosion resistance; fatigue strength	High modulus; availability	Dental castings; hip and knee joints
Ti and Ti-based alloys	Biocompatibility; corrosion; fatigue strength; low modulus; low density	Wear resistance; low shear strength	Modular total hip replacement (THR) (stems); dental implants; maxillofacial and craniofacial implants; permanent devices (nails, pacemaker cases); fixation elements (screws, staples)

Molybdenum (Mo) was added into the original stainless steel composition in order to improve its pitting corrosion resistance. The vacuum technology used in the production process reduced the carbon content from 0.08 to about 0.03 wt% maximum, yielding an increase in the corrosion resistance. The purpose of the addition of 9–15 wt% nickel (Ni) into stainless steel composition is to ensure an austenitic state at room temperature (RT) [11]. On the other hand, in body conditions, such as in a highly stressed and oxygen-depleted region, even type 316L stainless steels may corrode [13]. Therefore, the attempts to solve the problem of corrosion focus on Ni-free austenitic stainless steel. This steel has high nitrogen content to maintain the austenitic structure and higher levels of yield strength, fatigue strength, and improved resistance to pitting corrosion and crevice corrosion when compared to Type 316L [15].

When high wear resistance is required for implants, such as an artificial joint, Co-Cr alloys serve better than stainless steels [9]. They were originally developed for aircraft engines and as heat-resistant materials. Their mechanical properties, such as strength and toughness, castability, corrosion and wear resistance are excellent.

When compared to stainless steel, they have better corrosion resistance. Their wear resistance is better than that of stainless steel and Ti alloys; but their plasticity and workability are relatively low [14].

There are basically two Co-Cr alloys: castable CoCrMo alloy and CoNiCrMo alloy which is usually wrought by hot forging [13]. Corrosion resistance of wrought Co–Cr alloy is less than that of cast alloy [14]. Therefore, their application areas differ in body. Since Ni content is a high risk element, which is responsible of allergic reactions, Ni-free Co–Cr alloys are required. Under wear conditions, small amount of Ni may dissolve out of CoCrMo implants [14]. Additionally, a recent *in vitro* study has shown that CoCrMo nanoparticles (29.5 ± 6.3 nm in diameter) may cause damage in DNA and chromosomes [16].

Magnesium alloys have attracted attention as a new kind of biodegradable biomaterial. Magnesium and its alloys are lightweight metals with a density about 1.75 g/cm^3. They have similar Young's modulus to human bones, which can prevent the stress shielding and enhance bone growth and remodeling [17]. With the advantage of their fast corrosion rate in the physiological environment, they can be used as biodegradable metallic biomaterials [18]. Although Mg is essential for human body, the biodegradability property of these alloys necessitates that all elements in the structure must be non-toxic. They are promising materials as absorbable stents; however, it is still questionable for Mg alloys to be used as load bearing implants [17].

Another metallic biomaterial for hard tissue replacement and repair is titanium and its alloys that will be mentioned in detail later. Moreover, there are several other metals, such as tantalum, that have been used for various implant applications. Each one has its own advantages and disadvantages but they have to meet the general biomaterial requirements. The selection of the material for a specific case depends on its properties and especially how much it is able to fulfill these requirements.

The main concern about metals as biomaterials is the release of toxic elements under corrosive conditions that can cause adverse tissue reactions and hypersensitivity [11].

Biological environmental conditions that metallic implant materials are subjected to are described in Figure 3.

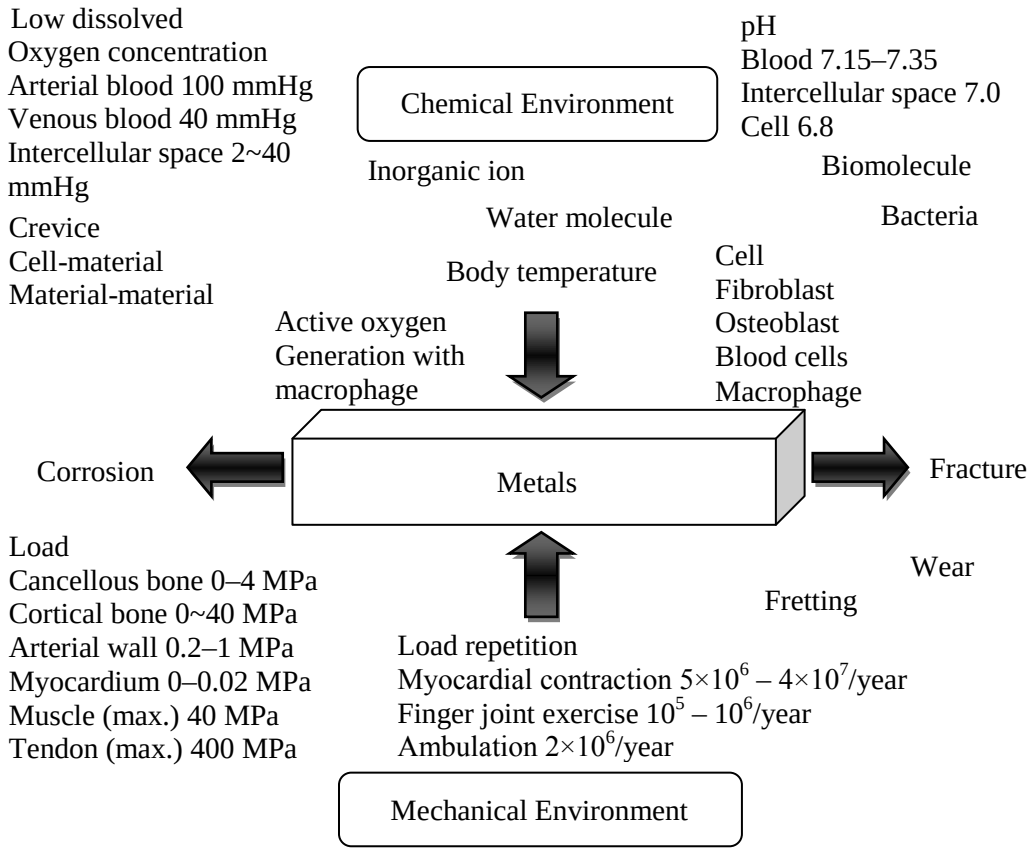

Figure 3 Biological environment of metallic materials implanted into human body. Redrawn from [14].

The chloride ion concentration in serum and interstitial fluid (113 and 117 mEq/L, respectively) tends to form a highly corrosive environment for metallic materials. In addition, various amino acids, proteins and dissolved oxygen in blood and intercellular spaces accelerate the corrosion of metals. Although pH of the body fluids changes in a very small range because the fluids are buffered solutions, critical local pH changes can occur around implant site [14]. On the other hand, oral environment is already more chemically aggressive. For instance, food intake and microbial flora can induce a decrease in the physiological pH of saliva and this can lead to ion release from the material [19].

Metallic biomaterials are exposed to not only chemical but also physical attacks. If the selected implant material and its design are not proper for the specified case, similarly, if the implant material is used outside of its designated area, the implant may fail in many ways. The possible reasons of failure that may end up with revision surgery are given in Figure 4.

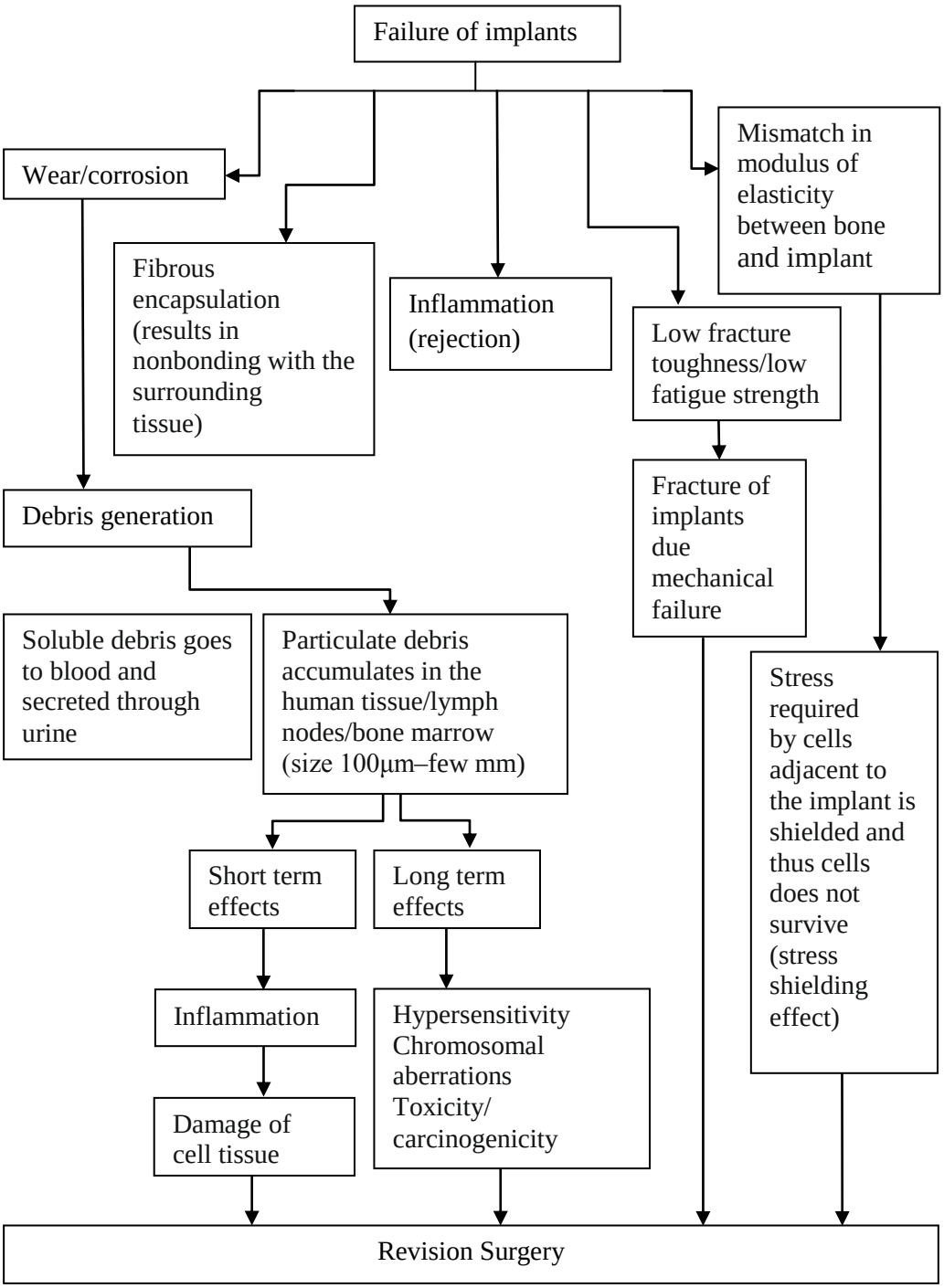

Figure 4 Main causes for failure of implants. Redrawn from [20].

Orthopedic implants are subjected to static or repetitive loads due to body weight and activity. In particular, the peak load can reach several times heavier than body weight in the lower extremities and this is repeated cyclically as a routine in the chemical environment of the body [14]. This condition requires an excellent combination of strength and ductility and this is why the metals are more preferred in load bearing applications [9]. In orthopedic implant applications, toughness, rigidity, elasticity, wettability, bioinertness, bioactivity, biodegradability and X-ray imaging are main concerns [14]. Additionally, for total joint replacement applications, wear resistance is another necessity to avoid debris formation from friction. Intra-oral applications require strong and rigid metals and even the shape memory effect for better results [9]. Before entering into the body, it is required to sterilize the implant therefore; the material must also be sterilizable.

1.3. Titanium and Its Alloys

Titanium element (Ti) was discovered by William Gregor in 1790, however it was named after Titans of Greek mythology by Martin Heinrich Klaproth in 1795. It is one of the transition elements with an atomic number of 22 and an atomic weight of 47.9 [21]. The studies about titanium as an implant material began in the 1950s at Cambridge University [22]. In 1952, Per Ingvar Brånemark implanted a titanium cylinder by screwing into rabbit bone for observing healing reactions. He fortuitously discovered that it was tightly integrated in the bone while he was trying to remove it from the bone after completion of the experiment [3]. Brånemark named this phenomenon osseointegration and later, he developed pure titanium screws for dental implant fixtures [3,22]. Nowadays, more than 1000 tons of titanium is implanted into patients in various forms worldwide annually [23].

Titanium, which is a low-density element (approximately 60% of the density of steel), can be strengthened by alloying and deformation processing [22]. For example, the addition of aluminum (Al) and vanadium (V) into pure Ti greatly increases its tensile strength [9]. Titanium alloys have Young's modulus about half that of stainless steel and Co–Cr alloys, and they are preferred materials for bone fixators because of their low Young's modulus [14].

In addition, titanium is covered by a regular titanium dioxide (TiO_2) layer immediately when it comes into contact with oxygen (air). The thickness of this layer is 4 nm and it serves as a powerful barrier against metal dissolution [24]. This layer is also formed on the surface of titanium alloys and their corrosion resistance is better than that of stainless steel and Co–Cr alloys, accordingly. In addition, when compared with Co–Cr alloys, titanium and its alloys demonstrate a 33% increase in bonding strength to HA coatings which will be mentioned later [17]. On the other hand, they have low torsion strength (torque) and torsion angle to fracture and therefore they are not suitable for bone fixation wires and sternal wires [14].

Commercial titanium alloys are classified into three main phase groups: alpha (α), alpha-beta (α+β) and beta (β) [25]. In this regard, titanium alloy elements are grouped into three categories: (1) α-stabilizers, such as Al, O, N, C; (2) β-stabilizers, such as Mo, V, Nb, Ta (isomorphous), Fe, W, Cr, Si, Co, Mn, H (eutectoid); (3) neutrals, such as Zr [21]. The most widely used alloys are α+β alloys and their β volume fraction is in the range of 5–40% at RT [11]. Among these, Ti6Al4V alloy is the most common biomedical alloy and normally used in annealed condition. Owing to the α + β structure, it has higher strength, higher ductility and higher low cycle fatigue while the β alloys have higher fracture toughness [20].

As stated before, when compared to conventional stainless steels and cobalt alloys, pure titanium and particularly the extra-low interstitial variant (ELI) of the Ti6Al4V alloy have better biocompatibility, lower modulus and enhanced corrosion resistance. Therefore, their use is continuously increasing. There are metallurgically quite similar alloys to Ti6Al4V, such as Ti6Al7Nb and Ti5Al2.5Fe. They are specifically developed to be used as biomaterials with the purpose of eliminating the vanadium, which may be considered as a toxic element [11].

1.4. Calcium Phosphates and Other Bioceramics

The word ceramic traces from the Greek word keramikos meaning pottery. Ceramics are inorganic, non-metallic solids prepared by the application of heat. Their structure can be crystalline, partly crystalline, or may be amorphous (e.g., a glass). Bioceramics (or biomedical ceramics) can be defined as biomaterials of the ceramic origin. The use of bioceramics began in the late 1960s, with the purpose of preventing some biocompatibility problems associated with the metallic implants in orthopedics [26]. Currently, bioceramics are used in many different applications. Generally they are used as joint or tissue replacements and coatings to improve biocompatibility of metal implants. Additionally, they function as resorbable lattices, providing temporary structures and frameworks those are biodegraded as body heals. Some types of bioceramics can be used as drug-delivery vehicles [27].

Bioceramics are classified as almost bioinert, bioactive and resorbable, according to their reactivity inside the living body. Almost bioinert ceramics are considered to be the first generation while bioactive and resorbable ceramics are known as the second generation bioceramics [28]. Figure 5 gives the most important first and second generation ceramics of each type as well as their clinical applications.

The first generation bioceramics were zirconia (ZrO_2) and alumina (α-Al_2O_3) which were used to fabricate femoral heads of total hip prostheses. Their common properties are bioinertness and good mechanical properties, especially, high wear resistance [26]. The applications of alumina and zirconia in medicine are similar and these oxides are mainly used as femoral heads [28].

As stated before, alumina does not directly bond to the bone. The resulting fibrous tissue between the bone and alumina implant can cause osteolysis, pain and loosening. In addition, alumina itself is not suitable for bone replacement therapies due to its very brittleness and a Young's modulus which is very different from that of bone tissue [29]. However, it is superior as dental crowns in terms of its aesthetic match to tooth and suitable mechanical properties.

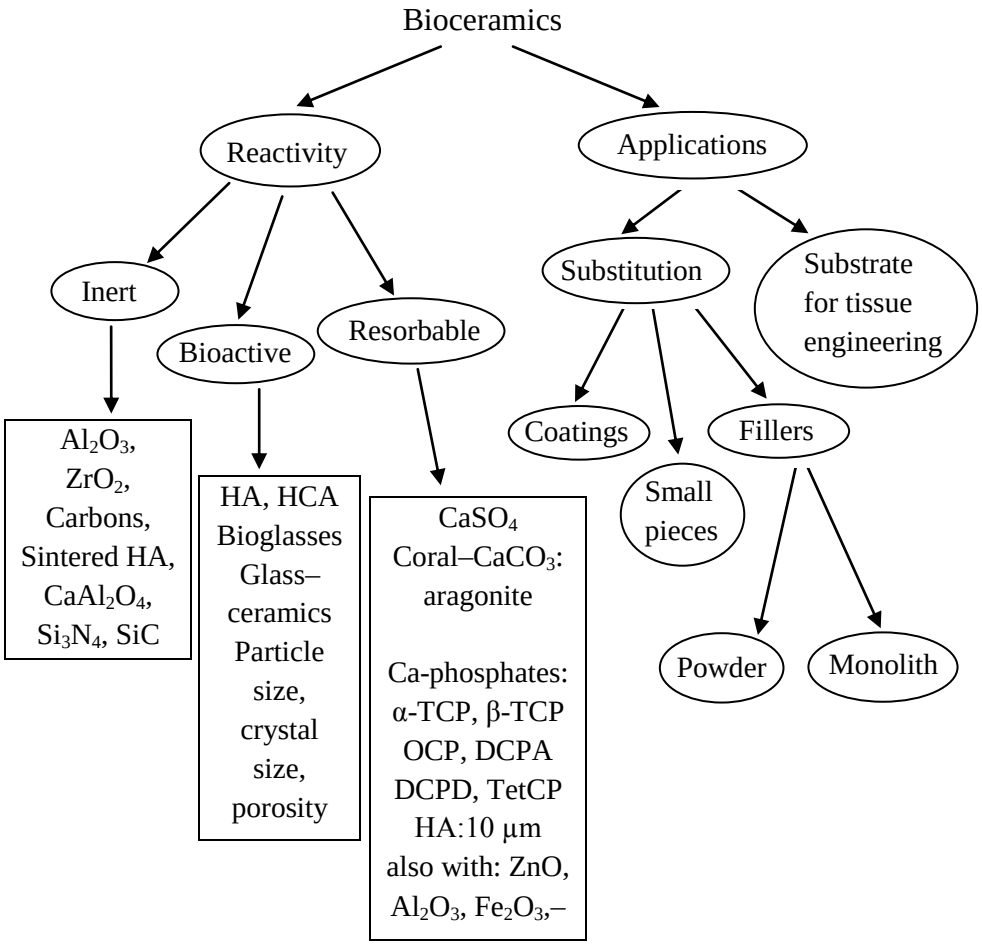

Figure 5 Main bioceramics and their clinical applications. Redrawn from [28].

Zirconia was introduced in 1985 as a ceramic femoral head in order to find an alternative to alumina [3]. The main advantages of zirconia compared to alumina are greater failure strength, mainly bending strength, as well as a good resistance to fatigue. Moreover, zirconia also presents advantages over alumina in terms of its lower friction and wear [28]. On the other hand, one of the disadvantages of zirconia is that it may be weakened under stress in the presence of moisture and this weakening occurs more rapidly at high temperature treatments such as steam sterilization (autoclaving). Zirconia can be strengthened by phase transformation and control of grain size. Yttrium-stabilized zirconia (YSZ) has been used as a femoral head of total hip joint prostheses and has two advantages over the alumina. One is YSZ has fine grain size and a well-controlled microstructure without any residual porosity. The other is YSZ has high fracture strength and toughness [13].

Silica-based bioactive glasses are one of the representatives of second generation bioceramics. They were first prepared in 1969 by Hench et al. [30]. They are the first man-made materials that are capable of making interfacial bond with host tissues. They were named as Bioglass® trademark later. The typical composition of a Bioglass® (45S5) is SiO_2 (45 wt%), Na_2O (24.5 wt%), CaO (24.5 wt%), and P_2O_5 (6 wt%). Its tensile strength is 42 MPa, about one in three and a half of that of human cortical bone. Therefore, they are mostly used in areas under reduced loads, such as, periodontal fillers [31]. At around the same time that Bioglass® was started to be used in clinic (1985) [30], Kokubo et al. developed a new glass-ceramic material: apatite-wollastonite (A-W) glass-ceramic which is an assembly of small apatite particles effectively reinforced by wollastonite. A-W glass-ceramic has higher bending strength, fracture toughness and Young's modulus that enables it to be used in some compression load bearing applications, such as vertebral prostheses [32].

Calcium phosphates were used as a bone regenerating medicine in 1890s but there were no positive findings until Albee found the stimulation of bone formation by tricalcium phosphate in 1920s [33]. In the same decade, the similarities between the X-ray diffraction patterns of natural bone mineral and a calcium phosphate (CaP) compound (hydroxyapatite) were first observed by de Jong [32]. Today, most of the crystalline bioactive and biodegradable ceramics used for bone regeneration are based on calcium phosphates [28]. Calcium phosphates vary in composition and form but all of them are biocompatible, osteoconductive, non-toxic, antigenically inactive and non-carcinogenic [33].

The list of all of the known calcium orthophosphates with standard abbreviations and their solubility and pH stability at 25ºC are given in Table 4. Among these, the compounds having a Ca/P ionic ratio less than 1 are not suitable for implantation into the body due to their high solubility and acidity. Therefore, they are not used as biomaterials. Similarly, tetracalcium phosphate itself is also not suitable due to its alkalinity. However, these calcium orthophosphates might be used in combination with either other calcium orthophosphates or other chemicals for biomedical applications [27].

Table 4 Existing calcium orthophosphates, their solubility and pH stability [27].

Ca/P molar ratio	Compound	Formula	Solubility at 25ºC, -log(K_s)	pH stability in aqueous solutions 25ºC
0.5	Monocalcium phosphate monohydrate (MCPM)	$Ca(H_2PO_4)_2 \cdot H_2O$	1.14	0.0–2.0
0.5	Monocalcium phosphate anhydrous (MCPA)	$Ca(H_2PO_4)_2$	1.14	[c]
1.0	Dicalcium phosphate dihydrate (DCPD), mineral brushite	$CaHPO_4 \cdot 2H_2O$	6.59	2.0–6.0
1.0	Dicalcium phosphate anhydrous (DCPA), mineral monetite	$CaHPO_4$	6.90	[c]
1.33	Octacalcium phosphate (OCP)	$Ca_8(HPO_4)_2(PO_4)_4 \cdot 5H_2O$	96.6	5.5–7.0
1.5	α -Tricalcium phosphate (α -TCP)	α-$Ca_3(PO_4)_2$	25.5	[a]
1.5	β -Tricalcium phosphate (β -TCP)	β-$Ca_3(PO_4)_2$	28.9	[a]
1.2–2.2	Amorphous calcium phosphate (ACP)	$Ca_xH_y(PO_4)_z \cdot nH_2O$, n=3–4.5; 15–20% H_2O	[b]	~5–12[d]
1.5–1.67	Calcium-deficient hydroxyapatite (CDHA)[e]	$Ca_{10-x}(HPO_4)_x(PO_4)_{6-x}(OH)_{2-x}$ [f] (0 <x < 1)	~85.1	6.5–9.5
1.67	Hydroxyapatite (HA or OHAp)	$Ca_{10}(PO_4)_6(OH)_2$	116.8	9.5–12
1.67	Fluorapatite (FA or FAp)	$Ca_{10}(PO_4)_6F_2$	120.0	7–12
2.0	Tetracalcium phosphate (TTCP or TetCP), mineral hilgenstockite	$Ca_4(PO_4)_2O$	38–44	[a]

[a] These compounds cannot be precipitated from aqueous solutions.
[b] Cannot be measured precisely. However, the following values were found: 25.7±0.1 (pH=7.40), 29.9±0.1 (pH =6.00), 32.7±0.1 (pH=5.28). The comparative extent of dissolution in acidic buffer is: ACP>>α-TCP>>β-TCP>CDHA>>HA> FA.
[c] Stable at temperatures above 100ºC.
[d] Always metastable.
[e] Occasionally, CDHA is named as precipitated HA.
[f] In the case x=1 (the boundary condition with Ca/P=1.5), the chemical formula of CDHA looks as follows: $Ca_9(HPO_4)(PO_4)_5(OH)$.

CaP based ceramics have been mostly used as bone substitutes, implants and coatings on dental and orthopedic implants. They can take the forms of granules, pastes, self-hardening cements, coatings and porous devices [26].

Synthetic hydroxyapatite (HA, $Ca_{10}(PO_4)_6(OH)_2$) is the most widely studied CaP because it is a complete chemical and crystalochemical analogue of bone mineral [4]. However, bone is not a completely inorganic material. Roughly, it consists of inorganic substances (69 wt%) whose main component is HA, organic substances (22 wt%) whose main component is collagen and water (9 wt%) [34]. Bone HA, forms crystalline platelets with the approximate dimensions of (1.5–3.5)×(5.0–10.0)×(40.0–50.0) nm^3. The mass percentage of HA crystals can reach up to 70% in cortical bones and the remaining material in the composite is collagen fibers. On the other hand, tooth enamel consists of 97% inorganic compound which is fluorine containing HA ($Ca_{10}(PO)_4(OH,F)_2$) [4].

The Ca/P ratio of stoichiometric HA is 1.67. The crystal structure of HA can be thought as hexagonal alignment of PO_4^{3-} ions creating two tunnels parallel to the c axis. Ca^{2+} ions, noted as Ca(I), occupy the first tunnel, coinciding with the ternary axis of the structure. The second tunnel, which is lined by oxygen and other calcium ions, noted Ca(II), is occupied by OH^- ions (see, Figure 6) [35].

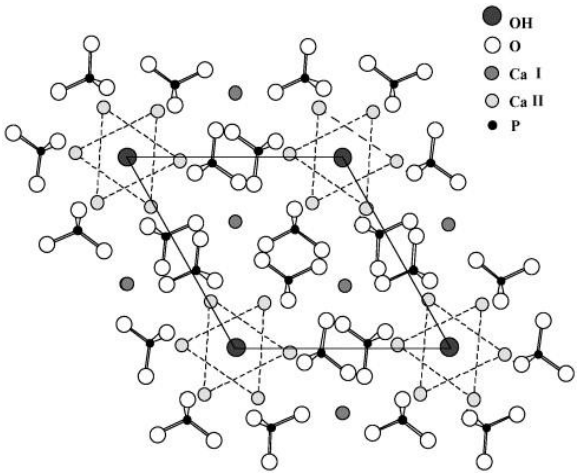

Figure 6 Projection of HA structure on the (001) plane. The two Ca^{2+} triangles lining the "tunnels" of the structure are located at *z*1/4 and *z*3/4. OH^- ions are slightly under or above the triangles [35].

HA can be prepared via various methods. For example, exactly stoichiometric quantities of calcium and phosphate containing aqueous solutions are mixed at pH>9, and boiled for several days under a CO_2-free atmosphere, filtered and dried. Microcrystalline HA can be produced by solid-state reactions of other calcium phosphates (e.g. MCPM, DCPA, DCPD, OCP) with CaO, $Ca(OH)_2$ or $CaCO_3$. During these reactions, sintering temperatures must exceed 1200ºC in an atmosphere of equal volumes of water and nitrogen. It is possible to produce single crystals of HA with hydrothermal synthesis. A water-free synthesis can be performed in ethanol from $Ca(OEt)_2$ and H_3PO_4 [36].

Clinical applications of HA can range from drug delivery systems to orthopedic devices. Unfortunately, as a bulk material, pure HA has poor mechanical properties. For example, fracture toughness (K_{1c}) of HA cannot exceed the value of 1.0 $MPa \cdot m^{1/2}$, therefore it is very low when compared to that of human bone (see, Table 5). Accordingly, HA ceramics cannot be used as heavy-loaded implants. Its mechanical properties limit the clinical applications to small unloaded implants, powders, coatings, and low-loaded porous implants [37].

Table 5 Summary of the physical and mechanical properties of various implant materials and natural bone [38].

Properties	**Natural bone**	**Magnesium**	**Ti alloy**	**Co–Cr alloy**	**Stainless steel**	**Synthetic HA**
Density (g/cm^3)	1.8–2.1	1.74–2.0	4.4–4.5	8.3–9.2	7.9–8.1	3.1
Elastic modulus (GPa)	3–20	41–45	110–117	230	189–205	73–117
Compressive yield strength (MPa)	130–180	65–100	758–1117	450–1000	170–310	600
Fracture toughness ($MPa \cdot m^{1/2}$)	3–6	15–40	55–115	N/A	50–200	0.7

Nowadays, bioceramics with more advanced properties are studied. Scientists are working to develop the third generation bioceramics with the purpose of substituting ‘replace’ tissues by ‘regenerate’ tissues [28]. These bioceramics are expected to be not only bioactive but also involved in the healing process.

HA is similar to a large extent to the inorganic structure of bone, but unlike pure HA, the inorganic component of the bone contains F^{-}, Mg^{2+}, CO_3^{2-}, Cl^{-}, Na^{+}, K^{+}, Fe^{2+}, Zn^{2+}, Sr^{2+} ions in its crystal lattice [39]. As can be understood, the crystal structure of HA is suitable to be changed by doping a variety of ionic and chemical groups. This has emerged the idea of adding various ions into HA in order to acquire the desired structural, mechanical and biological properties, and the recent successful applications in this direction have induced the attention of the biomaterials scientists. For example, the use of strontium in the treatment of osteoporosis [40], the antibiotic properties of silver [41] and the positive effect of zinc on bone formation [42] opened a door to the use of these elements in the studies intended to functionalize HA for orthopedic applications. Additionally, there are many dopant elements in literature, which normally cannot be found in the human body, such as yttrium, lanthanum, indium and bismuth [43].

1.5. Hydroxyapatite Coatings

As mentioned before, the term “osseointegration” was originally introduced by Brånemark to describe “a close implant–bone contact at the light microscopic level.” When the implant surface is not able to integrate with the adjacent bone, implant loosening is inevitable due to micromotions. Therefore, the implants must have appropriate surface chemistry, roughness and topography for the development of good osseointegration [20]. In order to enhance osseointegration, several surface modifications have been developed. These modifications can be classified into two general categories: (1) surface treatments to modify topography and (2) deposition of bioactive surface coatings, such as calcium phosphates [44].

Furlong and Osborn first began clinical trials using the HA coated implants in 1985 [45]. Today, there are various techniques for coating HA on metallic implants. These techniques with their advantages and disadvantages are summarized in Table 6.

Table 6 Various techniques to deposit bioresorbable coatings of calcium orthophosphates on metal implants [27].

Technique	Thickness	Advantages	Disadvantages
Thermal spraying	30–200 μm	High deposition rates; low cost	Line of sight technique; high temperatures induce decomposition; rapid cooling produces amorphous coatings
Sputter coating	0.5–3 μm	Uniform coating thickness on flat substrates; dense coating	Line of sight technique; expensive; time consuming; produces amorphous coatings
Pulsed laser deposition	0.05–5 μm	Coating by crystalline and amorphous phases; dense and porous coating	Line of sight technique
Dynamic mixing method	0.05–1.3 μm	High adhesive strength	Line of sight technique; expensive; produces amorphous coatings
Dip coating	0.05–5 mm	Inexpensive; coatings applied quickly; can coat complex substrates	Requires high sintering temperatures; thermal expansion mismatch
Sol–gel technique	<1 μm	Can coat complex shapes; low processing temperatures; relatively cheap as coatings are very thin	Some processes require controlled atmosphere processing; expensive raw materials

Table 6 Cont'd.

Technique	Thickness	Advantages	Disadvantages
Electrophoretic deposition	0.1–2.0 mm	Uniform coating thickness; rapid deposition rates; can coat complex substrates	Difficult to produce crack-free coatings; requires high sintering temperatures
Biomimetic coating	<30 μm	Low processing temperatures; can form bonelike apatite; can coat complex shapes; can incorporate bone growth stimulating factors	Time consuming; requires replenishment and a pH constancy of simulated body fluid
Hot isostatic pressing	0.2–2.0 μm	Produces dense coatings	Cannot coat complex substrates; high temperature required; thermal expansion mismatch; elastic property differences; expensive; removal/ interaction of encapsulation material
Electrochemical deposition	0.05–0.5 mm	Uniform coating thickness; rapid deposition rates; can coat complex substrates; moderate temperature, low cost	The coating/substrate bonding is not strong enough

Among these techniques, plasma spraying is used widely due to its simplicity and economy. However, it has been reported that plasma spraying exhibited variation in bond strength between the coatings and the metallic substrates, non-uniformity in coating thickness and coating density, changes in the phase composition and crystallinity of HA and alteration in the characteristics of metallic substrates due to the elevated temperature of the process [46,47].

In addition to these problems, plasma spraying is a line-of-sight process; therefore it is not very useful in coating complex implant surfaces [47]. At this point, biomimetic method, which is based on dipping the metallic implants in simulated body fluid (SBF) at the physiological temperature and pH, offers a promising alternative although it is time consuming.

1.6. Biomimetics and Simulated Body Fluid (SBF)

In general, biomimetics is the application of methods and systems that are present in nature to technology and engineering. In particular, it is an area of great interest for bone tissue engineering [48].

As stated before, biomimetics can be used as a route for HA coating on various substrates. Biomimetic method is based on dipping the metallic implants in SBF at the physiological temperature and pH. It has four main advantages: (i) it is applicable to any heat-sensitive substrate (including polymers) because of being a low temperature process; (ii) bonelike apatite crystals having high bioactivity and good resorption characteristics can be formed; (iii) it can be deposited even on porous or complex implant geometries; and (iv) it can incorporate bone-growth-stimulating factors [49].

The biomimetic apatite coating route is mainly mimicking the bone mineralization process by immersing implants in SBF that mimics the inorganic composition, pH, and temperature of human blood plasma [50]. SBF simulates just the inorganic part of human blood plasma and does not contain proteins, glucose, vitamins, hormones, etc.

Since the first formulation proposed by Kokubo for the SBF calcifying solution, a number of slightly different compositions were proposed [51]. A comparison of the concentrations of ions (mmol/l) in human plasma and in several different SBF solutions is given in Table 7.

Table 7 Ionic concentrations [mM] of blood plasma and several different SBF solutions in literature.

Ion	Na^+	K^+	Mg^{2+}	Ca^{2+}	Cl^-	HCO_3^-	HPO_4^{2-}	SO_4^{2-}	Buffer
Blood plasma [51]	142.0	5.0	1.5	2.5	103.0	27.0	1.0	0.5	
Original SBF [52]	142.0	5.0	1.5	2.5	148.8	4.2	1.0	0	TRIS
Corrected (c-SBF) [53]	142.0	5.0	1.5	2.5	147.8	4.2	1.0	0.5	TRIS
Tas-SBF [54]	142.0	5.0	1.5	2.5	125.0	27.0	1.0	0.5	TRIS
Bigi-SBF [51]	141.5	5.0	1.5	2.5	124.5	27.0	1.0	0.5	HEPES
Revised SBF (r-SBF) [55]	142.0	5.0	1.5	2.5	103.0	27.0	1.0	0.5	HEPES
Modified (m-SBF) [55]	142.0	5.0	1.5	2.5	103.0	10.0	1.0	0.5	HEPES
Ionized (i-SBF) [55]	142.0	5.0	1.0	1.6	103.0	27.0	1.0	0.5	HEPES
Newly improved SBF (n-SBF) [56]	142.0	5.0	1.5	2.5	103.0	4.2	1.0	0.5	TRIS
5×SBF [49]	714.8	0	7.5	12.5	723.8	21.0	5.0	0	

It can be noted that the original SBF used by Kokubo et al. [52] lacks the SO_4^{2-} ions contained in human blood plasma. This was corrected then as c-SBF (sometimes referred as conventional SBF [55]) and has been used as 'SBF' by many researchers. However, corrected c-SBF was still rich in Cl^- ion and poor in HCO_3^- ion when compared to human blood plasma [52]. Oyane et al. [55] tried to correct this difference. They prepared r-SBF and i-SBF which had ion concentrations equal to that of blood plasma and m-SBF whose HCO_3^- ion concentration was different from that of blood plasma only. However, r-SBF and i-SBF lacked long-term stability due to a strong tendency to precipitate both apatite and calcite from these SBF [50,55].

In 2004, Takadama et al. [56] proposed a newly improved SBF (n-SBF) in which they decreased only the Cl^- ion concentration to the level of human blood plasma, leaving the HCO_3^- ion concentration equal to that of c-SBF. This improved SBF was compared with c-SBF in its stability and the reproducibility of apatite formation on synthetic materials via round robin testing. As a result, it was confirmed that the c-SBF does not differ from n-SBF in stability and reproducibility [52,56].

As stated before, titanium and its alloys are generally chemically durable, since they are covered with a passive thin titania (TiO_2) layer [31]. Kim et al. [57] showed that even this TiO_2 layer can react with sodium hydroxide (NaOH) solution to form a sodium titanate hydrogel layer. They introduced alkali and subsequent heat treatment in order to enhance the bioactivity of Ti and its alloys.

The structural changes of Ti or its alloys during the alkali and heat treatments, and the process of the apatite formation on them in SBF, are demonstrated in Figure 7.

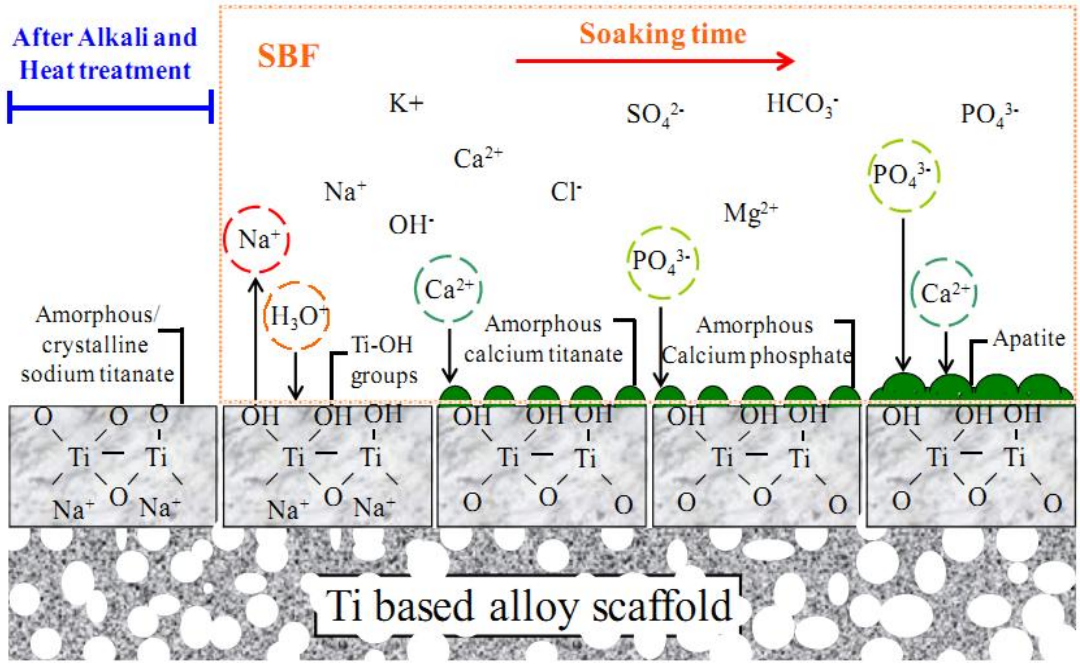

Figure 7 A schematic illustration of the apatite formation on the surface of alkali-heat treated porous Ti based alloy scaffold soaking in SBF [58].

When titanium metal and its alloys are soaked in alkaline solution, a hydrated titanium oxide gel layer containing alkali ions is formed on their surfaces [59]. During heat treatment, the hydrogel layer is dehydrated and densified to form a stable alkali titanate layer [57]. Actually, when the metal is treated with 5M NaOH aqueous solution at 60°C for 24 h, a sodium titanate hydrogel layer can be formed on its surface [60]. If the NaOH and heat-treated metal is soaked in SBF, it releases Na^+ ions via ion exchange with the H_3O^- ions in the SBF and form Ti–OH groups on its surface [59]. The Ti–OH groups formed immediately combine with Ca^{2+} ions in the SBF to form calcium titanate. This calcium titanate later combines with phosphate ions in the SBF to form amorphous CaP during this complex process of apatite formation. This can be interpreted in terms of the electrostatic interaction of the functional groups with the ions in the SBF. The Ti–OH groups formed on the surface of sodium titanate after soaking in SBF are negatively charged and, hence, combine selectively with the positively charged Ca^{2+} ions in the fluid to form calcium titanate. As the calcium ions accumulate on the surface, the surface gradually gains an overall positive charge. As a result, the positively charged surface combines with negatively charged phosphate ions to form CaP [61]. Once the apatite nuclei are formed, they spontaneously grow by consuming the calcium and phosphate ions from the surrounding fluid, since the body fluid is already supersaturated with respect to the apatite [62]. This is also the reason of the necessity of SBF replenishment (e.g. in every two days) during the coating process with the purpose of supplying calcium and phosphate ions for continuation of the apatite formation.

The equation of precipitation of HA is as follows [63]:

$$5Ca^{2+} + 3PO_4^{3-} + OH^- \rightarrow Ca_5(PO_4)_3(OH) \downarrow \quad (1)$$

The possible equilibrium chemical reactions involved in the process are listed in Table 8.

Table 8 Association/dissociation reactions in SBF and their equilibrium constants (K) [63].

Reaction	***K***
$H_2CO_3(aq.) \rightleftharpoons H^+ + HCO_3^-$	$10^{-6.31}$
$HCO_3^- \rightleftharpoons H^+ + CO_3^{2-}$	$10^{-10.25}$
$H_3PO_4(aq.) \rightleftharpoons H^+ + H_2PO_4^-$	$10^{-2.196}$
$H_2PO_4^- \rightleftharpoons H^+ + HPO_4^{2-}$	$10^{-7.185}$
$HPO_4^{2-} \rightleftharpoons H^+ + PO_4^{3-}$	$10^{-12.19}$
$Ca^{2+} + HCO_3^- \rightleftharpoons CaHCO_3^+$	$10^{1.16}$
$Ca^{2+} + CO_3^{2-} \rightleftharpoons CaCO_3(aq.)$	$10^{3.38}$
$Ca^{2+} + OH^- \rightleftharpoons CaOH^+(aq.)$	25.12
$Ca^{2+} + H_2PO_4^- \rightleftharpoons CaH_2PO_4^+$	31.9
$Ca^{2+} + HPO_4^{2-} \rightleftharpoons CaHPO_4(aq.)$	6.81×10^2
$Ca^{2+} + PO_4^{3-} \rightleftharpoons CaPO_4^-$	3.46×10^6
$Mg^{2+} + HCO_3^- \rightleftharpoons MgHCO_3^+$	$10^{0.62}$
$Mg^{2+} + CO_3^{2-} \rightleftharpoons MgCO_3(aq.)$	$10^{1.87}$
$Mg^{2+} + OH^- \rightleftharpoons MgOH^+$	$10^{2.19}$
$Mg^{2+} + H_2PO_4^- \rightleftharpoons MgH_2PO_4^+$	$10^{0.4}$
$Mg^{2+} + HPO_4^{2-} \rightleftharpoons MgHPO_4(aq.)$	$10^{1.8}$
$Mg^{2+} + PO_4^{3-} \rightleftharpoons MgPO_4^-$	$10^{3.3}$

There have been many studies done recently, in which metallic implant surfaces coated with HA via biomimetic method. In a study conducted by Pasinli et al. [64], in order to coat CaP on Ti6Al4V alloy substrates, a new SBF solution was developed, in which Ca^{2+}, Na^+, Mg^{2+}, K^+, HPO_4^{2-}, HCO_3^-, Cl^-, and SO_2^- ion concentrations similar to those of human blood plasma. The coating thickness was reported as 4 μm after 48 h. The binding force of surface coatings was measured by scratch test and differed as 9mN or 3mN according to the processes applied to Ti6Al4V plates before the coating process. It is reported that Ca^{2+} and HPO_4^{2-} rich solutions (compared to traditional solutions) resulted in shortening of the coating time.

Chakraborty et al. [65] coated HA on 316L stainless steel substrate and investigated the gradual development of crystallinity along with a morphological variation in deposited HA crystals with a transmission electron microscopy (TEM) study. After a period of 6 days of 316L stainless steel substrate immersion in SBF, a gradual growth in the HA nano-crystals from crystallite size of 20 nm to a crystallite size of 50 nm was observed. X-ray diffraction (XRD) analysis of coated substrates revealed a pure HA as the only phase present in the coating.

As it is mentioned before, functioning of HA by adding various ions has attracted growing interest in recent times. When compared to the pure HA, ion doped HA is more advantageous in terms of enabling the production of orthopedic implants with functionalized coatings. Li et al. [66] performed a study which was designed to investigate the effects of strontium-substituted HA coatings on implant fixation in ovariectomized rats. After a 12-week healing period, even only 10% strontium doped HA coated implants revealed improved osseointegration compared to pure HA.

However, there are a limited number of studies to produce orthopedic implants with functionalized surfaces, which are designed to prevent cancer occurrence or the proliferation of cancerous cells. When this is achieved, one of the difficulties in systemic drug delivery, which is failure in sending the proper amount of a drug to the intended target, should have been overcome. It makes sense to use the implant itself as a drug delivery system (local drug delivery), which has been problematic for currently used metals [67]. In this sense, selenium and integration of selenium to the HA coatings are promising solutions.

1.7. Bone Structure

Bone tissue is a natural composite that exhibits a highly hierarchical structure. The anatomy of bone can be considered hierarchically, starting from sub-microscopic (nanoscale) level to macroscopic level. The levels of human bone tissue are given in Figure 8.

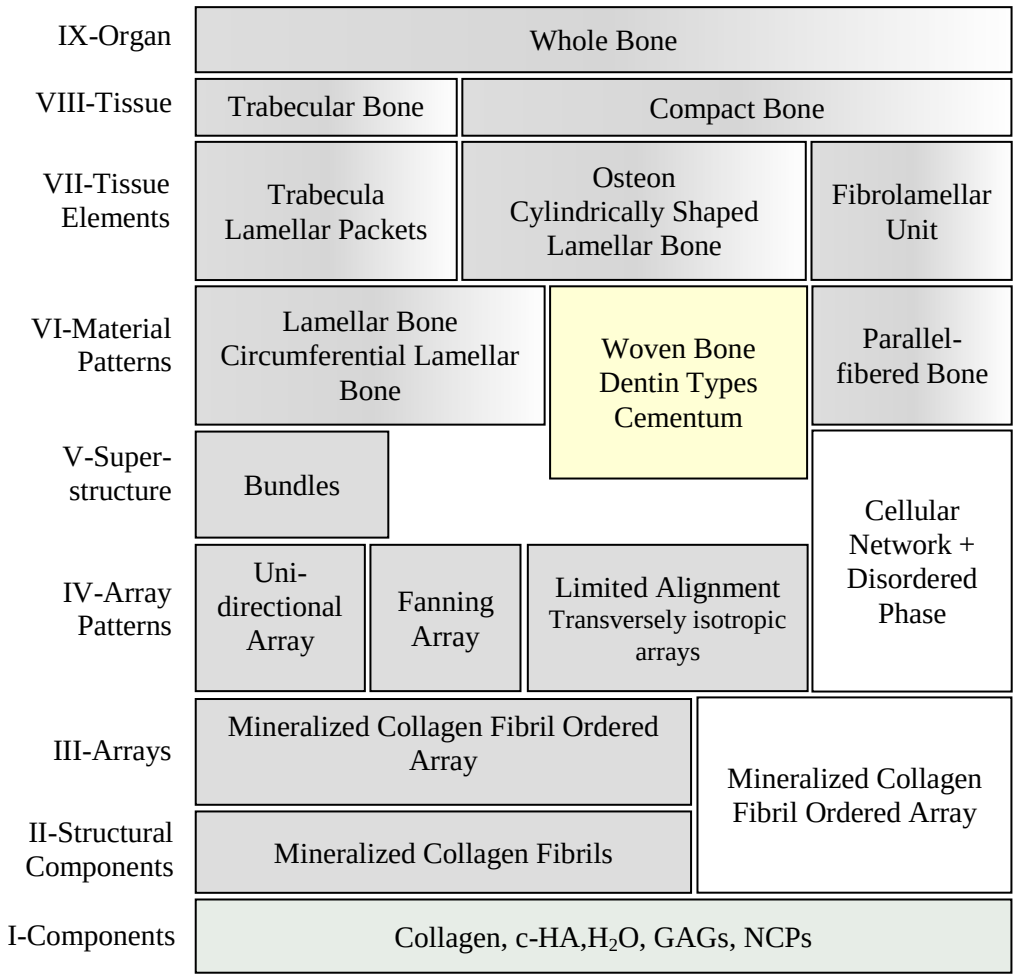

Figure 8 Hierarchical organization of bone (c-HA: carbonated hydroxyapatite; GAGs: glycosaminoglycans; NCPs: non-collagenous proteins). Redrawn from [68].

In Figure 8, up to level V, the hierarchical levels of bone can be divided into: (1) the ordered material (shown in grey) and (2) the disordered material (shown in white). At level VI, these two materials combine in lamellar bone and parallel fibered bone. Other members of the bone, which are still need to be investigated with respect to the presence of both material types, are depicted in a light yellow box. At level VII, the lamellar packets that make up trabecular bone material and the cylindrically shaped lamellar bone that makes up osteonal bone are shown. The fibrolamellar unit comprises the primary hypercalcified layer, parallel fibered bone and lamellar bone [68].

The schematic drawing of human cortical bone in microscopical level is given in Figure 9. The collagen molecules are organized into fibrils and the crystals of c-HA nucleate within the gaps inside these fibrils. The growth of HA extend into the overlapped zones. The end product is the mineralized collagen fibrils forming layers of plate-shaped crystals that span the cross-section of the fibrils [68].

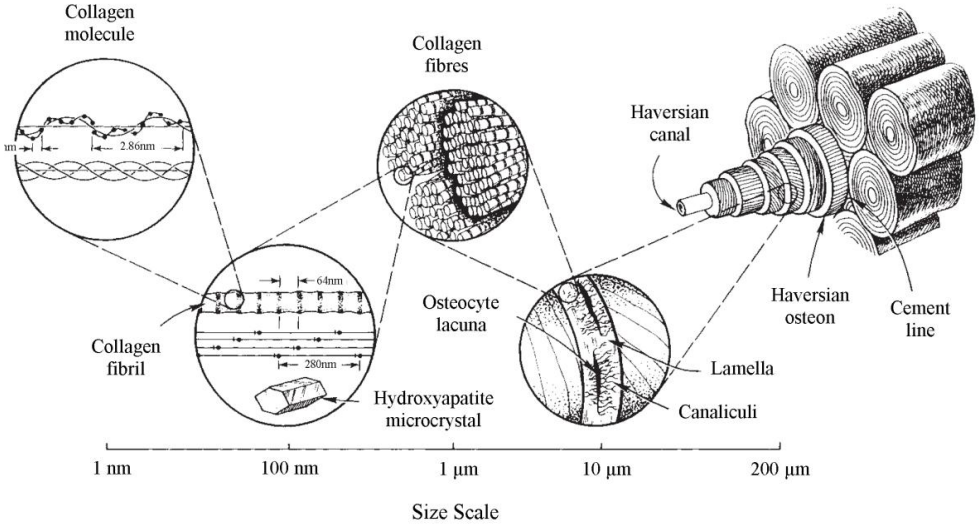

Figure 9 Macroscopical hierarchical structure of cortical bone [69].

Mineralized Type I collagen fibrils constitute the cylindrical arrays which may be organized in different ways to form different patterns. These cylindrical arrays are aligned side-by-side to form extensive sheets of bundles which are separated by thin layers of disordered material. In the disordered material, the super-structure is the combination of the material itself (mineralized collagen fibrils and ground mass) and the embedded osteocyte lacuna and canaliculi. In some cases these sheets of mineralized collagen fibers wrap in concentric layers around a Haversian canal to form an osteon. When no pattern of the mineralized collagen fibers can be distinguished, the bone type is called woven bone [68].

1.8. Cancer and Infection in Orthopedics

Primary bone cancer is rare, but as a secondary cancer form, which is a result of the spread of cancer from other organs (such as lungs, breasts and prostate), it is one of the most commonly seen cancer type [70,71]. Nevertheless, according to statistics

published by the American Cancer Society, in United States, in 2014, it was estimated that there will be new 3020 cases of primary bone and joint cancer (1680 male and 1340 female) and 1460 individuals were expected to lose their life from these cancers [72]. On the other hand, past studies suggested that 1.2 million new cases of cancer occurs each year in the USA, about 300000 eventually develops a bone metastasis [73]. The true numbers of bone cancer deaths are underreported in clinical literature, because many deaths are officially attributed to the original cancer source [70]. However, autopsy studies have shown that 70% of patients with breast and prostate carcinoma develop skeletal metastases, numbers are less but still significant in thyroid (40%), renal (35%), bronchus (35%) and rectal (10%) carcinoma [73].

A common technique for the treatment of bone cancer is insertion of an orthopedic implant to restore patient function after the surgical removal of cancerous tissue [74]. However, if cancer cells are not completely removed from the environment, recurrence of cancer can be seen around the implant.

In a study conducted by Yalnız et al. [75], 23 patients (12 males, 11 females; mean age 49 years; range 14-81 years) who underwent wide resection and cemented endoprosthetic replacement with prosthesis for bone tumors were included. Twelve patients (52.2%) had metastatic, 11 patients (47.8%) had primary tumors. It is reported that postoperative complications were noted for seven patients (30.4%), being local recurrences in 3 patients. During the follow-up period, 11 patients were lost due to tumoral causes, distant metastasis developed in three patients, and 9 patients were tumor-free. Ten of these 11 patients were among metastatic tumor group and one patient from the primary tumor group. Additionally, after the treatment, the most common complication was the reformation of tumor in same site (local relapse) with a rate of 13%.

Although biomaterials used in orthopedic devices are generally considered non-toxic, in animal studies, some constituents of these devices have been shown to be potentially carcinogenic. In humans, the development of an orthopedic implant associated malignancy is a rare, but a well recognized complication [76].

On the other hand, with the technological advances in recent years and the advances in biology and materials science at the molecular level, it has become possible to add a number of features to orthopedic implants for obtaining better results. For example, bioactive materials, which can actively promote the integration of bone tissue, ensure success of the cell attachment, proliferation and differentiation into a functionally and structurally appropriate tissue. HA can be given as an example of widely used orthopedic bioactive materials [77].

Apart from the development of cancer, infection following surgical fixation is a common complication occurring around the implant. The cause of two-thirds of these infections is the staphylococci bacteria [78]. *Staphylococcus epidermidis* and *Staphylococcus aureus* are the most frequently isolated bacteria from infected biomaterial surfaces. Additional organisms that may cause infection around the implant site are *Escherichia coli*, *Peptococci*, *Pseudomonas aeruginosa*, *Proteus mirabilis* and beta hemolytic *Streptococcus*. *S. epidermidis*, usually thought as a nonpathogenic, commensal, human skin saprophyte, has emerged as a serious pathogen in biomaterial-related infections and is a leading cause of infections of vascular prostheses, neurosurgical shunts, and orthopedic implants [79].

In order to prevent infections of biomaterials, two different materials are preferred: (1) anti-bacterial and (2) anti-adhesive. The first type of materials contains anti-bacterial substances that are incorporated into the biomaterial. Anti-bacterial coatings consisting of antibiotics (e.g., rifampicin and minocycline), silver ions, chlorhexidine, and silver sulphadiazine have been proposed. However, it was reported that no single anti-bacterial substance has been developed that accomplishes total and long-term eradication of adherent bacteria [80].

In a study carried out to investigate the effects of four different selenium compounds on the proliferation of *Staphylococcus aureus*, selenium was found to be successful in inhibition of the proliferation of these bacteria [81]. In addition, most of the researches that aimed to prevent the infections around the orthopedic implants are centered on the local delivery of anti-microbial agents, such as antibiotic loaded device coatings [82].

This reveals the possibility and importance of the implementation of selenium, which is promising in terms of prevention and treatment of many types of cancer [83-85], as an antibiotic agent, to the implant surfaces. However, the implant materials in the literature cannot make it possible to take advantage of the high biocompatibility and bioactivity of HA coatings, which are almost associated with Ti6Al4V implants in orthopedics.

1.9. Selenium and Its Importance

In humans and animals, selenium is an essential element naturally present in the structure of selenoproteins and plays important roles in many processes such as defense systems, thyroid hormone metabolism, and redox control of cell reactions [86]. Its functions in the body include regulating metabolism, improving immunity, enhancing reproductive performance and preventing cancer [87]. The association between selenium deficiency and the risk for cancers, including the lung, breast, prostate, lymph node and gastro-intestine, has been widely studied. The blood selenium levels were found to be significantly lower in cancer patients than in control groups. Although the exact mechanism involved in tumor suppression by selenium is still unknown, it has been reported to be a potential cancer preventive and inhibitory agent [88]. Therefore, it has a promising potential in cancer prevention and also in treatment.

As stated before, although the exact mechanism in cancer prevention is still not known exactly, it is reported that selenium has effects on DNA replication, transcription and translation [89]. In some studies, selenium containing selenodiglutathione, which is the selenium analogue of the sulfur containing essential amino acid methionine, is shown to induce apoptosis, the programming of the cell to destroy itself [90].

Selenium can get in the body through the foods that contain various amounts and chemical forms of it. The metabolism of dietary selenium is shown in Figure 10.

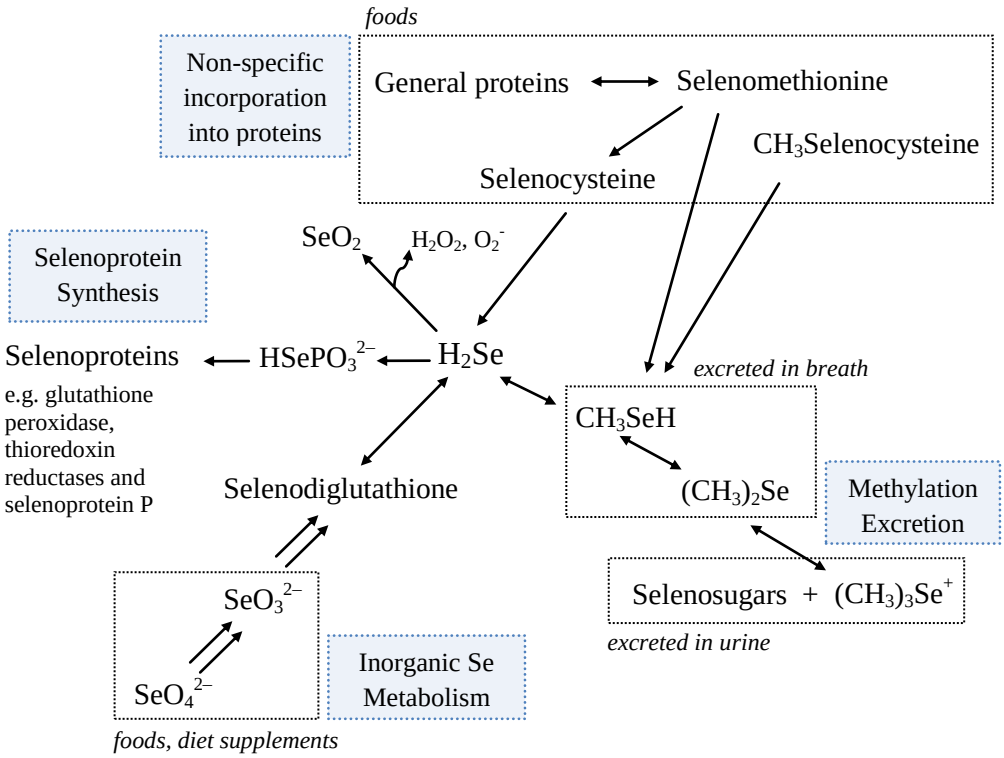

Figure 10 Intermediary metabolism of selenium. Adapted from [91,92].

The selenium compounds in cells may be biologically active in many ways as shown in Figure 11. Although these pathways are characterized in different cell types, these events also occur in bone cells.

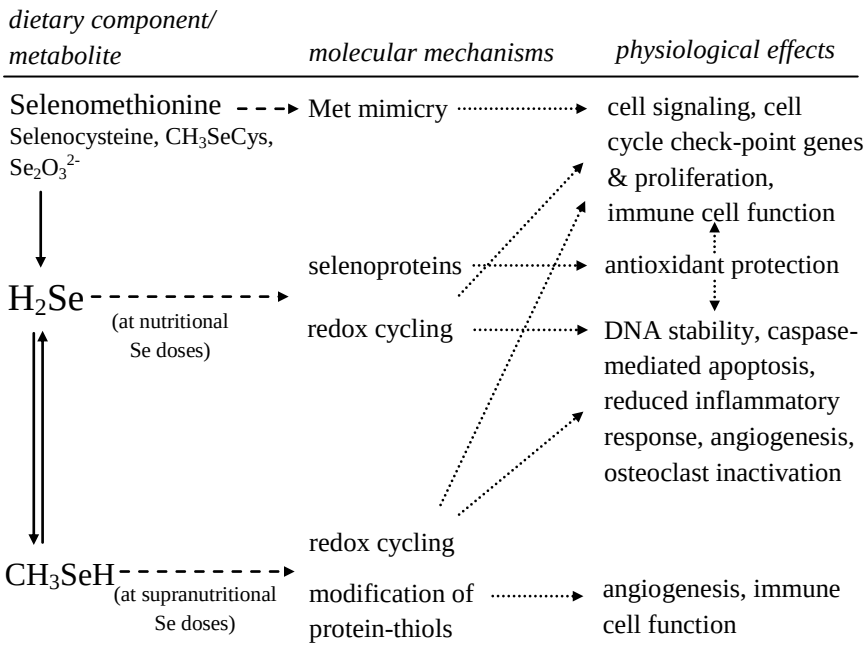

Figure 11 Molecular mechanism of selenium related to bone health [91].

Based on this, Hiraoka et al. [88] studied selenium oral medication given as a method for blocking the proliferation of osteosarcoma cells. It was shown that selenium inhibited the tumor growth *in vitro* and morphological changes indicative of apoptosis were demonstrated. More importantly, osteosarcomas in mice were inhibited in growth by selenium with no cytotoxic change in normal tissues. These findings suggested that selenium may offer a novel therapeutic modality for osteosarcoma. Additionally, in particular for secondary bone cancers, it was previously reported that osteoblast response to metastatic breast cancer cells is effectively suppressed by selenium supplementation and selenium may prevent osteoblast inflammatory response and metastasis process [93].

In addition, selenium was shown to be a radioprotective agent that can be beneficial when malignant lesions are treated by surgery and radiotherapy procedures. In a study [94], bone repair was examined in a bone defect formed in rats after intraperitoneal injection of sodium selenite (1.0 mg/kg). During healing, volumetric bone density of the rats treated with sodium selenite was reported to be closer to or higher than those of the control group that received distilled water. This outcome was reported to be in correlation with the antioxidant mechanisms of selenium. When gamma radiation was applied to the rats, spongy trabecular bone between the cortical plates was totally absent on the 45^{th} day of healing. However, in the rats which were treated with sodium selenite, thick cortical bone plates with spongy bone were preserved, showing the benefit of selenium in the process of bone repair in individuals undergoing radiotherapy.

Selenium doped HA nanpoparticles embedded in chitosan matrix to form a composite implant biomaterial was previously shown to enhance the rat calvarial critical size defect [95]. Twelve weeks after surgery, when compared to the HA/chitosan applied group, selenium doped HA/chitosan group had more fibrous cells, osteoid cells and stromal cells in the area of defects with visible blood vessels. It was also noted that some multinucleated giant cells anchored in degraded scaffolds engulfed the material, penetrated into the pores of it and supported new bone formation. In addition to the role of selenium in cancer treatment and bone healing,

the role of its deficiency in osteoporosis and its potential in the treatment of this bone disease were also studied [96,97].

Selenium is also known as the most toxic of all metalloids [88]. Therefore, its controlled release from the surfaces of implants and/or adjustment of appropriate dose must be achieved. Webster and his colleagues did several researches in which selenium is applied directly to the surface of orthopedic implants via deposition method, for providing this release mechanism as well as for creating a nano-sized rough surface [67,70,74,98-100]. The production of pressed cylindrical selenium structures and selenium nano-clusters deposited on titanium substrates, *in vitro* examination of the effects of these structures on healthy bone cells and osteosarcoma cells and determination of the release profile of the elemental selenium are examples of these studies. The common point of the three of these studies is the deposition of selenium nano-clusters exhibiting a colloidal texture on titanium surfaces and subsequent surface characterization and cell density tests. Selenium deposition process was carried out by dipping titanium substrates into the solution of glutathione and sodium selenite.

In the first study [70], the surface with selenium nano-clusters was developed and it was found that selenium suppresses the functions of cancer osteoblasts, while promoting functions of healthy osteoblast cells. In the second study [98], it was shown that the competitive proliferation of cancerous bone cells was also inhibited on the surface of titanium coated with nano-clusters of selenium when they were co-cultured with normal osteoblasts. In the last study [74], together with separate and co-culture experiments of healthy and cancerous osteoblasts, the effect of selenium on the growth of *S. epidermidis* (one of the leading bacteria that infect implants) was investigated. It was reported that functions of *S. epidermidis* were inhibited on titanium coated with selenium nano-clusters compared to uncoated materials.

A recent study presented selenium-doped c-HA coatings on titanium and silicon via pulsed laser deposition (PLD) by using commercial HA and selenium powders. Biological evaluation of the coatings illustrated that if 0.6 at% Se was added to the coatings, no cytotoxicity was observed and MC3T3-E1 preosteoblasts proliferated

well. It was also shown that proliferation of *P. aeruginosa* and *S. aureus* bacteria was inhibited by this coating [101]. The bacterial infection around the implant is one of the reasons leading to the failure of the implant and a new surgical operation for removing the implant. The potential anti-bacterial property of selenium indicated by this study proves the fact that orthopedic use of this element is a very good choice in terms of postoperative success. However, the potential implant materials produced in these studies cannot make possible to take advantage of high biocompatibility and bioactivity of HA coatings, which are almost associated with Ti6Al4V implants in orthopedics.

1.10. Aim of the Study

The present work was aimed to produce a functionalized surface coating with anti-cancer and anti-bacterial properties by doping selenium into the HA lattice. The mentioned coating was applied upon the plates composed of Ti6Al4V implant material in order to improve the well known biocompatible and bioactive HA coating applied on dental and orthopedic prosthesis as to serve better.

For this purpose, firstly, a novel and modified 1.5×SBF solution was produced with additional selenate ion content to be used in the biomimetic coating process. The Ti6Al4V plates were coated by immersing in euther normal or selenate ion added 1.5×SBF solutions for different period and these solutions yielded pure and selenium doped HA coatings, respectively. The coated plates were evaluated in terms of their structural and mechanical properties by the use of SEM, EDS, XRD, FTIR, Raman spectroscopy, ICP-MS and scratch test methods. In addition, cell culture studies with healthy bone cells (osteoblasts) and osteosarcoma cells were carried out for determining the cytotoxicity of selenium and viability of these cells on the coatings. To investigate the anti-bacterial property of the selenium doped HA coating, the survival of the *S. epidermidis* (the most common bacterial strain isolated from orthopedic implants) on the surface of the implant was determined.

CHAPTER 2

MATERIALS AND METHODS

The titanium alloy, Ti6Al4V, was selected as the substrate material because of its widespread use in orthopedic area. Ti6Al4V plates (Grade 5 ELI ASTM B265-10) with the dimensions of 20×20×2 mm^3 were used.

2.1. Pretreatment of Ti6Al4V Substrates

Before applying the alkali-heat treatment, two different Silicon carbide (SiC) abrasives were used in order to obtain rough surfaces on the plates; 400 grit SiC paper and 1200 grit SiC paper. According to surface characterization studies that will be described later, 400 grit SiC paper yielded rougher surface as it is expected and 1200 grit SiC paper had almost no effect on the surface. Therefore, 400 grit SiC paper was decided to be utilized. The plates were abraded by using a horizontal wet sanding machine (Buehler Metaserv 2000, USA).

2.2. Ultrasonic Cleaning

Ultrasonic cleaning was performed using ethanol (70%), acetone and distilled water in an ultrasonic bath (Bandelin Sonorex RK100, Germany). In each cleaning step, 10 plates were placed in a glass beaker which was attached to the stand and filled with the solvent. The beaker was submerged in the ultrasonic bath of distilled water. Cleaning was performed at ambient temperature for a period of 15 min in each solvent. After removal from the distilled water, the plates were placed on a clean tissue paper and dried using a fanned convection laboratory oven (Carbolite Eurotherm,England).

2.3. Alkali Treatment

The ultrasonically cleaned Ti alloy plates were exposed to a sodium hydroxide solution (NaOH) of 5 M concentration. The treatment temperature was 80°C, and the specimens were treated for 3 days. Following the treatment, the specimens were gently washed with distilled water and dried at 40°C in a fanned convection laboratory oven overnight.

2.4. Heat Treatment

The alkali treated titanium alloy plates were washed and dried as described above. The specimens were then heat-treated at 600°C for 1 h in a high temperature furnace (Alserteknik Protherm PLF 140/5, Turkey) and left to cool in the oven overnight. The plates were then stored in paraffin film wrapped airtight containers.

2.5. Preparation of Simulated Body Fluid

In the biomimetic technique, HA coatings can be obtained by placing the substrates into a biocompatible aqueous medium kept at the body temperature of 37°C and at the blood pH of 7.4. Conventional simulated body fluid (c-SBF, referred as SBF in this text) solution was chosen as the starting point of this research and the method for preparing SBF given by Kokubo et al. [52] was followed. Since SBF is supersaturated in terms of apatite precursor ions, a careless preparation of apatite in the solution may cause precipitation. Therefore, attention was paid to ensure that the solution was colorless and transparent at any time, and there was no precipitate at the bottom or side surfaces of the beakers used.

For the preparation of 1000 ml of SBF solution, the reagents given in Table 9, were dissolved in 700 ml of ion-exchanged distilled water (autoclaved, sterile), which was maintained at 36.5±1.5°C, by following the order from the 1^{st} to the 8^{th} under constant stirring. Each weighing bottle was washed with several drops of ion-exchanged distilled water, which was added to the solution. After the first eight reagents were dissolved, the amount of the solution was completed to 1000 ml with ion-exchanged distilled water at 36.5±1.5°C.

Table 9 Order, amounts, weighing containers, purities and formula weights of reagents for preparing 1000 ml of SBF [52].

Order	Reagent	Amount	Container	Purity (%)	Formula weight
1	NaCl	8.035 g	Weighing paper	99.5	58.4430
2	$NaHCO_3$	0.355 g	Weighing paper	99.5	84.0068
3	KCl	0.225 g	Weighing bottle	99.5	74.5515
4	$K_2HPO_4.3H_2O$	0.231 g	Weighing bottle	99.0	228.2220
5	$MgCl_2.6H_2O$	0.311 g	Weighing bottle	98.0	203.3034
6	1 M HCl	39 ml	Graduated cylinder	—	
7	$CaCl_2$	0.292 g	Weighing bottle	95.0	110.9848
8	Na_2SO_4	0.072 g	Weighing bottle	99.0	142.0428
9	TRIS	6.118 g	Weighing paper	99.0	121.1356
10	1 M HCl	0–5 ml	Syringe	—	—

The reagents of 9^{th} (TRIS) and 10^{th} order (small amount of HCl) were dissolved in the process of pH adjustment. Just before dissolving TRIS, the pH of the solution should be between 2.0±1.0. At this pH, with the solution temperature between 35 and 38°C, preferably 36.5±0.5°C, TRIS was dissolved gradually taking careful note of the pH change. When the pH was set to 7.30±0.05, the temperature of the solution was maintained at 36.5±0.5°C and more TRIS was added to raise the pH to 7.45. Then, 1 M HCl was added by dribbling with a syringe to lower the pH to 7.42±0.01, taking care of the pH not to decrease below 7.40. When this pH was maintained, the remaining TRIS was dissolved again gradually until the pH has risen to 7.45. 1 M HCl and TRIS were added alternately into the solution, until the whole amount of TRIS was dissolved keeping the pH within the range of 7.42–7.45. Lastly, the pH of the solution was adjusted to 7.40 exactly at 36.5°C by dropping 1 M HCl little by little. The resulting solution was used in the biomimetic coating process immediately after the preparation without delay or storing.

2.6. Preparation of 1.5 Times Concentrated SBF

Biomimetic coating process in SBF with conventional composition was noted to be very slow and there were nearly no coating after 20 days. Therefore, 1.5×SBF was preferred for biomimetic coating. The ionic concentrations of blood plasma and 1.5×SBF are given in Table 10.

Table 10 Ionic concentrations of blood plasma and 1.5×SBF [102].

Ions (mM)	Na^+	K^+	Mg^{2+}	Ca^{2+}	Cl^-	HPO_4^{2-}	SO_4^{2-}	HCO_3^-
1.5×SBF	212.3	7.5	2.3	3.8	186.8	1.5	0.75	40.5
Blood	142.0	5.0	1.5	2.5	103.0	1.0	0.5	27.0

According to the given ionic concentrations of 1.5×SBF, the amounts of reagents were calculated as given in Table 11.

Table 11 Order, amounts, weighing containers, purities and formula weights of reagents for preparing 1000 ml of 1.5×SBF.

Order	Reagent	Amount	Container	Purity (%)	Formula weight
1	NaCl	10.003	Weighing paper	99.5	58.4430
2	$NaHCO_3$	3.419	Weighing paper	99.5	84.0068
3	KCl	0.337	Weighing bottle	99.5	74.5515
4	$K_2HPO_4.3H_2O$	0.346	Weighing bottle	99.0	228.2220
5	$MgCl_2.6H_2O$	0.467	Weighing bottle	98.0	203.3034
6	1 M HCl	50ml	Graduated cylinder	—	
7	$CaCl_2$	0.438	Weighing bottle	95.0	110.9848
8	Na_2SO_4	0.108	Weighing bottle	99.0	142.0428
9	TRIS	Appropriate	Weighing paper	99.0	121.1356
10	1 M HCl	0–5 ml	Syringe	—	—

For the preparation of 1000 ml of 1.5×SBF, the reagents given in Table 11 were dissolved in 700 ml ion-exchanged distilled water, which was at 36.5±1.5°C, by

adding in the order from the 1st to the 8th under constant stirring. Each weighing bottle was washed with several drops of ion-exchanged distilled water, which was added to the solution. After the first eight reagents were dissolved, the amount of the solution was completed to 1000 ml with ion-exchanged with distilled water at 36.5±1.5°C.

The 9th reagent TRIS, was dissolved in the process of pH adjustment. Just before dissolving it, the pH of the solution was checked whether it is between 2.0±1.0 range. At this pH, with the solution temperature preferably at 36.5±0.5°C, TRIS weighing less than about 1 g was dissolved gradually, in order to avoid local increase in pH of the solution. 1.5×SBF was buffered at pH 7.2 in order to prevent spontaneous precipitation. The resulting solution was used immediately after preparation without delay or storing.

2.7. Preparation of Selenate Added 1.5 Times Concentrated SBF

While preparing the selenate added 1.5×SBF, the ionic concentration of 1.5×SBF given in Table 10 was kept constant, only 0.15 mM selenate ion was added. The resulting ionic composition of selenate added 1.5×SBF is given in Table 12.

Table 12 Ionic concentrations of blood plasma and selenate added 1.5×SBF.

Ions (mM)	Na^+	K^+	Mg^{2+}	Ca^{2+}	Cl^-	HPO_4^{2-}	SO_4^{2-}	HCO_3^-	SeO_4^{2-}
Selenate added 1.5×SBF	212.3	7.5	2.3	3.8	186.8	1.5	0.75	40.5	0.15
Blood	142.0	5.0	1.5	2.5	103.0	1.0	0.5	27.0	-

For the preparation of selenate added 1.5×SBF, the same method used for the normal 1.5×SBF was followed. However, while dissolving the chemicals, sodium selenate (Na_2SeO_4) was added into the solution in the fourth order and the remaining reagents were added subsequently. The amounts of the reagents other than sodium selenate were recalculated in order to keep the ionic concentrations of common ions same as in the normal 1.5×SBF.

2.8. Biomimetic HA Coating in Selenate Added and Normal 1.5×SBF

The alkali-heat treated Ti6Al4V substrates were soaked in normal 1.5×SBF and selenate added 1.5×SBF separately at 37°C for apatite depositing. The plates, after being placed into plastic bottles, were introduced into the SBFs of 50 ml per 1cm^2 plate. Every two days, new solutions were prepared and renewed. At each refreshment of solution, by considering the possibility of precipitation on the walls, the bottles were replaced with the clear ones. The solutions, in which the plates were soaked, were kept at 37°C by using a shaking water bath (Nüve ST402, Turkey). Ti6Al4V substrates were taken out of the coating solutions on the 4th, 7th, 10th 14th and 21st days of immersion. After the samples were taken out of the solutions, the loose precipitations were rinsed gently with distilled water and the plates were left to dry at 37°C overnight.

2.9. Sterilization

In order to perform cell and bacterial culture experiments, the coated plates were sterilized prior to these tests. Bacterial growth can be inhibited by adding sodium azide (NaN_3, 1.5 g/l) in SBF solutions [103]. However, addition of a NaN_3 (or any other preservatives) into SBF solution can modify the composition of the solution and even alter the antibiotic effect of the coatings obtained from selenate added 1.5×SBF. Therefore, the preparation of SBF solutions was carried out with autoclaved distilled water and the coated plates were sterilized after biomimetic deposition process.

The coated Ti6Al4V plates were sterilized in a dry-heat furnace at 200°C with for 2 h. In order to prevent spontaneous crack formation on the HA coatings, the samples were left to cool slowly during overnight in the furnace.

2.10. Surface and Structure Analyses

The surface morphology of the abraded, pretreated and biomimetically coated plates were observed with a scanning electronic microscope (SEM). The microscopic images were taken by a field emission scanning electron microscope (FE-SEM, FEI Quanta 400F, USA). The pretreated and biomimetically coated plates were first sputter-coated with Au/Pd in order to obtain a thin layer of conducting material. In addition, elemental composition of the coatings was analyzed by using the energy dispersive X-ray spectroscopy (EDS) set-up.

X-ray diffraction (XRD) analysis was performed with a diffractometer (Rigaku Ultima-IV, Japan) with Cu-Kα radiation at 40 kV and 30 mA. A pretreated plate without a coating was introduced as the blank and therefore, the pattern of substrate itself was subtracted from the XRD data of the coated samples. The phases present in the coatings were determined by using the pdf database of International Centre for Diffraction Data® (ICDD). From the XRD data collected on the coatings, the proportions of the phases of calcium phosphates were quantified by means of a Rietveld based software.

For Fourier transform infrared spectroscopy (FTIR) analysis, the compound system consisting of a spectrometer and a microscope (Bruker IFS 66/S and Hyperion 1000, Germany) was used. The samples were examined in the mid-infrared (MIR) range (between 4000-400 cm^{-1}). Similar to the XRD analysis, a pretreated Ti6Al4V was introduced to the device as a blank sample and its IR spectrum was subtracted.

Raman spectroscopy can be more sensitive than IR spectroscopy in most cases. For further analysis of selenium incorporation into HA structure, this technique was applied to the pure and selenium added HA coatings. The analysis was performed with a spectrometer (Renishaw inVia, UK) argon ion laser at a wavelength setting of 532 nm for excitation.The range was between 100 and 2000 cm^{-1} for monitoring any changes in the phosphate and hydroxyl groups.

Scratch tests were run with a scanning scratch tester (Shimadzu SST-W101, Japan). The scratch velocity was 5 μm/s and the scratch length was 1000 μm. The maximum applied load was 250 mN. The test was repeated 5 times for each sample and the measured values of the critical lateral force were averaged.

Inductively coupled plasma-mass spectrophotometry (ICP-MS) analysis was performed by using a Thermo Electron X7 device (Thermo Fisher Scientific USA). For ICP-MS analysis, the coatings on the surfaces of Ti6Al4V plates were scraped by using a spatula and each powder was dissolved in 2% nitric acid (HNO_3) solution.

2.11. Human Osteoblast Cell Culture

Normal human osteoblasts (NHOst, CC-2538, Lonza, USA) were obtained as proliferating cells in a T-75 flask. The complete growth medium of these cells were prepared by adding OGM SingleQuots supplements and growth factors (Lonza, USA) including 50 ml fetal bovine serum (FBS), 0.5 ml ascorbic acid and 0.5 ml gentamicin/ amphotericin-B to a 500 ml bottle of osteoblast basal medium (OBM, Lonza, USA). Upon arrival, the flask was placed in 37°C, 5% CO_2, humidified incubator and allowed to equilibrate for 3 h. After cells had equilibrated, the shipping medium was removed from the flask and replaced with fresh complete growth medium. The next day, the cells were 80% confluent and subcultured. The medium was removed and the cells were rinsed with phosphate buffered saline solution (PBS, pH 7.4). In order to detach the cells from the surface, 0.25% trypsin/EDTA (Biochrom AG, Germany) solution was used. After neutralizing the trypsin solution with medium, the detached cells transferred to a sterile 15 ml centrifuge tube and centrifuged at 1000 rpm for 5 min. The cells were diluted in 2 ml of growth medium and counted by using a cell counter (Nucleocounter, Chemometec, Denmark). The cells were diluted again and seeded to new flasks at a density of 5000 viable cells/cm^2. 10 ml complete growth medium was added to each flask and the cells were incubated in a 37°C, humidified incubator with 5% CO_2. The medium was changed the day after seeding and every other day thereafter.

The proliferating cultures are assured for experimental use for five population doublings by the manufacturer. At the second passage, the cells were observed to change their shape and differentiate. Since their growth rate, biological responsiveness and function may deteriorate; these cells were not used in any further experiments. Due to the finite lifespan of normal human osteoblasts, it was decided to use SV40 large T antigen transfected osteoblasts hFOB 1.19 (CRL-11372, ATCC, USA) which have the ability to differentiate into mature osteoblasts expressing the normal osteoblast phenotype.

Human fetal osteoblastic cell line (hFOB 1.19) was obtained in the cryopreserved form in a cryovial. After receiving the vial, the cells were removed from dry ice packaging and thawed by gentle agitation in a 37°C water bath immediately. The base medium of this cell line is a 1:1 mixture of Ham's F12 medium and Dulbecco's Modified Eagle's medium, with 2.5 mM L-glutamine (without phenol red). This mixture was purchased in the commercially available form (Thermo Scientific HyClone, USA). To make the complete growth medium, the following components was added to the base medium: 0.3 mg/ml G418 (Geneticin®, Thermo Scientific HyClone, USA) and FBS (Biochrom AG, Germany) to a final concentration of 10%. After thawing the cryopreserved cells, the content of the vial was transferred to a centrifuge tube containing 9.0 mL complete growth medium and centrifuged at 1500 rpm for 5 min. The cell pellet was resuspended in complete growth medium and transferred to a cell culture flask.

When the cells reached about 80% confluency, the medium was discarded and they were rinsed with PBS solution. The cells were detached by using 0.25% trypsin/EDTA (Biochrom AG, Germany) solution at 37°C. Trypsin was neutralized with complete medium and detached cells spun at 1500 rpm for 5 min. The cells were diluted in complete growth medium and seeded to flasks with a subcultivation ratio of 1:4. The cells were incubated in a 37°C, humidified incubator with 5% CO_2. The growth medium was changed every 2 to 3 days.

2.12. Human Osteosarcoma Cell Culture

Cancerous human bone cells Saos-2 (HTB-85, ATCC, USA) were obtained in the cryopreserved form in a cryovial. Upon receipt, the cells were removed from dry ice packaging and thawed by gentle agitation in a 37°C water bath immediately. The base medium of this cell line is McCoy's 5A modified medium. In order to obtain a complete growth medium, 10% FBS (Biochrom AG, Germany) and 1% penicillin/streptomycin solution (Biochrom AG, Germany) were added to McCoy's 5A modified medium (PAA, France). After thawing the cryopreserved cells for 2 min, the vial content was transferred to a centrifuge tube containing 9.0 mL complete culture medium and centrifuged at 1000 rpm for 5 min. The cell pellet was resuspended in complete medium, transferred to a cell culture flask and incubated at 37°C in a humidified incubator with 5% CO_2.

When the cells reached 80% confluency, they were subcultured. The medium was removed and the cells were rinsed with PBS. The cells were detached by using 0.25% trypsin/EDTA (Biochrom AG, Germany) solution at 37°C. Trypsin was neutralized with complete medium and the detached cells were centrifuged at 2000 rpm for 5 min. The cells were diluted in growth medium, seeded to flasks with a subcultivation ratio of 1:3 and incubated in a 37°C, humidified incubator with 5% CO_2. The medium was changed 2 times per week.

2.13. Cell Viability Tests with PrestoBlue

PrestoBlue reagent is a resazurin-based solution that functions as a cell viability indicator by using the reducing power of living cells in order to measure the proliferation of cells quantitatively. It contains a cell-permeant compound which is blue and virtually nonfluorescent. When added to culture media, PrestoBlue reagent is modified by the reducing environment of the viable cell and turns red in color. This fluorescent color can be detected using fluorescence or absorbance measurements [104].

In this study, PrestoBlue reagent was used to obtain the colorimetric data of the Saos-2 and hFOB 1.19 cells seeded on pure or selenium added HA coated Ti6Al4V plates and the results were compared with the control group in order to determine the effect of coatings on the cell viability. Dose dependent cytotoxic effect of selenium on Saos-2 and hFOB1.19 cells was investigated by using PrestoBlue assay.

2.13.1. Preparation of the Selenium Solutions

For cell viability test, several selenium containing solutions were prepared. 1.3160 g Na_2SeO_4 was dissolved in 10 mL PBS, in order to obtain a stock solution which is 100000× more concentrated than the solution with the desired concentration to be tested. The stock solution was serially diluted to obtain test solutions in 5 different concentrations. Table 13 summarizes the selenium content of the growth medium of the cells when 100 μL of each solution was added to 1mL of medium.

Table 13 Cell viability assay solutions and final selenium content of the growth medium when 100 μL of each solution was added to 1mL of medium.

Solutions	**Control PBS**	**Stock 100000×**	**Solution A 1000×**	**Solution B 100×**	**Solution C 10×**	**Solution D 1×**	**Solution E 0.1×**
Selenium Content	0	5×10^{-3} g	5×10^{-5} g	5×10^{-6} g	5×10^{-7} g	5×10^{-8} g	5×10^{-9} g

The selenium solutions were sterilized by using syringe filters with a porosity of 0.22 μm (Cellulose Acetate GyroDisc®, Orange Scientific, Belgium) before addition to the cell culture media for the cell viability tests.

2.13.2. Cell Viability Test Procedure for Selenium Solutions

Saos-2 cells were grown in McCoy's 5A modified medium containing 10% FBS and 1% penicillin/streptomycin solution. When the cells reached about 90–95% confluency, they were counted and seeded into two 24-well plates at a density of 50000 cells/well. The cells were allowed to attach to the surfaces for 30 min in an

incubator. After this period, phenol red free Dulbecco's Modified Eagle's medium (DMEM, Biochrom AG, Germany) with 10% FBS and 1% penicillin/ streptomycin was added into the wells. The cells were incubated in a humidified incubator at an atmosphere of 5% CO_2 at 37°C.

Similarly, hFOB 1.19 cells were seeded into two 24-well plates at a density of 50000 cells/well in 1:1 mixture of Ham's F12/DMEM (without phenol red) containing 0.3 mg/ml G418 and 10% FBS and they were incubated in a humidified incubator at an atmosphere of 5% CO_2 at 37°C.

After seeding two types of cells into two 24-well plates for each type, selenium containing solutions were added into the media of the cells immediately. The configuration of the 24-well plates for either of the two cell types is given in Figure 12. Same configuration was used for both Saos-2 and hFOB1.19 cells. The number of replicates for each group was 6. The experiment was repeated 2 times separately (n=2).

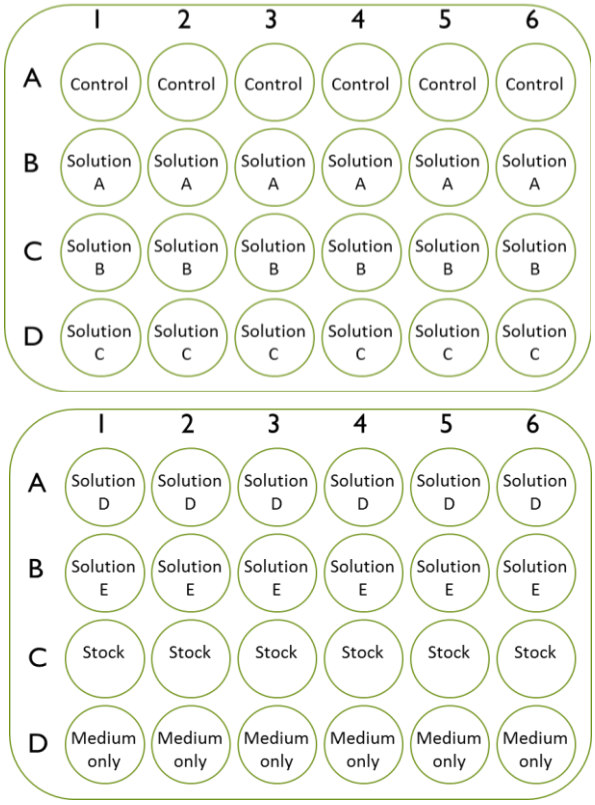

Figure 12 Configuration of the media of the cells for the cell viability tests of selenium containing solutions.

The cells treated with 100 µL of each selenium solution, control cells and culture medium were left in a humidified incubator at an atmosphere of 5% CO_2 at 37°C for 24 h. 100 µL PBS was added to complete the growth media of the untreated control cells.

PrestoBlue reagent is supplied as a 10× solution and it can be added directly to cells in culture medium. Therefore, after 24h, 122 µL of the reagent was added into each well. After 1h and 2h of incubations of cells with PrestoBlue reagent, the supernatant media were transferred to clean well plates and the absorbances were read at 570 nm and 600 nm (reference) with a multi-well plate reader. As this is a live cell assay, readings may be taken at multiple time points, in this case 1h and 2h, to determine optimal performance. However, since longer incubation times increase the sensitivity of detection and visible observation of color change at 2h was better, the data obtained after 2h of incubation with PrestoBlue reagent were used in any of the calculations presented hereafter.

After taking the supernatant media for absorbance reading, the complete growth media, which were containing 100 µL of each selenium solution, were refreshed for both kinds of cells. The absorbance readings with PrestoBlue reagent were repeated after 3 days and 5 days of incubation with selenium containing media. For consistency, same experiment was repeated once more independently.

In order to obtain background corrected absorbance data the following calculations were made. The absorbance at 600 nm was subtracted from the absorbance at 570 nm for each individual well. Then, the absorbances of the media only control wells were averaged and the average control well value was subtracted from the absorbance of the each experimental well. By doing this, the background (absorbance of culture media) was corrected. Statistical comparison of the results was performed using the Mann-Whitney U-test.

2.13.3. Cell Viability Testing of Coated Ti6Al4V Plates

Similar to the cell viability tests of selenium containing solutions, Saos-2 cells and hFOB 1.19 cells were seeded on pure HA and selenium added HA coated Ti6Al4V plates at a density of 100000 cells/plate. The cell seeded plates were placed into 6-well plates. The control group was directly seeded on the tissue culture plate. The test configurations of the 6-well plates for either of the cell types are given in Figure 13. Same configuration was used for both Saos-2 and hFOB1.19 cells. Total number of the repeated wells was 3 for each sample and the complete experiment was repeated separately for 2 times (total n=6).

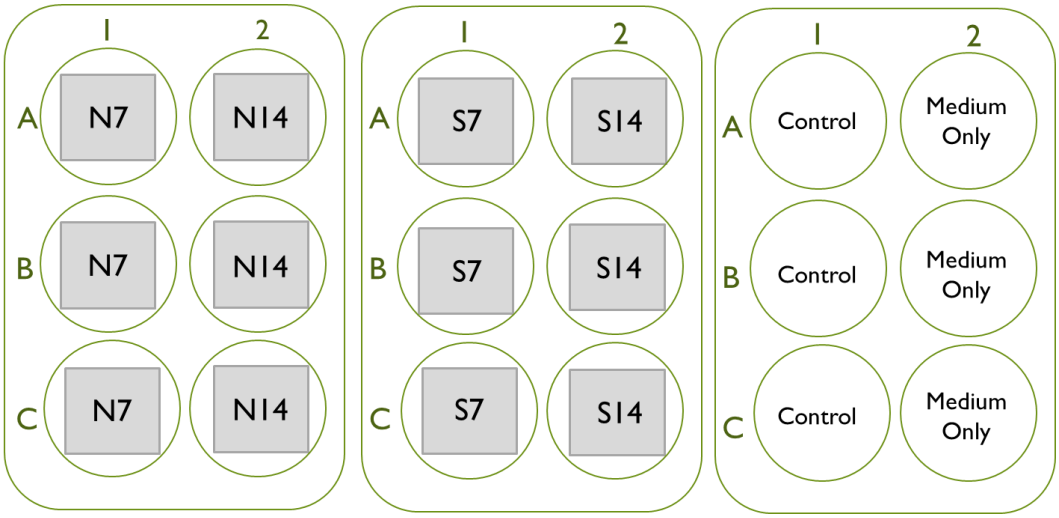

Figure 13 Wells prepared for the cell viability tests of pure HA and selenium added HA coated Ti6Al4V plates.

The nomenclature of the pure or selenium added HA coated Ti6Al4V plates are listed in Table 14.

Table 14 Nomenclature of the coated plates.

No	Name	Coating SBF	Coating Time
1	N7	Normal 1.5×SBF	7 days
2	S7	Selenate added 1.5×SBF	7 days
3	N14	Normal 1.5×SBF	14 days
4	S14	Selenate added 1.5×SBF	14 days

After waiting for 30 min of incubation for the cells to attach on the surfaces (Figure 13), 2.5 mL of the own complete growth media of each cell were added into the wells. The cells seeded on the plates, control cells and culture medium were left in a humidified incubator at an atmosphere of 5% CO_2 at 37°C for 24 h.

After 24h of incubation, 277 µL of PrestoBlue reagent was added into the medium of each 6-well and the cells were incubated for 2h. The resulting purplish supernatant media were transferred to clean well plates and the absorbances were read at 570 nm and 600 nm (reference) with a multi-well plate reader. The complete growth media of both cell types were refreshed. Absorbance reading with PrestoBlue reagent was repeated after 3 days and 5 days of incubation. For consistency, same experiment was repeated once more independently.

Similar to the calculations done in cell viability tests of selenium solutions; the absorbance at 600 nm was subtracted from the absorbance at 570 nm for each individual well. Then, the absorbances of the media only control wells were averaged and the average control well value was subtracted from the absorbance of the each experimental well. Statistical comparison of results was performed using the Mann-Whitney U-test.

2.14. Determination of Cell Morphology with SEM Imaging

In order to examine the morphology and attachment of Saos-2 cells on the pure and selenium added HA coatings, SEM studies were performed. After growing in T-75 flasks to 90–95% confluency, the cells were detached from the surface by 0.25% trypsin/EDTA solution. 100000 cells were seeded on each plate in McCoy's 5A modified medium containing 10% FBS and 0.5% penicillin/streptomycin. The plates were incubated in 6-well plates for 1 day and 7 days. After incubation, the medium in the wells were aspirated and the cells were washed twice with PBS. The plates were immersed in 4% paraformaldehyde solution for 15 min at RT in order to preserve the cell morphology by fixation. After fixation, the cells were gently rinsed with PBS. Then, the cells were dehydrated with graded series of ethanol (30%, 50%, 70%, 80%, 90% and 100%) for 10 min of immersion in each solution, consequently. For a

complete dehydration, hexamethyldisiloxane (HMDSO, Sigma, USA) was dropped onto the plates and they were left in a laminar flow cabin for 10 min. The plates were coated with platinum (Pt) prior to SEM imaging. The sputter coated samples were observed by SEM (JEOL, JSM 6400, Japan) operating at an acceleration voltage of 15 kV.

2.14.1. Aging of Coated Plates in Cell Culture Media

In order to evaluate the durability of the coatings in the culture medium, the pure and selenium added HA coated plates (N14 and S14, see Table 14) were placed into the 6-well plates and cell culture media was added. The lid of the 6-well plate was sealed with paraffin film. The plates were placed onto an orbital shaker (Biosan OS-10, Latvia) and left for constant shaking at 100 rpm for 7 days.

2.14.2. Seeding Cells on Aged Coatings for SEM Imaging

SEM studies were performed in order to examine the morphology and attachment of Saos-2 cells and hFOB1.19 cells co-cultured on the aged pure and selenium added HA coatings. After growing the cells in T-75 flasks to 90–95% confluency, the cells were detached from the surface by 0.25% trypsin/EDTA solution. 50000 cells/plate were seeded from each cell type (total 100000 cells/plate) in 1:1 mixture of complete growth media of each cell type. The plates were incubated in 6-well plates for 3 days. After incubation, the medium in the wells were aspirated and the cells were washed twice with PBS. The plates were immersed in 4% paraformaldehyde solution for 15 min at RT in order to preserve the cell morphology by fixation. After fixation, the cells were gently rinsed with PBS. The cells were dehydrated with graded series of ethanol (30%, 50%, 70%, 80%, 90% and 100%) for 10 min in each. For a complete dehydration, HMDSO was dropped onto the plates and they were left in laminar flow cabin for 10 min. The plates were sputter coated with Au-Pt prior to SEM imaging. The samples were observed by FE-SEM (FEI Quanta 400F, USA) operating at an acceleration voltage of 30 kV.

2.15. Determination of Cell Proliferation with Confocal Imaging

2.15.1. Seeding Cells for Confocal Imaging

Saos-2 cells were grown in T-75 flasks. These cells were detached from the flask surface with 0.25% trypsin/EDTA solution when they reached to 90–95% confluency. The pure and selenium added HA coated plates were placed to 6-well plates after sterilization for cell seeding. The detached cells were counted and seeded onto the plates at a density of 100000 cells/plate. Then, the plates were incubated in a humidified incubator at an atmosphere of 5% CO_2 at 37°C for half an hour. The wells were slowly filled with 3 ml of McCoy's 5A modified medium containing 10% FBS and 0.5% penicillin/streptomycin and placed in 5% CO_2 humidified incubator at 37°C for 1 day and 3 days.

2.15.2. Phalloidin and PI Staining

Phalloidin is a toxin peptide isolated from the deadly Amanita phalloides mushroom and is commonly used in imaging applications to selectively label F-actin. Fluorescein phalloidin in its conjugated form to the green fluorescent dye, is fluorescein isothiocyanate (FITC). Phalloidin binds to the F-actin with high selectivity while fluorescein provides the present green fluorescence and together they allow high-contrast discrimination of actin staining. Propidium iodide (PI) is a popular red-fluorescent nuclear and chromosome counterstain [105]. In this study, these cell stains were used together in order to observe the cell nucleus and cytoskeleton of the Saos-2 cells which were seeded on the coated plates. Since PI staining is normally performed after all other stainings, the FITC-phalloidin staining was performed first. In order to prepare the FITC-phalloidin stock solution, FITC-phalloidin (Invitrogen, USA) vial content was dissolved in 1.5 mL methanol to yield a final concentration of 200 units/mL, which is equivalent to approximately 6.6 μM. In order to make a stock solution of PI from the solid form, PI (Invitrogen, USA) was dissolved in deionized water (dH_2O) at a concentration of 1 mg/mL (1.5 mM). The PI stock solution was stored at 4°C, while fluorescein phalloidin stock solution was frozen at –20°C. Both of the solutions were protected from light.

Saos-2 cells were previously seeded on the plates that were coated either in normal or selenate added 1.5×SBF for 7 and 14 days. After 1 and 3 days of incubation in McCoy's 5A modified medium containing 10% FBS and 0.5% penicillin/streptomycin, the medium was aspirated and the cells were rinsed with PBS pH 7.4 at 37°C. The cells were fixed by using 4% paraformaldehyde solution for 15 min at RT. After rinsing with PBS, the cells were permeabilized with 0.1% Triton X-100 (Applichem, Germany) at RT for 5 min. Triton X-100 was aspirated and the cells were rinsed with PBS two more times. To reduce nonspecific background staining, the fixed cells were pre-incubated with PBS containing 1% bovine serum albumin (BSA) for 30 min. The BSA solution was aspirated and 200 µL 0.1% BSA in PBS solution containing 5 µL methanolic stock solution of phalloidin was added to each plate. The plates were left in the staining solution in an incubator at 37°C for 1 h.

After staining with FITC for 1 h, the staining solution was aspirated and the cells were rinsed with PBS. The cells were equilibrated in 2×SSC solution containing 0.3 M NaCl and 0.03 M sodium citrate ($Na_3C_6H_5O_7$) at pH 7.0. The cells were then incubated in 100 µg/mL DNase-free RNase (Fermentas, Thermoscientific, Canada) containing 2×SSC at 37°C for 20 min. The plates were rinsed three times in 2×SSC, 1 min each. The 1 mg/mL (1.5 mM) stock solution was diluted 1:3000 in 2×SSC to make a 500 nM solution of PI. The plates were incubated in 300 µL diluted solution at 37°C for 5 min. The plates were rinsed several times in 2×SSC and observed with confocal microscopy without a delay.

2.16. Bacterial Adherence Tests

Staphylococcus epidermidis is one of the members of normal bacterial flora of the human skin. It accounts for most of the device-related infections [106]; it is one of the most common factors of primary bacteremia due to the formation of biofilm adherent to the implants.

S. epidermidis bacteria were obtained in the form of dispersed colonies on a LB-agar petri dish. Firstly, LB medium was prepared by dissolving 2.5 g premixed LB

powder (Applichem, Germany) in 100 ml distilled water and it was sterilized by autoclaving. Two 5 ml LB medium containing centrifuge tubes were inoculated with bacteria collected from the petri dish and incubated in normal atmosphere at 37°C with constant shaking of 220 rpm for 18h. For the second passage, bacteria from these suspensions were plated on LB-agar petri dishes and incubated in normal atmosphere at 37°C for 18 h. Inoculation of two LB medium containing centrifuge tubes was repeated by using the bacteria collected from the petri dishes of the second passage. After incubation at 37°C for 18 h, at normal atmosphere with constant shaking of 220 rpm; when the bacteria reached to a stationary phase, the tubes with bacteria were centrifuged and resuspended in LB to an optical density of 0.52 at 562 nm using a microplate reader (Multiskan GO, Thermo Scientific, USA). This value was correlating to 3 on the McFarland Scale, or 9×10^8 *S. epidermidis* bacteria per ml of medium [74].

Three copies from each batch of S14 and N14 coated plates and uncoated Ti6Al4V plates were placed into 6-well plates containing 3 ml of LB medium. The bacterial suspension was diluted and inoculated at 15×10^6 cells per well onto these substrates. Sterile LB medium served as a control. While inoculating 3 wells containing with the same amount of bacteria, 3 LB medium containing wells were left sterile to serve as a control of the color or opacity of the medium itself. After 3 days of incubation at 37°C at normal atmosphere, substrates were put into 15 ml centrifuge tubes and vortexed vigorously to collect the bacteria. 200 µL of each medium containing bacteria was placed into a well of a 96 well plate and analyzed for cell concentration using a microplate reader. Light absorbance values were measured at a wavelength of 562 nm.

CHAPTER 3

RESULTS AND DISCUSSIONS

3.1. SEM and EDS Results

3.1.1. Effects of Pretreatment

In order to enhance the mechanical interlock between the coating and the surface of the metal plate by changing the surface topography, abrading was applied to the Ti6Al4V plates. SEM micrographs of the surfaces after abrasion with SiC papers are given in Figure 14.

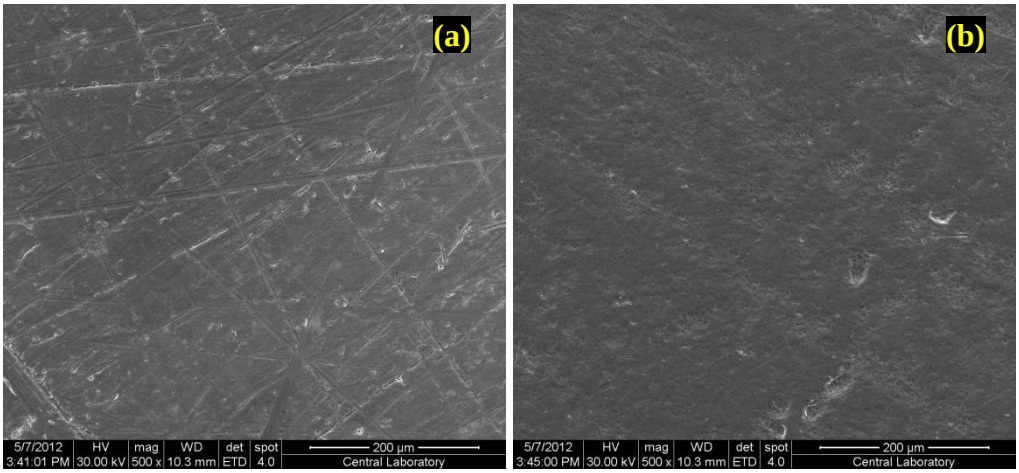

Figure 14 SEM images of surfaces of Ti6Al4V plates after abrading (a) with a 400 grit SiC abrasive paper and (b) with a 1200 grit SiC abrasive paper (500×).

When the surfaces of the Ti6Al4V plates were examined after abrasion, it was noted that the plate abraded with a 400 grit SiC paper had multidirectional scratches, whereas the plate abraded with a 1200 grit SiC paper represented a less roughened surface.

The 1200 grit SiC paper, which is less coarse, leaved nearly none or very fine scratches on the metal surface, therefore the 400 grit SiC paper was selected as the abrasive.

SEM images belonging to the Ti6Al4V plates after abrasion with a 400 grit SiC abrasive paper and alkali-heat treatment are given in Figure 15.

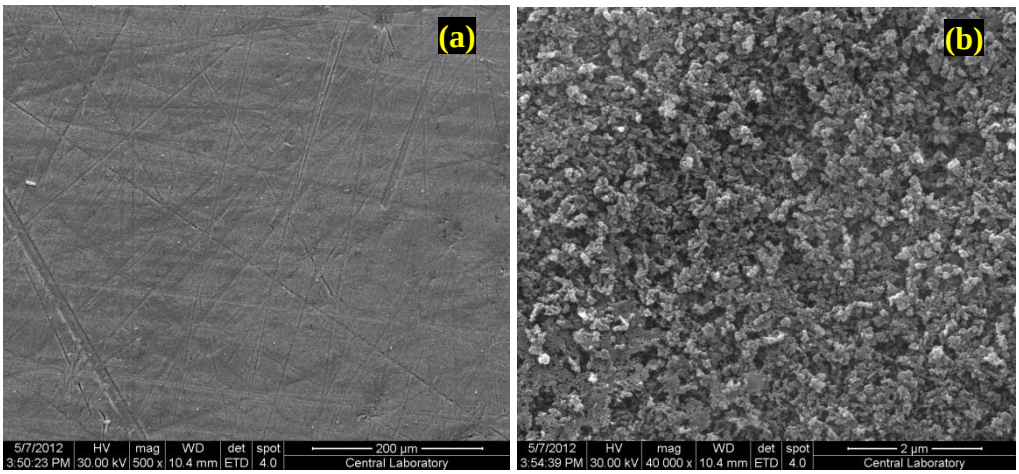

Figure 15 SEM images of surfaces of Ti6Al4V plates after abrading with a 400 grit SiC abrasive paper and pretreatment. Magnification: (a) 500× and (b) 40000×.

As can be seen in the SEM images (Figure 15), the surfaces of the Ti6Al4V plates, which were soaked in a 5 M sodium hydroxide (NaOH) solution at 80°C for 3 days, then heat treated at 600°C for 1 h, gained a micro-porous and loose structure.

The purpose of the alkali treatment was to obtain a porous network layer of sodium titanate, on which apatite formation could be induced. In addition, in order to increase the stability of titanate layer, the plates were heated to 600°C for 1 h after alkali treatment. This would transform the amorphous titania gel to crystalline phase [107]. However, if the temperature exceeds 600°C during the heat treatment; this might cause a decrease in Na^+ release thus formation of less TiOH groups [108], which would negatively affect the apatite forming ability of the surface. Therefore, higher sintering temperatures (over 600°C) were avoided.

3.1.2. Coatings in SBF

SEM images of the abraded and pretreated plates that were kept in SBF solution for 5 days and 20 days are given in Figure 16 together with the EDS analysis results.

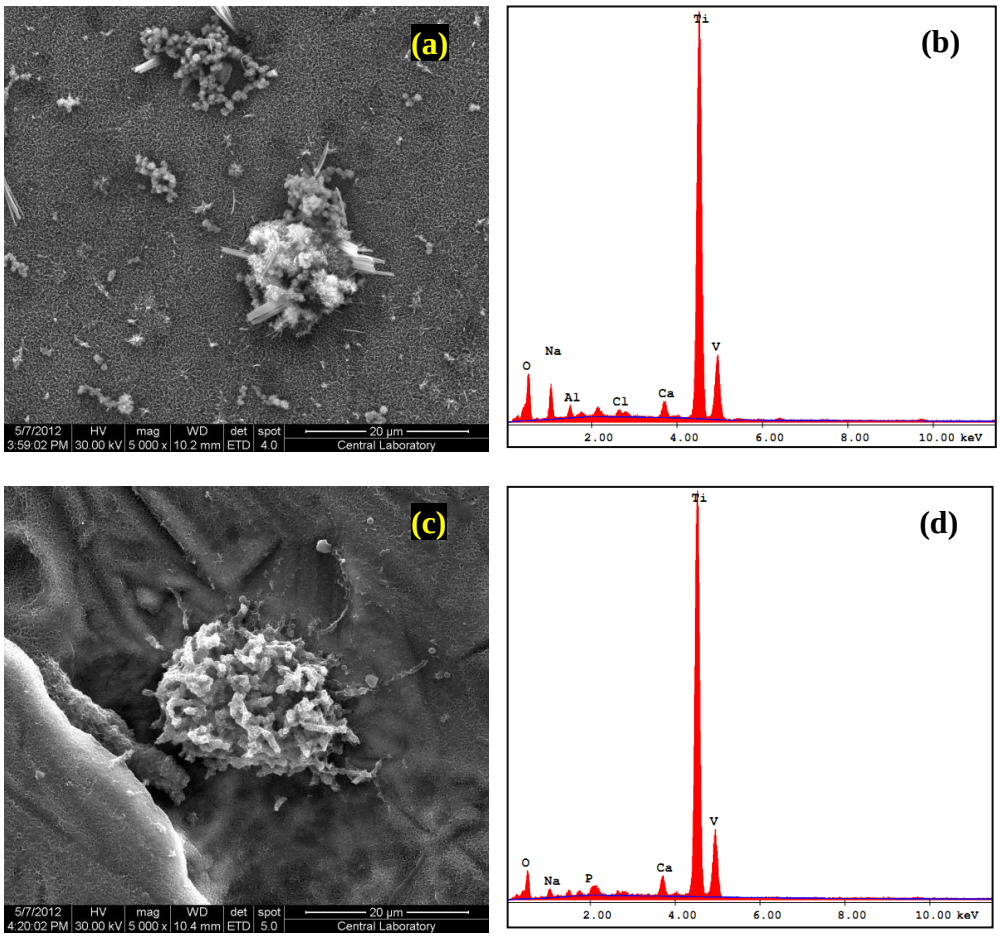

Figure 16 Surface of the abraded and pretreated Ti6Al4V plate after immersion in SBF (a) SEM image after 5 days of immersion (5000×); (b) EDS spectrum of (a); (c) SEM image after 20 days of immersion (5000×) and (d) EDS spectrum of (c).

From the SEM images and EDS analysis of the plates that were immersed in SBF, it can be said that CaP nuclei were formed after 5 days. However, there was not a complete coating on the surface even though 20 days had passed. In fact, this observation is in agreement with results described in the literature. Jalota et al. [109] prepared different SBF solutions (i.e. c-SBF, Tas-SBF, r-SBF) and tested the formation of calcium phosphates on alkali-treated Ti6Al4V strips for 1 week of soaking at 37°C. They reported that there was almost no coating observed, regardless

of the replenishment rate with these 1×SBF solutions. It was concluded that, for 1×SBF solutions, more than 3 weeks of soaking is required to observe only the onset of the coating. Therefore, 1.5×SBF solutions were also prepared in order to accelerate the coating process in that study.

Additionally, in the surface of the coatings obtained from SBF, the presence of sodium on the surface was observed. In Figure 16(b), the sodium peak can be attributed to the excess undissolved sodium chloride in SBF together with the sodium titanate formed during the alkali treatment. The chlorine peak, which was probably arising from the undissolved NaCl at the early times of immersion into SBF, was not observed in the coating obtained by immersion in SBF for 20 days.

Related to Figure 16(d), it can be stated that the amount of sodium was also reduced on the 20^{th} day, since it was released also from the sodium titanate layer which was formed in the pretreatment process. As stated before, during pretreatment with NaOH aqueous solution and heat, an amorphous sodium titanate layer forms on the surfaces of the plates. The plates release Na^+ ions from their surface sodium titanate layers into SBF via exchange with H_3O^+ ions. As a result, Ti-OH groups are formed on the surfaces of plates, which induce the apatite nucleation [62]. Besides, sodium removal during the pretreatment process would have been possible by immersion in distilled water between the alkali-heat treatments, but that option was not preferred. This is because the previous studies have reported that removal of sodium decreases the adhesive strength of the treated layer to the substrate [110].

3.1.3. Coatings in Normal 1.5×SBF

The SEM images of the surfaces of pretreated Ti6Al4V plates after soaking in 1.5×SBF with normal ionic concentration for a period of 4, 7, 10, 14 and 21 days are given in Figure 17.

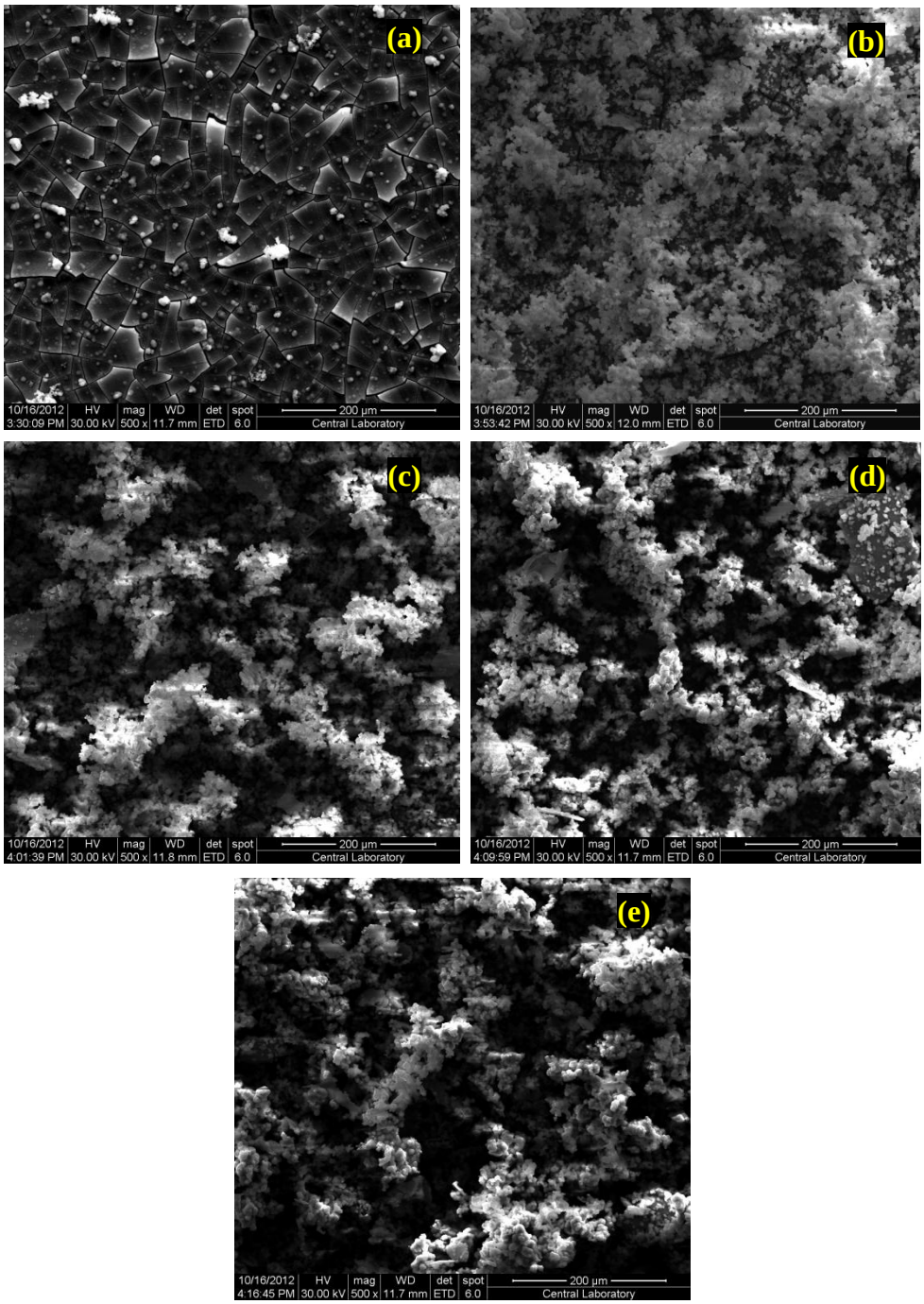

Figure 17 SEM images of Ti6Al4V plates after soaking in 1.5×SBF with normal ionic composition for a period of (a) 4; (b) 7; (c) 10; (d) 14 and (e) 21 days (500×).

From the SEM images given in Figure 17(a), it can be said that the nucleation of CaP had already started on the 4th day and increased with the increasing incubation period in SBF. The surface of the Ti6Al4V plates was entirely covered with numerous and almost spherical granular CaP precipitates after 7 days in 1.5×SBF.

The alkali-heat treatment, which was applied as a pretreatment to provide bioactivity on Ti6Al4V surface, is of great importance in the formation of this structure. This method was first applied by Kim [57] and Kokubo [59] on Ti and its alloys to improve the bioactivity. Through this process, TiO_2 layer on the surface can be partially dissolved by the hydroxyl groups of the sodium hydroxide solution. It is followed by hydration of titanium and a negatively charged sodium titanate hydrogel layer is formed on the surface. Since this gel layer is an unstable structure, the plates are generally heat treated in order to condense and increase the mechanical strength of the layer.

During the aging in SBF, the sodium ions from the sodium titanate layer on the surface are replaced with hydronium ions (H_3O^+) in the SBF by means of ion exchange and released to the medium. Since Ti-OH layer is negatively charged, it binds selectively with the positively charged Ca^{2+} ions and forms calcium titanate. The positively charged surface, which becomes positively charged, binds with the negatively charged phosphate ions (PO_4^{3-}) in the SBF to form CaP precipitates. Finally, the apatite nuclei grow by consuming calcium and phosphate ions in the SBF spontaneously [58].

SEM images given in Figure 17, show the CaP layer which has grown steadily as a result of this process. The EDS analysis results obtained from SEM images, mass and atomic ratios of the elements in the coatings are listed in Figure 18.

The CaP composition of the coatings can be determined from the EDS analysis results. The Ca/P molar ratios of the coatings obtained from the 1.5×SBF with normal ionic concentration was calculated as follows: 1.09 on day 4, 1.79 on day 7, 1.83 on day 10, 1.78 on day 14 and 1.80 on day 21. Thus, it can be said that the Ca/P ratio of the coatings on the 4^{th} day was low and remained almost constant at around 1.80 in the following days. This could be due to the fact that the amount of coating was low and the coating was discontinuous on the 4^{th} day.

After the coating got thicker and became continuous, the Ca/P ratio reached to 1.8. Since Ca/P molar ratio of the average healthy adult human bone is around 1.71 [111], the obtained results were considered to be a satisfactory. In the literature, the Ca/P molar ratio of CaP coatings obtained by the biomimetic method is typically greater than 1.7, and is generally between 1.7 and 2.7 [112]. For this reason, the resulting Ca/P ratio was determined to be in a similar level of natural bone and in agreement with the literature.

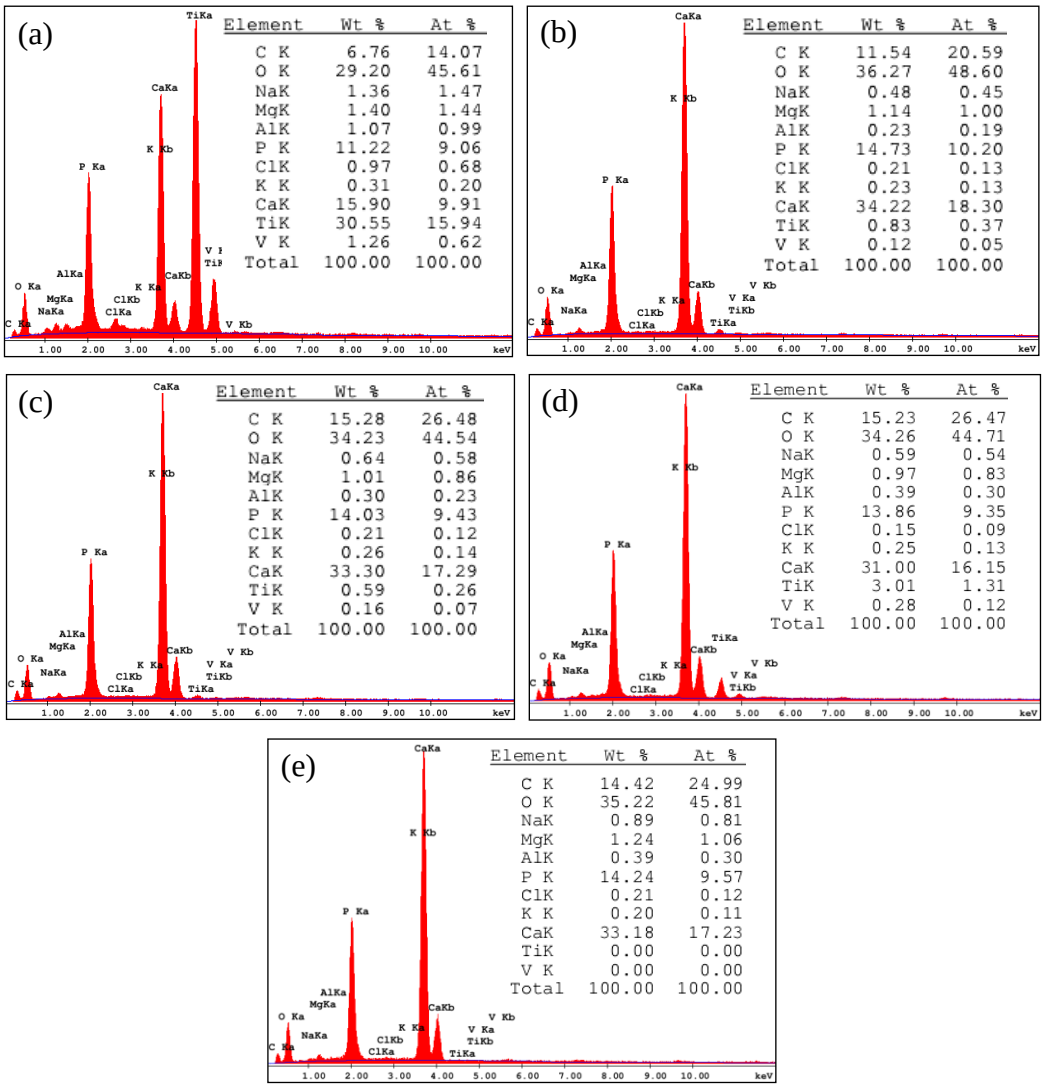

Figure 18 EDS analyses of Ti6Al4V plates after soaking in 1.5×SBF with normal ionic composition for a period of (a) 4; (b) 7; (c) 10; (d) 14 and (e) 21 days.

3.1.4. Coatings in Selenate Added 1.5×SBF

SEM images of the surfaces of pretreated Ti6Al4V plates after soaking in selenate ion added 1.5×SBF for a period of 4, 7, 10, 14 and 21 days are given in Figure 19.

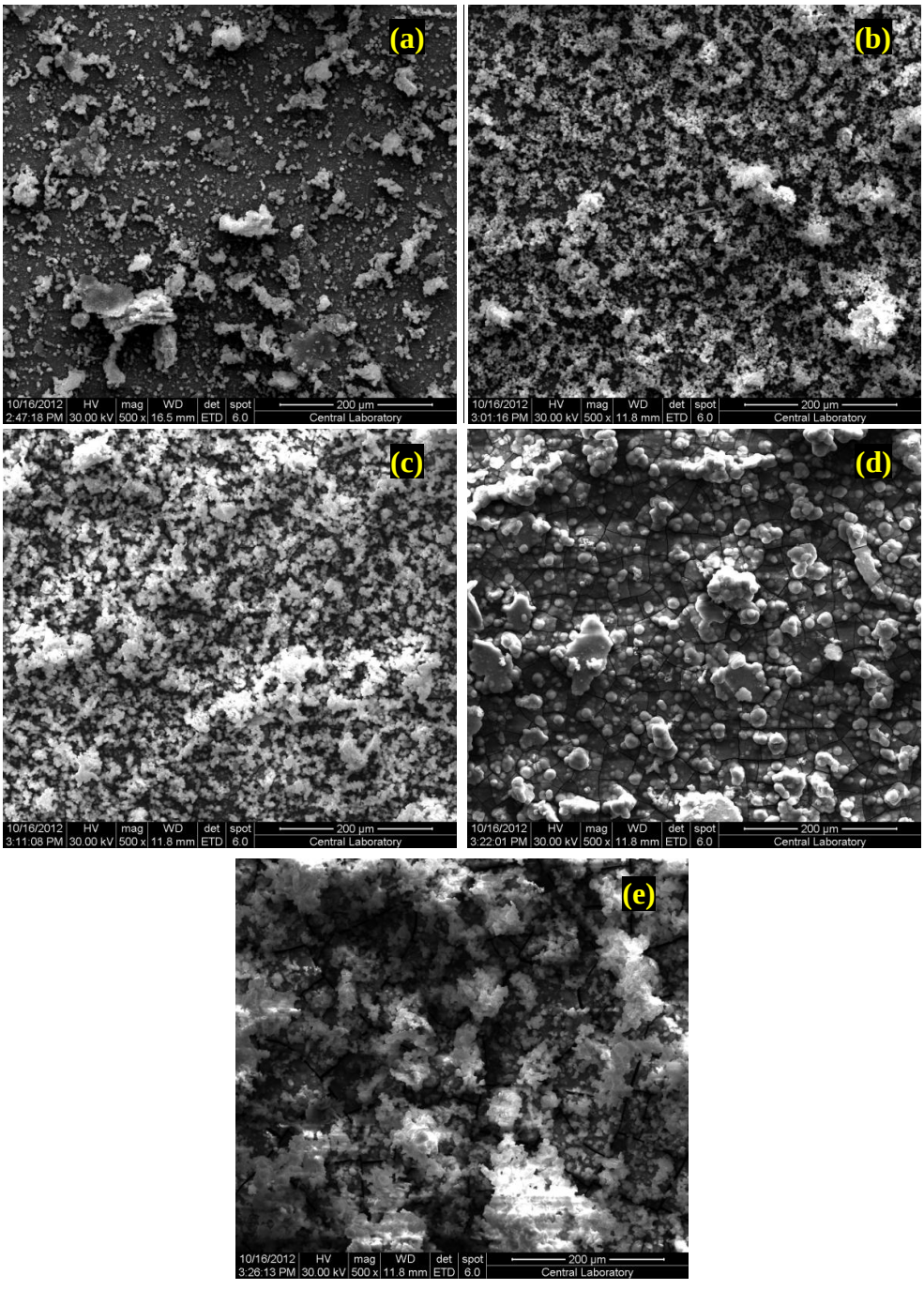

Figure 19 SEM images of Ti6Al4V plates after soaking in selenate added 1.5×SBF for a period of (a) 4; (b) 7; (c) 10; (d) 14 and (e) 21 days (500×).

It was observed that the nucleation started on the surfaces coated in selenate added 1.5×SBF on day 4, just as for the coatings obtained from the 1.5×SBF with normal ionic concentration (Figure 19). Similarly, it was seen that the deposition around the nuclei continued during the soaking period and the initial CaP precipitate in the form of half-spheres were covered with additional precipitates to form new and bigger half-spheres. The coating came to the desired morphology on the 14th day. However, on the 21st day, the uniform structure in the form of half-spheres turned to an uneven form in clusters. As can be seen in Figure 19(e), the SEM images contain charged areas due to the very high deposits of the coating. In order to compare the nanostructure of the pure and selenium added coatings, high-magnification SEM images of the surfaces of pretreated Ti6Al4V plates after soaking in normal or selenate ion added 1.5×SBF for a period of 14 days are given in Figure 20.

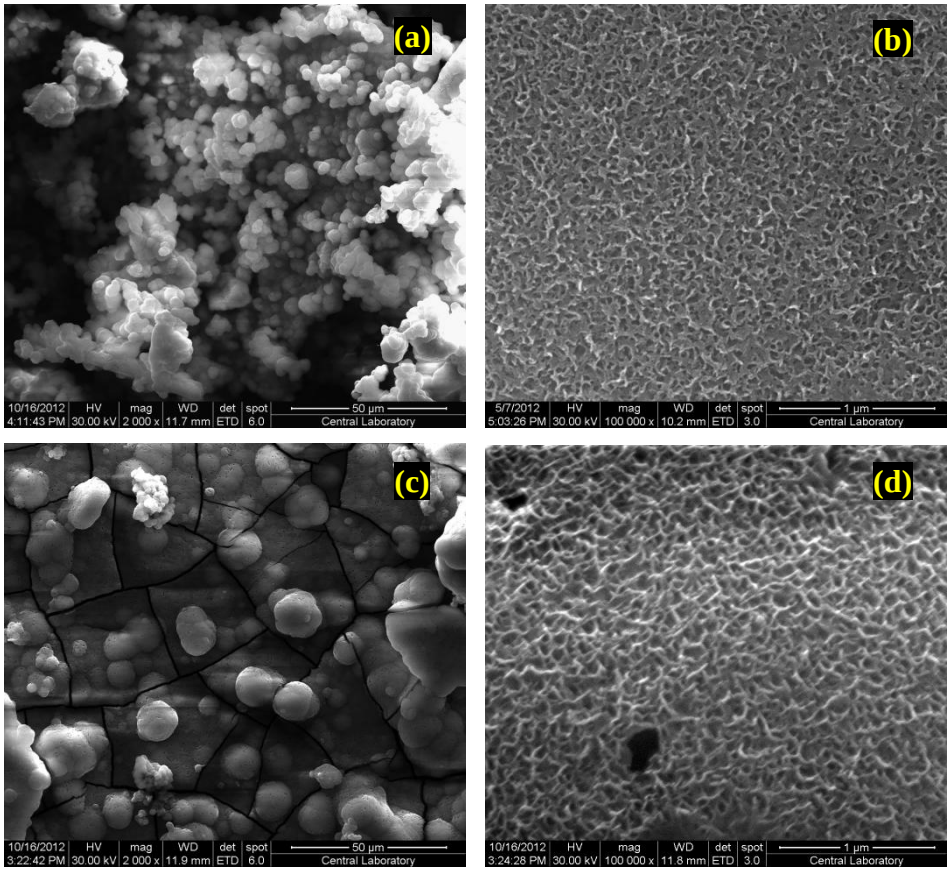

Figure 20 High-magnification SEM images of Ti6Al4V plates after soaking in normal 1.5×SBF for 14 days, magnification: (a) 2000×; (b) 100000× and selenate added 1.5×SBF for 14 days, magnification: (c) 2000×; (d) 100000×.

The higher magnification SEM images revealed that the spherical structures of both the pure and selenium added coatings were composed of nano-flakes.

Figure 21 displays the corresponding EDS analyses and the mass and atomic ratios of the elements of the coatings that are given in Figure 19.

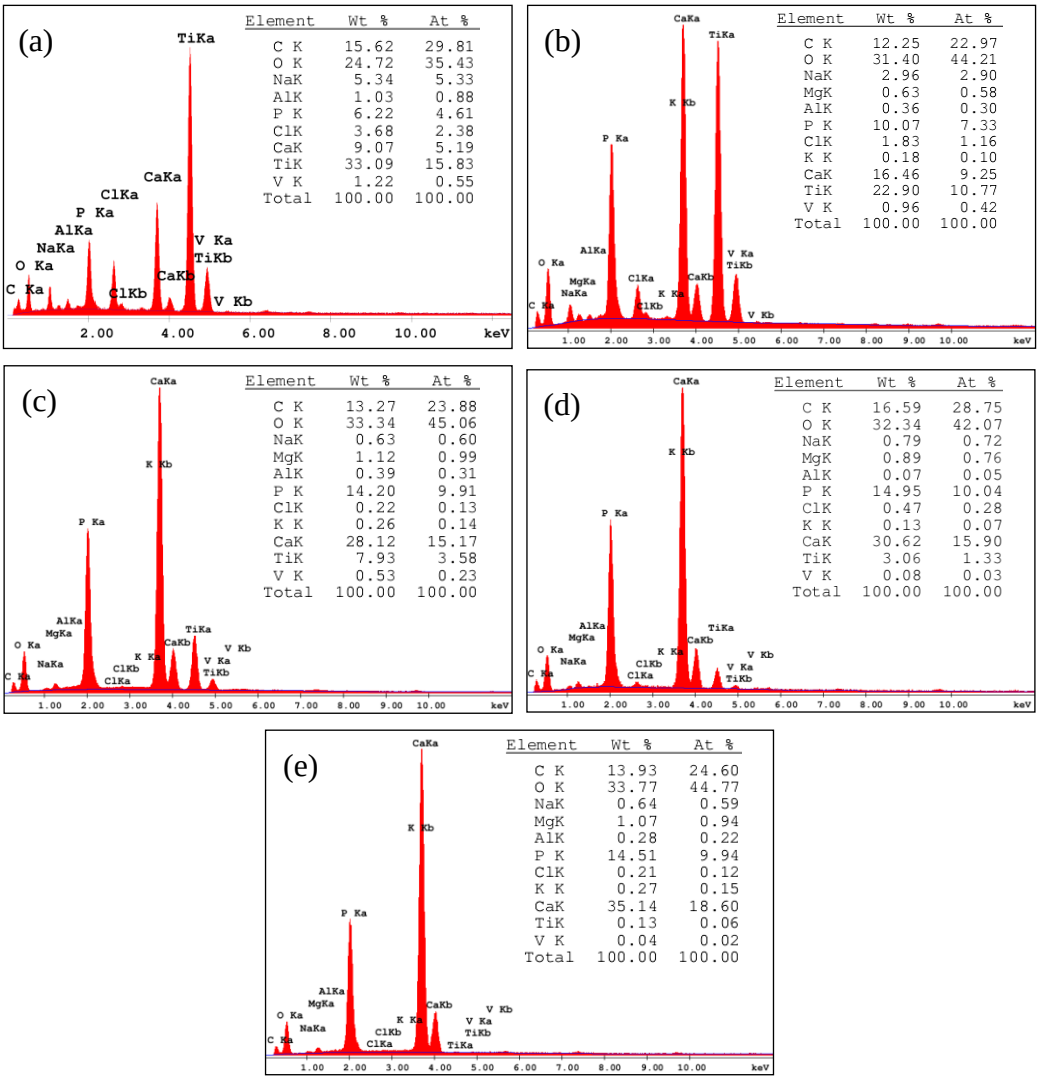

Figure 21 EDS analyses of Ti6Al4V plates after soaking in selenate added 1.5×SBF for a period of (a) 4; (b) 7; (c) 10; (d) 14 and (e) 21 days.

According to the EDS results, Ca/P molar ratio of the coatings varied depending to the immersion time in SBF. The Ca/P ratios were calculated as 1.13 on the 4th day, 1.26 on the 7th day, 1.53 on the 10th day, 1.58 on the 14th day and 1.87 on the 21st day, respectively.

Thus, it can be assumed that the Ca/P molar ratio was increased by the increasing immersion time of the plates in selenate added 1.5×SBF. However, the EDS technique is not enough by itself to determine the structure of CaP coating just by focusing on the Ca/P ratios. Therefore, XRD method was utilized for the detection of phases in the coatings.

On the other hand, the increase in the coating thickness can be observed from the reduction of elemental percentages of Ti, Al and V with increasing immersion time in selenate added 1.5×SBF, because these elements are the components of the base plate. For example, the atomic percentage of Ti, which was 15.83 on the 4th day, gradually decreased to 0.06 on the 21st day.

3.2. XRD Results

3.2.1. Coatings in Normal 1.5×SBF

The XRD patterns of the surfaces of pretreated Ti6Al4V plates after soaking in 1.5×SBF with normal ionic composition for a period of 4, 7, 10, 14 and 21 days are represented along with the standard HA spectrum (ICDD card No. 1-1008) in Figure 22.

As shown in Figure 22, CaP coatings, which were obtained by soaking the Ti6Al4V plates into the 1.5×SBF with normal ionic concentration, were in the form of HA independent from the immersion period in SBF solution. All coatings exhibited the standard HA (ICDD card No. 1-1008) XRD peaks. The 2θ degrees pertaining to the XRD peaks of the coatings derived from 1.5×SBF with normal ionic concentration are listed in Table 15.

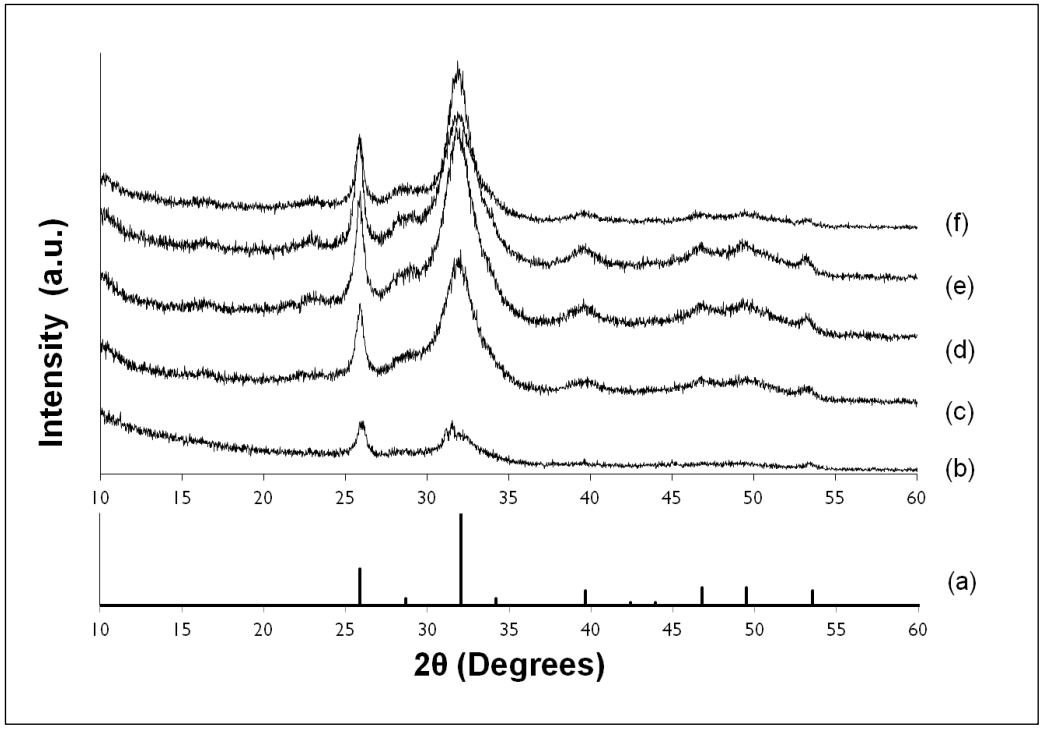

Figure 22 XRD patterns of (a) standard HA (ICDD card No. 1-1008) and Ti6Al4V plates after soaking in 1.5×SBF with normal ionic composition for a period of (b) 4; (c) 7; (d) 10; (e) 14 and (f) 21 days.

Table 15 XRD peaks of the coatings obtained in the 1.5×SBF with normal ionic concentration.

Coating Time	4 days	7 days	10 days	14 days	21 days
XRD Peaks 2θ (Degrees)	25.98	25.89	25.72	25.73	25.71
	32.04	32.06	32.18	32.16	32.14
	39.60 (weak)	39.80	39.58	39.54	39.60
	-	46.64	46.62	46.60	46.74
	-	49.80	49.20	49.16	49.20
	53.46	53.44	53.18	53.22	53.24

The coatings displayed strong peaks at 2θ angles of about 25.8 and 32.1 degrees independent of the immersion period in the solution. As the immersion time increases, XRD peaks were strengthened due to the increase in the thickness of the coating. The XRD peak intensity of the coating on the 21st day was less than the XRD peak intensities of the coatings on the 10th and 14th days. This was considered

to be due to the disintegration of the thick coating on the surface. From the XRD analyses, the coatings obtained by soaking the Ti6Al4V plates into the 1.5×SBF with normal ionic concentration for 10 and 14 days yielded very similar XRD patterns with highest intensities.

3.2.2. Coatings in Selenate Added 1.5×SBF

The XRD patterns of the surfaces of pretreated Ti6Al4V plates after soaking in selenate added 1.5×SBF for a period of 4, 7, 10, 14 and 21 days are given with standard HA (ICDD card No. 1-1008) in Figure 23.

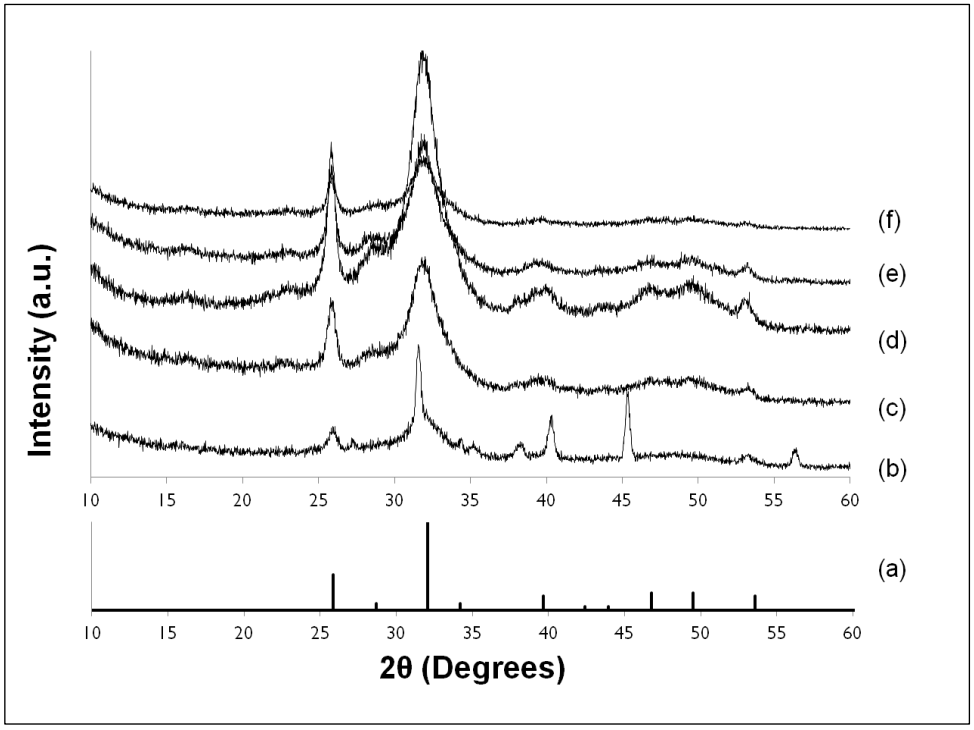

Figure 23 XRD patterns of (a) standard HA (ICDD card No. 1-1008) and Ti6Al4V plates after soaking in selenate added 1.5×SBF for a period of (b) 4; (c) 7; (d) 10; (e) 14 and (f) 21 days.

Similar to the pure coatings obtained by immersing the plates into 1.5×SBF with normal ionic concentration, CaP coatings derived from the selenate added 1.5×SBF showed standard HA (ICDD card No. 1-1008) pattern. The 2θ angle values pertaining to the XRD peaks of the coatings in selenate added 1.5×SBF are listed in Table 16.

Table 16 XRD peaks of the coatings obtained in the selenate added 1.5×SBF.

Coating Time	4 days	7 days	10 days	14 days	21 days
XRD Peaks 2θ (Degrees)	25.95	25.84	25.84	25.88	25.98
	31.51	28.60	28.86	28.50	28.60(weak)
	38.18	32.02	32.14	32.02	32.10
	40.35	39.46	39.77	39.54	39.42
	45.31	49.49	49.40	49.10	-
	53.30	53.28	53.13	53.24	53.36
	56.35	-	-	-	-

As seen in Figure 23(b), the coating obtained from the selenate added 1.5×SBF on the 4th day of immersion gave peaks at 2θ angles of about 38.18, 40.35 and 56.35, which were related to the substrate plate. The reason for this is that nucleation began in the form of spheres distant from each other. On the other hand, the coatings obtained from the selenate added 1.5×SBF on days 7, 10, 14 and 21 did not exhibit peaks of a secondary phase other than HA.

Similar to the un-doped coatings, the XRD peak intensity of the selenate added coating on the 21st day was smaller than the XRD intensities of the peaks of the coatings on 10th and 14th days. This was also assumed to be due to the disintegration of the thick coating on the surface. From the XRD analyses of the coatings obtained by the selenate added 1.5×SBF; it was observed that the strongest peaks are obtained from the coating which is immersed into the solution for a period of 10 days.

The Rietveld method is a full pattern analysis approach in which all factors contributing to the intensity measured for each 2θ step can be refined until the difference between the observed and calculated pattern is minimized. This method allows quantitative phase analysis with high accuracy [113]. The data obtained from the XRD analysis of the selenate added HA coatings were used in the Rietveld analysis. Figure 24 shows a representative XRD pattern of the coating obtained by immersing the Ti6Al4V plate into the selenate added 1.5×SBF for 10 days.

As seen in Figure 24, the observed intensities of the collected pattern of the selenate added HA coating fitted perfectly to the diffraction pattern of HA with 100%. There was no other phase detected in the structure.

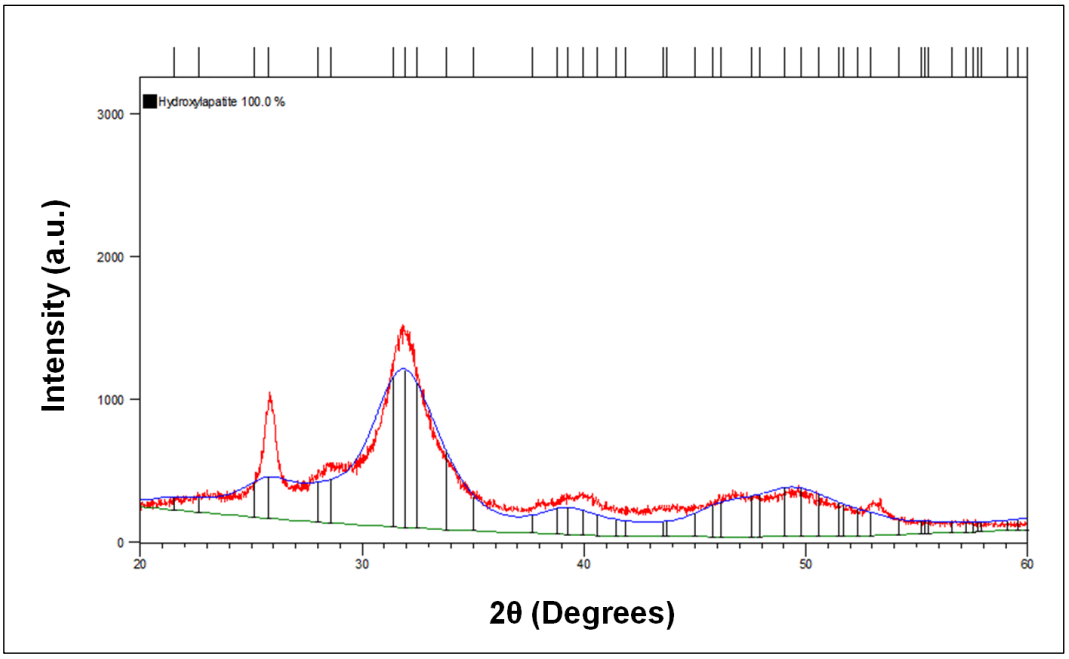

Figure 24 XRD pattern of the coating obtained by immersing the Ti6Al4V plate into the selenate added 1.5×SBF for 10 days together with the results from Rietveld analysis.

XRD results and visible physical conditions of both pure and selenate added coatings suggest that best coating characteristics were obtained after 14 days of immersion by taking the SEM images into consideration. On the 14th day, it can be said that the coating had the phase pure structure, optimum level of crystallinity and morphology together with the best visual impression in terms of the occurrence of the unbound precipitates that can easily detach from the surface.

On the other hand, the Rietveld refined values of lattice parameters a and c were found as 9.5557 Å and 6.9199 Å while they were known to be 9.4180 Å and 6.8840 Å, respectively for the assigned HA phase (ICDD card No. 9-0432). It is clear that both lattice parameters and the unit cell volume obtained accordingly from the coating were greater than the values of the standard HA.

The expansion in the unit cell volume of HA could be due to the incorporation of selenate ion which has larger ionic radius than phosphate ion. It was previously reported that since selenate (Se–O ~1.65 ± 0.01 Å) is larger than phosphate (P–O ~1.53–1.56 Å), it can push out the surrounding Ca atoms to slightly higher distances and therefore cause local distortions [114]. As a result of the larger selenium doped HA lattice parameters, the peaks were expected to shift slightly to lower values compared to the standard HA [115].

In HA crystal unit cell, there are two locations where either SeO_3^{2-} or SeO_4^{2-} ions can accommodate: the channels running along the c-axis, normally occupied by columns of structural hydroxyl groups and the orthophosphate sites. As stated above, SeO_4^{2-} ion has a tetrahedral structure as the PO_4^{3-} ion and it is slightly larger. On the other hand, although the SeO_3^{2-} ion has a very similar diameter to that of the PO_4^{3-} ion, it has a different geometry of a flat trigonal pyramid. The incorporation of both SeO_3^{2-} and SeO_4^{2-} ions into the HA crystal lattice is possible and they can easily replace the phosphate ions to form non-stoichiometric HA. For selenium-doped HA, the following chemical formula was proposed [116]:

$$Ca_{(10-x)}(PO_4)_{(6-x)}(SeO_n)_x(OH)_{(2-x)} \quad (2)$$

where $0<x<2$ and x refers to the amount of selenium in the form of selenium oxyanions and n is 3 or 4, for the selenite or selenate ions, respectively.

3.2.3. The Effects of Sterilization

The sterilization of the coated Ti6Al4V plates is necessary for the cell and bacterial culture studies or prior to *in vivo* use. In general, among the sterilization methods applied to the biomaterials, steam sterilization or autoclave sterilization, dry heat and ethylene oxide (EtO) sterilization methods are the most widely used methods, because they are simple and inexpensive [117]. For example, a standard procedure in biomedical applications is subjecting the biomaterial to a temperature of 120°C for 20 min in a steel autoclave [118].

However, the dry heat application at considerably low temperatures was accepted to be more appropriate for the CaP coated Ti6Al4V plates in terms of increasing the crystallinity of the coating. Therefore, the plates were subjected to heat at 200°C for 2 h.

Since this process consists of the application of higher temperatures than RT, the possibility of decomposition of the coating to different phases other than HA was considered; thus, XRD analysis was performed on the sterilized plates. The resulting XRD patterns are given in Figure 25.

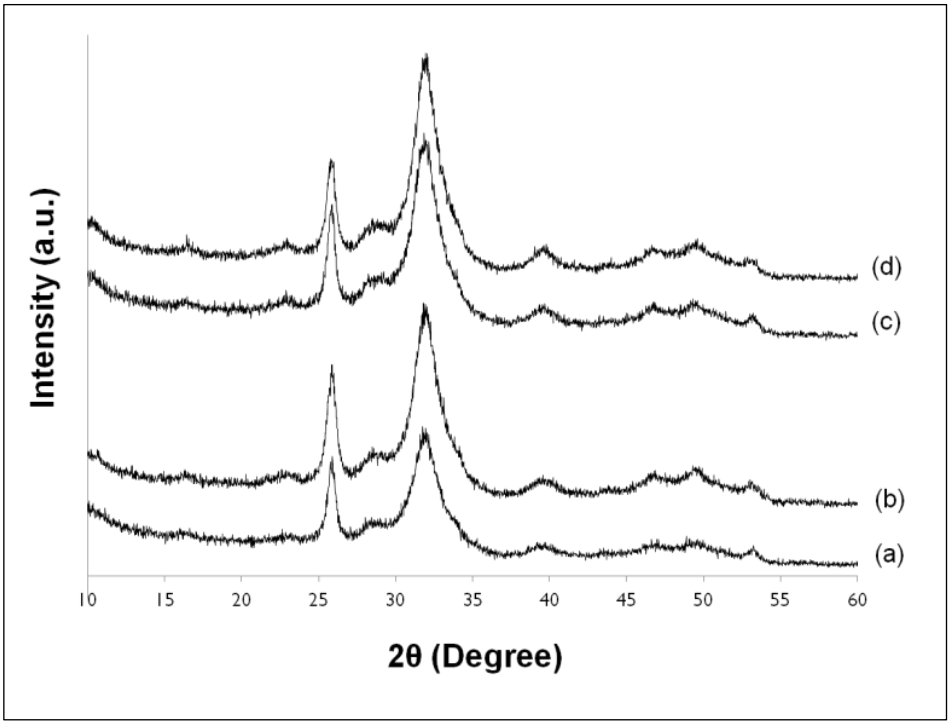

Figure 25 XRD patterns of Ti6Al4V plates (a) after soaking in selenate added 1.5×SBF for 14 days (S14); (b) after soaking in selenate added 1.5×SBF for 14 days (S14) and sterilization; (c) after soaking in 1.5×SBF with normal ionic composition for 14 days (N14) and (d) after soaking in 1.5×SBF with normal ionic composition for 14 days (N14) and sterilization.

In this study, sintering procedure was not applied to avoid crack formation which can be induced by the thermal expansion mismatch between the HA coatings and the Ti6Al4V substrates. It was previously shown that selenium substituted HA powders

with the Se/P ratio of 0.1 have thermal stability at the sintering conditions of 900°C for 2 h [119]. Considering this data; it was predicted that sterilization by dry heat would not cause HA coatings to decompose into other phases. As expected, the coatings obtained from selenate added or normal 1.5×SBF on 14th day did not yield the new phase formations after sterilization at 200°C for 2 h. Additionally, there was no visible disintegration of the coatings. In addition, the coatings subjected to a heat sterilization process gave higher intensity XRD peaks compared to the unsterilized equivalents, therefore, it was concluded that sterilization at 200°C for 2 h also improved the crystallinity of the coatings.

3.3. FTIR Results

3.3.1. Coatings in Normal 1.5×SBF

The FTIR spectra of the surfaces of pretreated Ti6Al4V plates after soaking in 1.5×SBF with normal ionic concentration for a period of 4, 7, 10, 14 and 21 days are given in Figure 26. The FTIR bands of the same coatings are listed in Table 17.

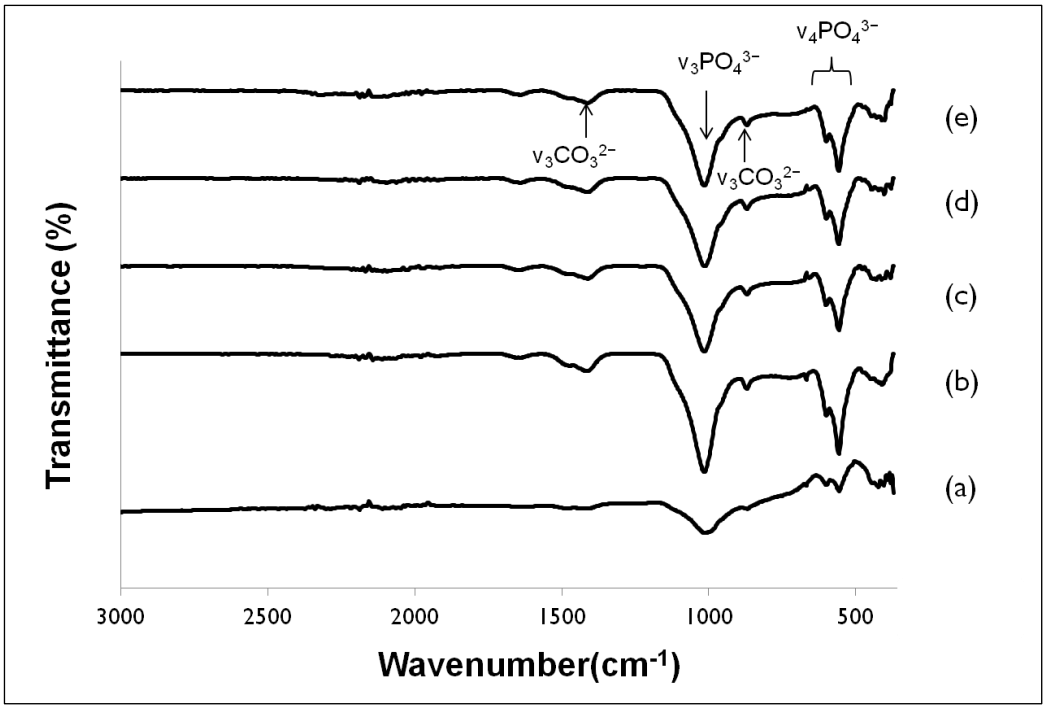

Figure 26 FTIR patterns of Ti6Al4V plates after soaking in 1.5×SBF with normal ionic composition for a period of (a) 4; (b) 7; (c) 10; (d) 14 and (e) 21 days.

Table 17 FTIR peaks of the coatings obtained in the 1.5×SBF with normal ionic concentration.

Coating Time	4 days	7 days	10 days	14 days	21 days
FTIR Bands Wavenumber (cm^{-1})	556.09	557.95	557.70	557.87	557.89
	599.55	599.79	600.29	600.05	600.10
	868.37	870.82	870.34	870.99	870.07
	1012.02	1015.53	1015.57	1014.39	1015.45
	1410.36	1414.14	1412.55	1412.42	1412.65
	-	1639.18	1641.58	1641.50	1641.56

In FTIR spectra, the characteristic bands belonging to $\nu_3PO_4^{3-}$ stretching mode at 1015 cm^{-1} and $\nu_4PO_4^{3-}$ bending mode with a maximum at 557 cm^{-1} and a shoulder at 600 cm^{-1} of the phosphate ion in the structure of HA were clearly observed. Bands at 870 cm^{-1} and 1412 cm^{-1} were attributed to $\nu_3CO_3^{2-}$ mode of carbonate, which are also known to present in bone and dentin [120]. EDS analysis supported the presence of carbonate ion via detection of carbon element. The weak band at 1640 cm^{-1} was attributed to absorbed water vapor [120,121]. The general characteristics of the FTIR bands of the coatings are very similar but the bands at the FTIR spectrum of the coating on the 4^{th} day were weaker since the coating was non-uniform and thinner.

3.3.2. Coatings in Selenate Added 1.5×SBF

The FTIR spectra of the surfaces of pretreated Ti6Al4V plates after soaking in selenate added 1.5×SBF for a period of 4, 7, 10, 14 and 21 days are given in Figure 27. The FTIR bands of these coatings are listed in Table 18.

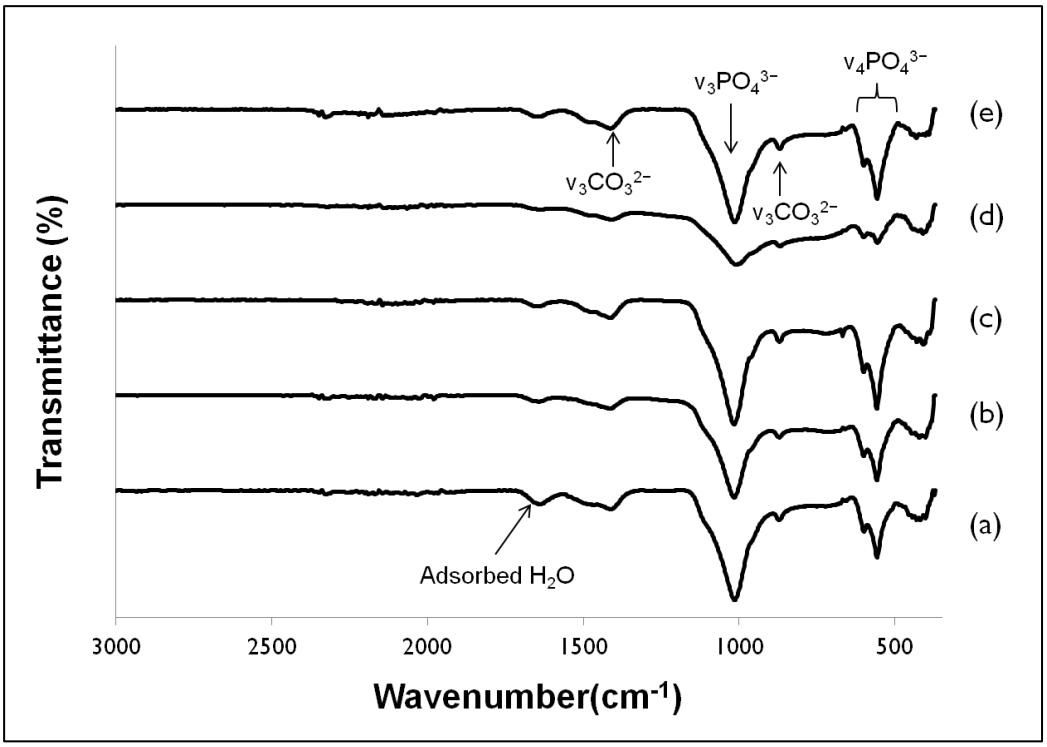

Figure 27 FTIR patterns of Ti6Al4V plates after soaking in selenate added 1.5×SBF for a period of (a) 4; (b) 7; (c) 10; (d) 14 and (e) 21 days.

In the FTIR spectra, the band at 1015 cm^{-1}, which was attributed to the $\nu_3PO_4^{3-}$ stretching mode, and the band with a maximum at 557 cm^{-1} and a shoulder at 600 cm^{-1}, which was attributed to $\nu_4PO_4^{3-}$ bending mode, were common. As for the coatings obtained from the 1.5×SBF with normal ionic composition, the bands at 870 cm^{-1} and 1412 cm^{-1} of $\nu_3CO_3^{2-}$ mode were observed.

Table 18 FTIR peaks of the coatings obtained in the selenate added 1.5×SBF.

Coating Time	4 days	7 days	10 days	14 days	21 days
FTIR Bands Wavenumber (cm^{-1})	557.40	558.01	558.25	555.59	557.30
	599.20	600.45	600.19	599.97	599.95
	871.96	871.69	870.92	868.27	870.25
	1014.83	1016.11	1016.35	1010.52	1014.83
	1412.81	1414.63	1413.74	1409.82	1413.40
	1641.24	1642.49	1641.99	1641.01	1642.06

The FTIR spectra of selenium doped coatings were found to exhibit no significant difference than pure HA. This result is consistent with the XRD analyses and showed that the coatings were phase pure. The obtained results are in compliance with the literature [114], in terms of examining no distinctive differences between selenium doped and pure HA in FTIR and XRD studies when the amount of selenium is at ppm level.

On the other hand, Wang et al. [122] prepared selenium doped HA in which Se/P molar ratios were between 0.4-1.1 by an aqueous precipitation method with the addition of sodium selenite (Na_2SeO_3) during synthesis. It was shown that FTIR spectra of selenium doped HAs have an additional band at 783 cm^{-1} which is assigned to the selenite (SeO_3^{2-}) group. Additionally, the band intensity of carbonate groups was shown to become stronger with the increasing selenium content. It was explained as follows: since the selenite group is divalent and has less negative charge than the trivalent phosphate group, more hydroxyl groups are replaced by carbonate groups due to the charge compensating mechanism. Therefore, the content of carbonate groups increases with the increasing content of selenite groups. The same charge mismatch between selenate (SeO_4^{2-}) group and phosphate group also exists. This could also result in increased intensities of the carbonate bands of the selenium doped HA coatings with respect to pure HA coatings. However, the results of this study did not provide detectable differences in the carbonate bands.

3.4. Raman Spectroscopy Results

In order to evaluate the incorporation of selenium ion into the structure of HA further studies were performed. Raman spectroscopy is a useful technique to study the incorporation of various ions in HA and it is used as a complementary method to FTIR technique.

Figure 28 represents the Raman spectra of the pure and selenium added HA coatings from 2500 to 100 cm^{-1}.

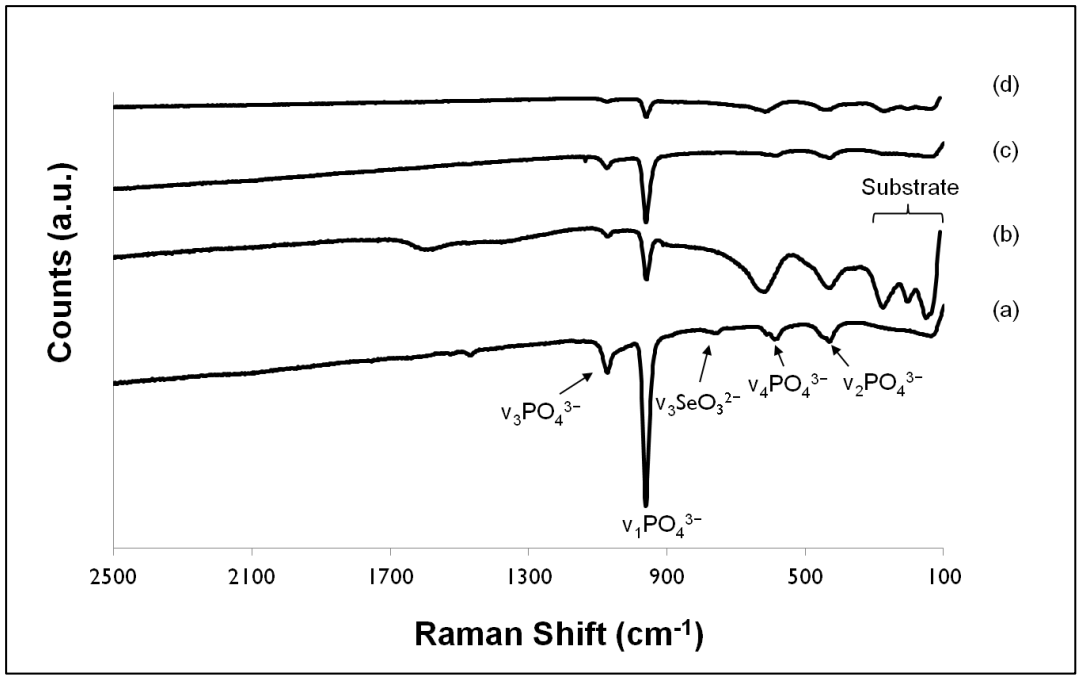

Figure 28 Raman spectra of (a) after soaking in selenate added 1.5×SBF for 14 days; (b) after soaking in selenate added 1.5×SBF for 7 days; (c) after soaking in 1.5×SBF with normal ionic composition for 14 days and (d) after soaking in 1.5×SBF with normal ionic composition for 7 days.

The intense peak around 961 cm^{-1}, which was attributed to the stretching mode (ν_1) of the phosphate group, was the main characteristic peak of all of the coatings. The other bands of phosphate groups were also identified at 1072 cm^{-1} (ν_3, stretching mode) and 429 cm^{-1} (ν_2, stretching mode). The band at 590 cm^{-1} was observed in Figure 28(a) and (b) which was attributed to the ν_4 bending mode of phosphate group [101,123]. The bands around 136 cm^{-1}, 209 cm^{-1}, 270 cm^{-1} and 629 cm^{-1} were assigned to the alkali-heat treated Ti6Al4V plates (substrate).

It is known that the chemistry of the selenite (SeO_3^{2-}) ion resembles the chemistry of the sulphite (SO_3^{2-}) ion and the symmetry of the selenite ion should be similar to that of sulphite. The selenite ion thus has four fundamentals: ν_1 (approximately 790–806 or 760–855 cm^{-1} – the symmetric stretching vibration; ν_2 (approximately 430–461 cm^{-1}) – the bending vibration; ν_3 (approximately 714–769 or 680–775 cm^{-1}) – the degenerate stretching vibration; ν_4 (approximately 387–418 cm^{-1}) – the doubly

degenerate in-plane bending vibration. All vibrations are Raman and infrared active [124].

Similarly, selenate (SeO_4^{2-}) and sulphate (SO_4^{2-}) ions are structurally very similar. The normal modes of vibration for the free selenate anion, which are all Raman active, are the nondegenerate ν_1 symmetric SeO stretching at 837 cm^{-1}, the doubly degenerate ν_2 OSeO bending at 349 cm^{-1}, the triply degenerate ν_3 asymmetric SeO stretching at 873 cm^{-1}, and the triply degenerate ν_4 OSeO bending at 417 cm^{-1} [125]. However, these selenate bands were not detected in any of the Raman spectra of selenium doped HA coatings.

On the other hand, in the Raman spectra of the plate, which was coated in the selenate added 1.5×SBF for 14 days, an extra weak band at 764 cm^{-1} was detected. This band was attributed to the antisymmetric SeO_3^{2-} unit [126]. However, since the amount of the selenium incorporated into the HA structure was very low, the bands could not be specified certainly.

3.5. Scratch Test Results

There are several methods to evaluate the interfacial strength between the coatings and substrates, such as pull-off, indentation and shockwave-loading and scratch test [127]. Scratch testing is a widely used method for determining the strength of the adhesion of applied coatings. It is performed with a specified indenter (commonly, diamond-shaped) to scratch of a coated surface under increasing load and constant speed or increasing speed and constant load or both constant. The adhesion can be estimated when the coating fails by knowing all test parameters and by a measurement of the critical load [128]. Due to the porous microstructure of CaP coatings, the scratch test was considered to be a convenient method to prevent artificial factors such as glue infiltration [127].

The scratch test results of the Ti6Al4V plates with different characteristics are given in Figure 29.

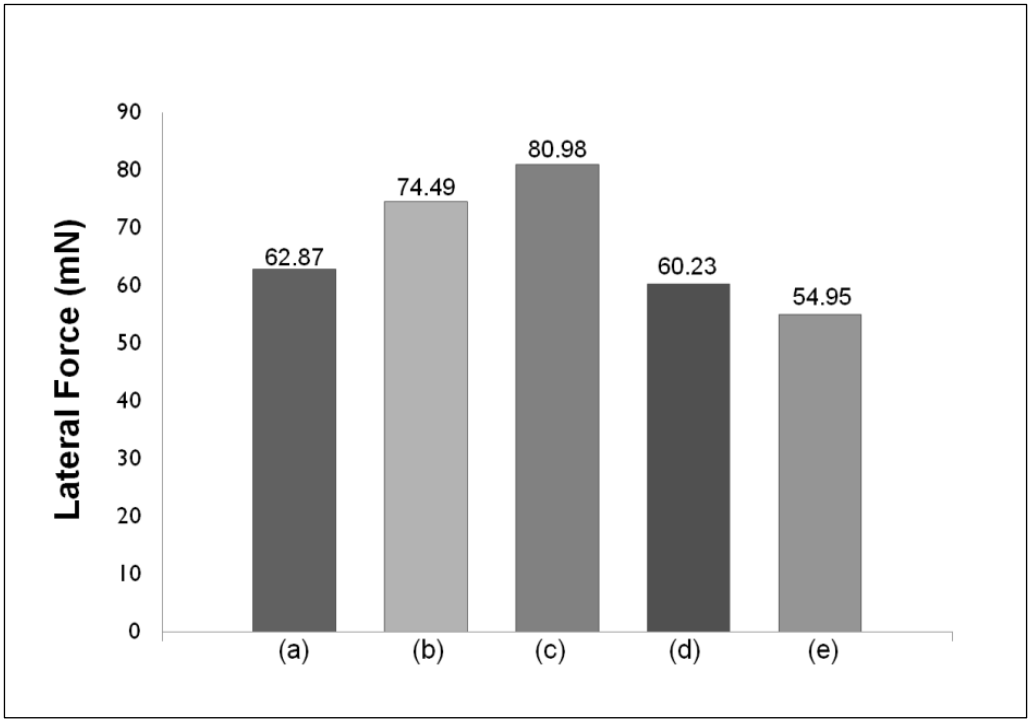

Figure 29 Scratch test results of the Ti6Al4V plates (a) after soaking in selenate added 1.5×SBF for 10 days; (b) after soaking in selenate added 1.5×SBF for 14 days; (c) after soaking in 1.5×SBF with normal ionic composition for 10 days; (d) after soaking in 1.5×SBF with normal ionic composition for 14 days and (e) after soaking in selenate added 1.5×SBF for 14 days and sterilization.

As can be seen in Figure 29, all of the critical lateral force values obtained at the moment of coating failure were above 50 mN. The coating obtained in the 1.5×SBF with normal ionic composition on the 10^{th} day of immersion gave the highest critical value (80.98 mN). There was no significant difference between the coatings obtained from selenate added 1.5×SBF or 1.5×SBF with normal ionic compositions for soaking periods of 10 and 14 days.

The strength values at the moment of fracture of the coatings were above the expected levels for all types. In a study consisting of the biomimetic CaP coating of alkali-heat treated Ti6Al4V plates, the adhesive strength of the coatings was reported at about 9 mN [64].

In addition, from Figure 29(e), it was observed that the lateral force of the coating in selenate added 1.5xSBF for 14 days did not decrease significantly after sterilization process. Therefore, the method of sterilization was considered as not detrimental to the coating in terms of mechanical properties.

3.6. ICP-MS Results

The Ca/Se atomic ratios of the coatings obtained by soaking the pretreated Ti6Al4V plates into the selenate added 1.5×SBF for a period of 7, 10, 14 and 21 days are given in Figure 30. The amount of the precipitates obtained in the selenate added 1.5×SBF at 4th day was very low and therefore ICP-MS analysis could not be possible.

In addition, the coatings obtained from the 1.5×SBF with normal ionic composition was defined as the control group and there was no selenium detected with the ICP-MS method on these coatings.

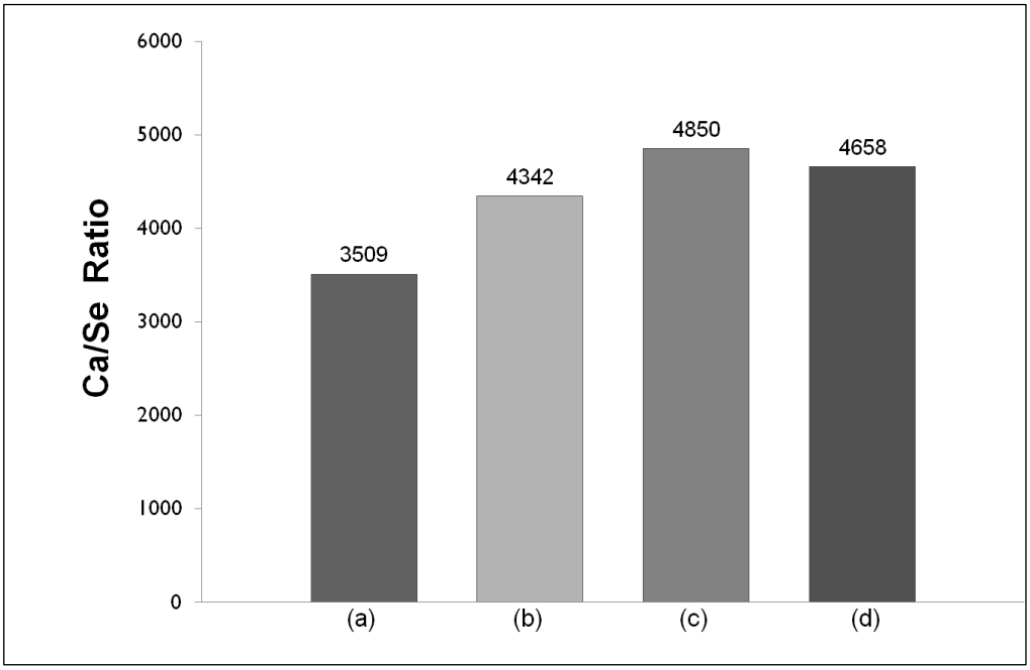

Figure 30 Calculated Ca/Se atomic ratios of the Ti6Al4V plates after soaking in selenate added 1.5×SBF for a period of (a) 7; (b) 10; (c) 14 and (d) 21 days.

As can be seen in Figure 30, all of the coatings on the Ti6Al4V plates soaked into the selenate added 1.5×SBF for a period of 7, 10, 14 and 21 days contain selenium. Since the plates were washed with distilled water after removal from the SBF solutions, the unbound precipitates were removed from the surface and the detected selenium was arising only from the content of the coatings. It is interesting that the Ca/Se ratio increased with the increasing soaking time which means the amount of the doped selenate was decreasing. However, due to the fact that the Ca/Se ratio was very high, the increment was considered to be insignificant in terms of incorporation of selenium into the structure.

3.7. Cell Viability Tests of Selenium Containing Solutions

The PrestoBlue test was performed in order to assess the dose dependent cytotoxicity of the selenium. The percent viabilities of the cells treated with the various test media with respect to the control group were determined from the following equation:

$$Percent\ Viability\ (\%) = \frac{\text{Absorbance of treated well}}{\text{Mean absorbance of control wells}} \times 100 \qquad (3)$$

The percent viabilities were calculated for each well with respect to the mean absorbance of the control wells and these were averaged. Figure 31 shows the average percent cell viability of the hFOB 1.19 cells treated with different concentrations selenium (see, Table 13 for the final selenium content of the growth media) with respect to the control (untreated) cells.

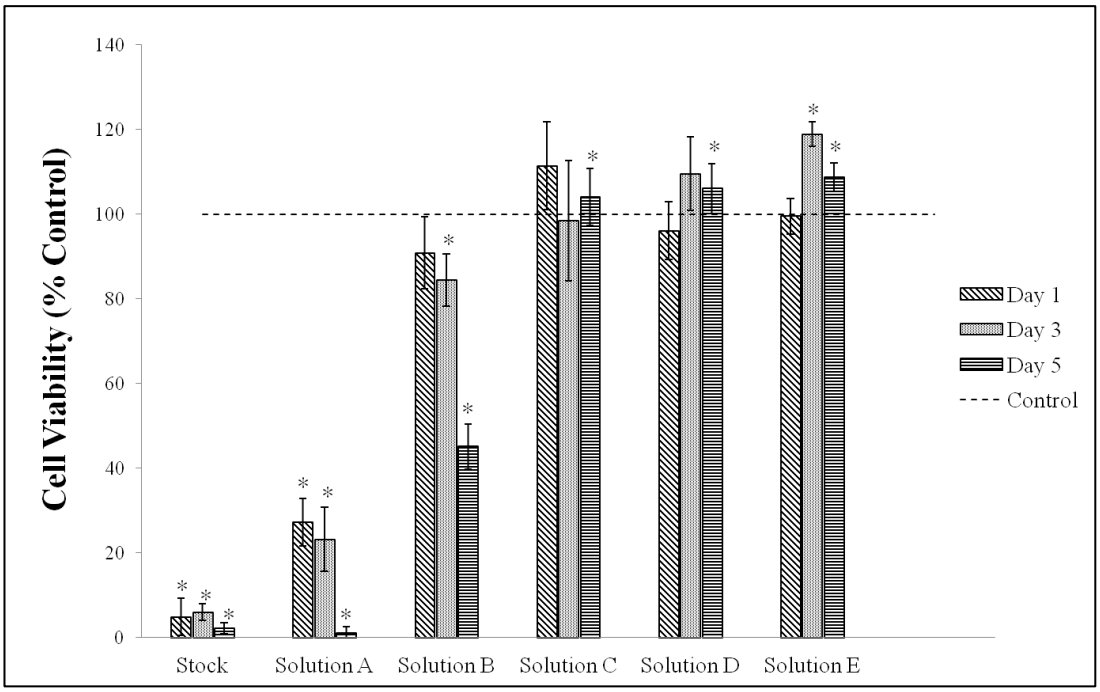

Figure 31 Cellular viability of hFOB 1.19 cells treated with selenium solutions at different concentrations for 1, 3 and 5 days (n=2). The error bars represent the standard error. Asterisks indicate differences of statistical significance (*$p<0.05$) with respect to control values of the same time point as determined by the Mann-Whitney U-test.

The normal human fetal osteoblast cells that were treated with solutions C, D and E showed higher overall viability than the control and the other groups, as can be seen in Figure 31. Solution A and stock solution showed high cytotoxicity. Similarly, solution B, which contains 5×10^{-6} g Se per 1.1 ml of the media, exhibited a statistically significant decrease in cell viability with respect to the control.

Similarly, the percent cell viabilities of the Saos-2 cells treated with the various selenium containing medium are given in Figure 32. The cell culture medium with the maximum selenium content (stock solution, 5×10^{-3} g Se) was shown to be cytotoxic to both Saos-2 and hFOB1.19 cells since the cells treated in this medium showed the very low viability, as determined from Figures 31 and 32. Similarly, solution A was cytotoxic for both types of cells. Solutions B and C did not show cytotoxicity on the cancerous cells (Saos-2), on the contrary, both of the solutions yielded better cell viabilities with respect to control.

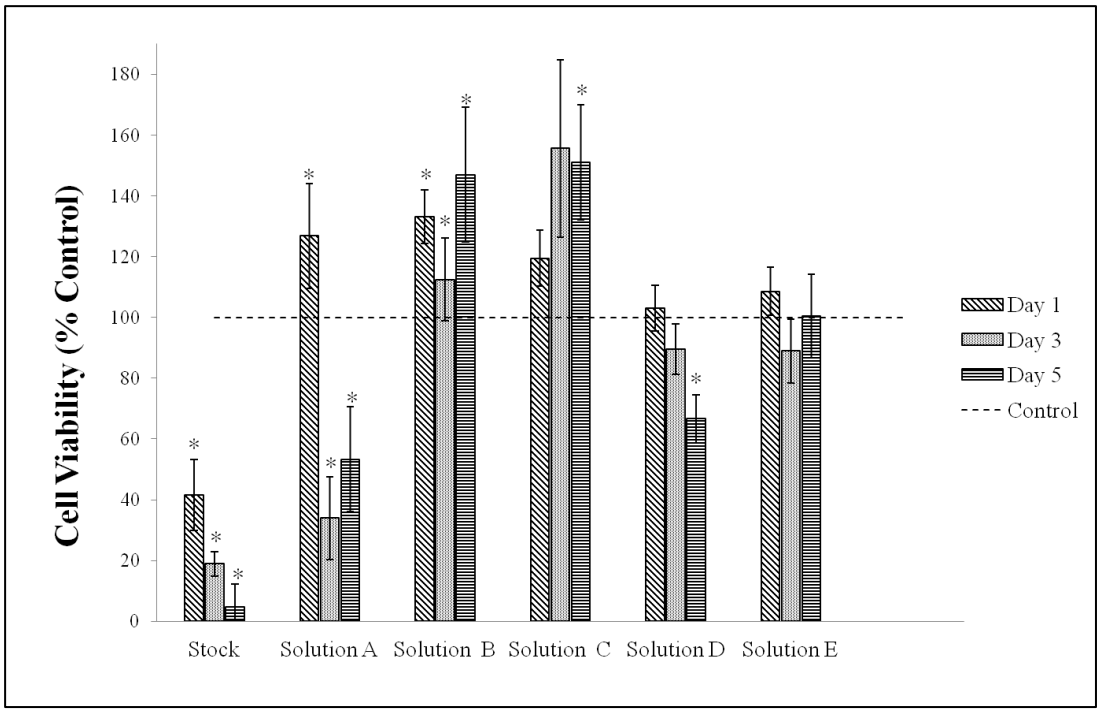

Figure 32 Cellular viability of Saos-2 cells treated with selenium solutions at different concentrations for 1, 3 and 5 days (n=2). The error bars represent the standard error. Asterisks indicate differences of statistical significance (*$p<0.05$) with respect to control values of the same time point as determined by the Mann-Whitney U-test.

Among the cells treated with the selenium containing media prepared by adding different solutions from A to E, the cells incubated in solution D added medium, which contained 5×10^{-8} g Se, provided the best result in terms of inhibiting cancerous (Saos-2) cell growth while preventing the inhibition of healthy (hFOB 1.19) cells. This concentration of selenium is the desired amount to be tested, since it is the mean concentration determined previously by ICP-MS analysis of the selenium added HA coatings. From the results of PrestoBlue test, it was shown that the selenium at this concentration is optimum for the aim of the study.

Several studies reported the association between selenium and the cell cycle, proliferation and apoptosis of different kinds of cells. The percent cell viabilities of various cell lines treated with different concentrations of selenium reported in the literature are summarized in Table 19.

Table 19 Percentages of the cell viabilities of various cell lines treated different concentrations of selenium.

Treatment	Cell Line	Treatment Duration	Cell Viability (% of control)	Reference
5 μg Se/ml (as sodium selenite)	BALB/c MK-2 Mouse keratinocyte cells	24h	81±6	[129]
10 μg Se/ml (as sodium selenite)	BALB/c MK-2 Mouse keratinocyte cells	24h	90±9	[129]
25-250 μg Se/ml (as sodium selenite)	BALB/c MK-2 Mouse keratinocyte cells	24h	Cell detachment occurred between these doses	[129]
1 μM sodium selenite (0.789 μg Se/ml*)	LNCaP Prostate carcinoma cells	72h	81	[130]
2.5 μM sodium selenite (1.973 μg Se/ml*)	LNCaP Prostate carcinoma cells	72h	8	[130]
5 ng/ml Se (as selenomethionine)	HT29 Human intestinal adenocarcinoma cells	24h-72h	~100 (for both of the time points)	[131]
50 ng/ml Se (as selenomethionine)	HT29 Human intestinal adenocarcinoma cells	24h-72h	~100 (for both of the time points)	[131]
500 ng/ml Se (as selenomethionine)	HT29 Human intestinal adenocarcinoma cells	24h-72h	80- ~100 (for the two time points, respectively)	[131]

*Calculated by knowing the atomic weight of selenium is 78.96 amu and the molecular mass of sodium selenite is 172.94 g/mol.

Table 19 demonstrates that all of the cells show a dose dependent survival rate depending upon the concentration of selenium in the cell growth media. A previous study aiming to determine the activity of selenium on cell proliferation, cytotoxicity, and apoptosis of intestinal adenocarcinoma cells (HT29) [131] revealed that selenium was not cytotoxic and did not interfere with cell proliferation at low doses, i.e. at any of the concentrations of 5, 50 and 500 ng/mL. More importantly, it was reported that selenium increases apoptosis, especially when it is associated with a damage-inducing agent and it has an important role in the expression of a gene which is related to cell cycle regulation.

Although these studies [129-131] related to determine the cytotoxicity of selenium compounds reported the dose dependent inhibitory effect of selenium on different kinds of cancer cell lines, they are unable to demonstrate the cytotoxicity of selenium on the healthy cells. On the other hand, the effect of different concentrations of selenium on both healthy and cancerous bone cells was determined in this study. It was shown that the viability of the healthy osteoblast cells (hFOB 1.19) increased at concentrations below about 0.5 μg Se/ml (i.e. solutions C, D, E) and the survival of the cells significantly decreases at concentrations ten times higher than that in cell culture media. However, the viability of cancerous cells (Saos-2) did not show a linear relationship with the varying concentrations of selenium.

3.8. Cell Viability Tests of Coatings

Similar to the cell viability assessment of the selenium containing media; the viability of the cells seeded on the pure and selenium added HA coatings that were obtained after 7 and 14 days of biomimetic coating process was determined by the Prestoblue test. The absorbance is a direct measure of cellular viability since it is a result of the ability of the cells to reduce the active ingredient. The absorbance values of the hFOB 1.19 cells seeded on N7, N14, S7 and S14 plates are given in Figure 33 (see Table 14 for the description of the coated plates).

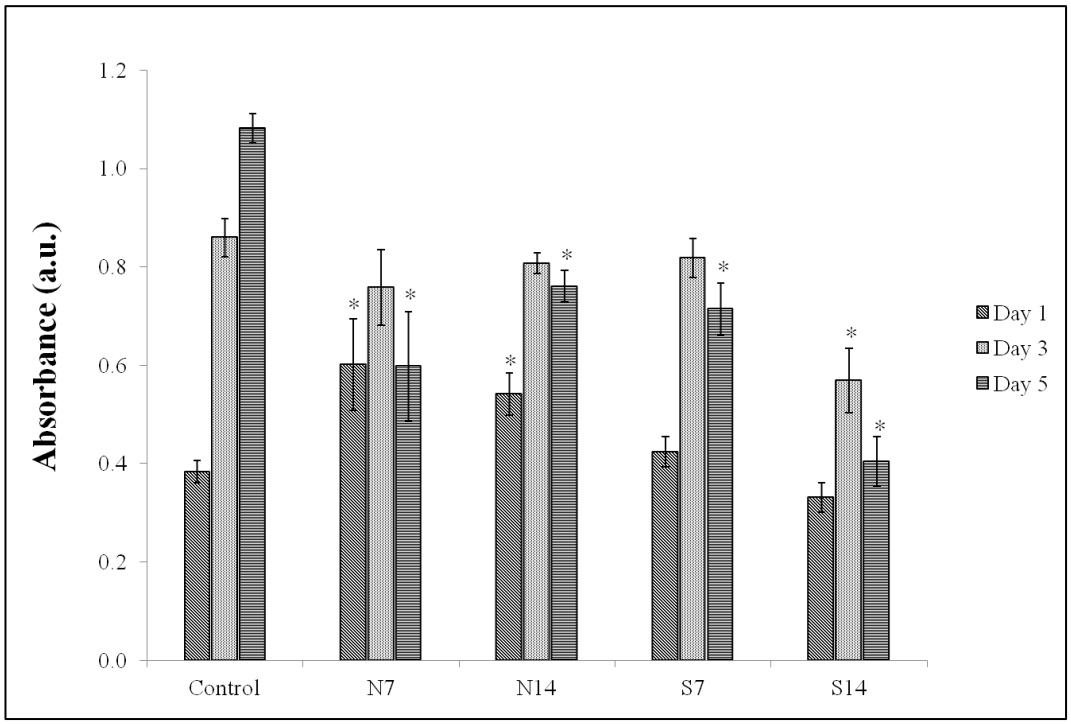

Figure 33 Cellular viability of hFOB 1.19 cells seeded on pure HA and selenium added HA coatings and incubated for 1, 3 and 5 days (n=2). The error bars represent the standard error. Asterisks indicate differences of statistical significance (*$p<0.05$) with respect to control values of the same time point as determined by the Mann-Whitney U-test.

As it can be seen from Figure 33, the viabilities of the hFOB 1.19 cells seeded on the plates were generally lower than that of the control group seeded on cell culture plate. The increase in the absorbance of the control group with time represents a normal proliferation of the cells. On the other hand, the viability of the cells on the test plates did not show a time dependent increment. There was an important factor contributing to these results that either of the selenium added or pure biomimetically obtained HA coatings disintegrates during the prolonged cell culture process. Therefore, the cells attached on the surface were also lost during medium renewals. The percent viability of the cells in all groups generally decreased with time because of the decreased number of the cells attached on the surface with time due to the mentioned cell loss.

Similarly, the absorbance values of the Saos-2 cells seeded on N7, N14, S7 and S14 plates are given in Figure 34.

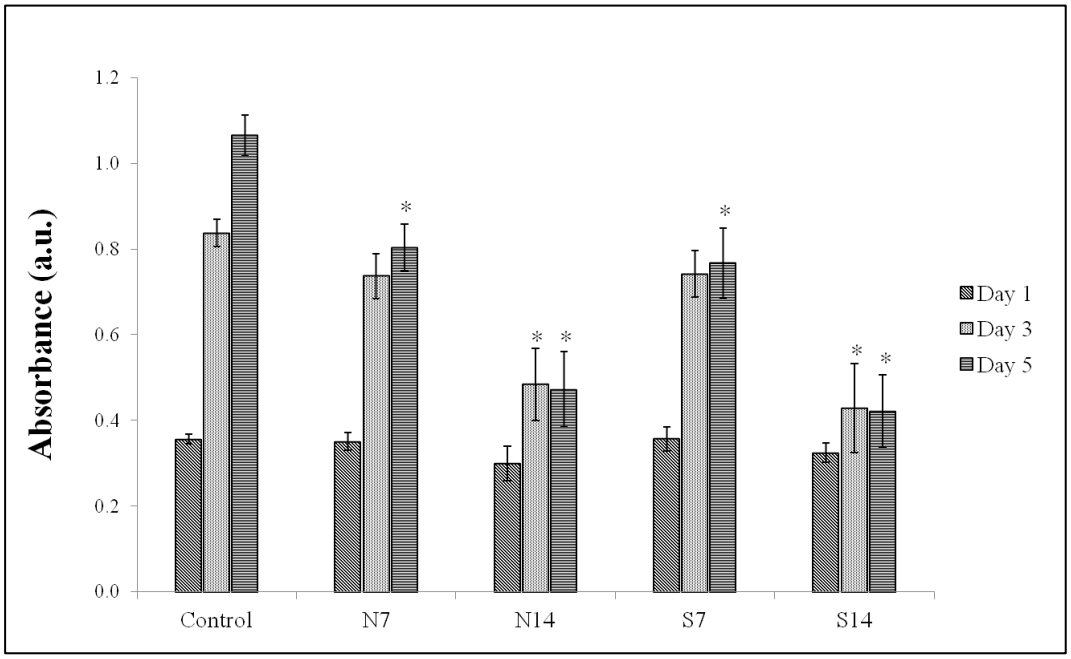

Figure 34 Cellular viability of Saos-2 cells seeded on pure HA and selenium added HA coatings and incubated for 1, 3 and 5 days (n=2). The error bars represent the standard error. Asterisks indicate differences of statistical significance (*$p<0.05$) with respect to control values of the same time point as determined by the Mann-Whitney U-test.

Similar to the viabilities of the hFOB 1.19 cells, the viabilities of Saos-2 cells seeded on the plates were generally lower than the control group which was seeded on cell culture plate. Lower overall viability of the cells on the plates that were coated for 14 days (N14 and S14) with respect to the viability of the cells on the plates that were coated for 7 days (N7 and S7) was more apparent for Saos-2 cells. This brings to mind again that the coating thickness is also important factor in terms of cell proliferation. The deposited apatite may have been lost with the attached cells on the coatings obtained at the 14^{th} day. The results were in accordance with the confocal microscopy images which will be discussed in following sections.

On the other hand, the tissue culture plastic, on which the control group was seeded, is an ideal substrate that supports the attachment and growth of cells. Therefore, the difference between the viability of the control cells and the viability of the cells seeded on the test samples was not an unexpected result.

It was previously shown that when selenium doped HA nanoparticles (Se/P molar ratio 1.1) were added to the culture medium of bone marrow mesenchymal stem cells (BMSC), there were no differences in viability with respect to the cells treated with pure HA nanoparticles [122]. However, when the same selenium doped HA nanoparticles were added to the culture medium of human osteosarcoma MG63 cells, less than 40% of MG63 cells survived after 72h. The reported Se concentration in the medium was 200 μg/ml at that point. This is much higher than the selenium concentration of most concentrated solution (Solution A, 5×10^{-5} g) tested in this study.

3.9. SEM Microscopy Results

The morphology and attachment of the Saos-2 cells on the plates coated in normal and selenate added 1.5×SBF were evaluated by using the SEM technique. The SEM images of the cells incubated on the plates with different coatings for 7 days are given in Figure 35.

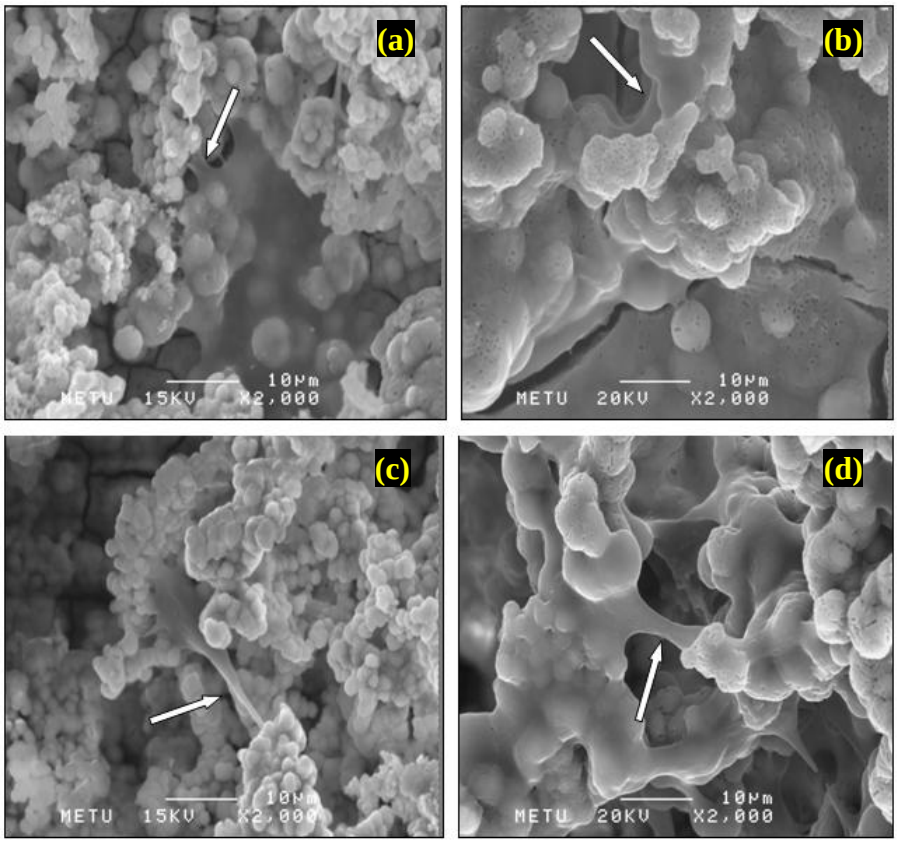

Figure 35 SEM images of the Saos-2 cells incubated for 7 days on: (a) N7; (b) S7; (c) N14 and (d) S14 (arrows indicate cell extensions) (2000×).

It can be stated that the cells attached firmly and spread on the coatings following the surface topography with regard to the SEM images. The migration of cells on the coated surfaces was demonstrated by the presence of lamellipodia and filopodia on all the materials studied, as indicated by arrows in Figure 35. SEM imaging was not used to determine the difference in the proliferation of Saos-2 cell on selenium added or pure HA coatings, rather it showed the reaction of cells to surface topography. The SEM images of the coatings after 7 days of aging in complete cell culture media are given in Figure 36.

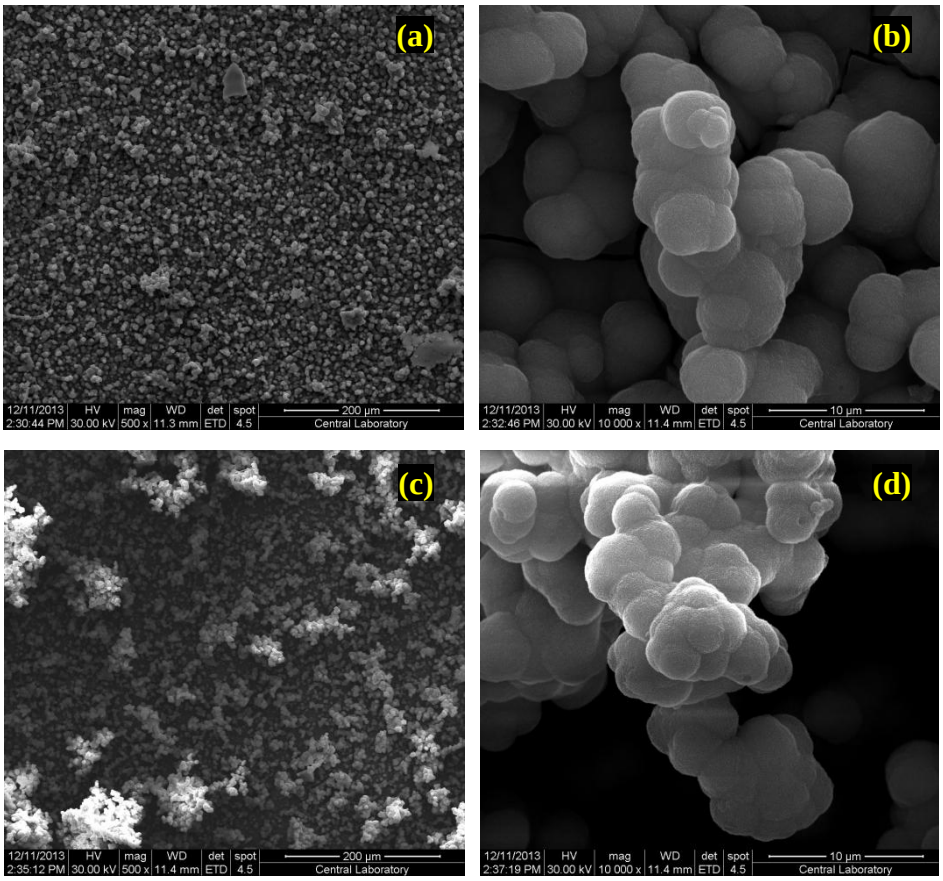

Figure 36 SEM images of (a) aged N14 (500×); (b) aged N14 (10000×); (c) aged S14 (500×) and (d) aged S14 (10000×).

From the SEM images of the aged coatings, it can be said that the selenium added HA coating obtained at 14th day of SBF immersion (S14) was more non-uniform when compared to the normal HA coating (N14). However, there were no pieces of HA flakes detached from the surface despite the detected HA flakes on the surfaces of the coatings that were aged and seeded with cells.

The morphology and attachment of the co-cultured hFOB1.19 and Saos-2 cells on the aged plates, which were coated in normal and selenate added 1.5×SBF, were evaluated by using SEM. The SEM images of the co-cultured cells incubated on the different coatings for 3 days are given in Figure 37.

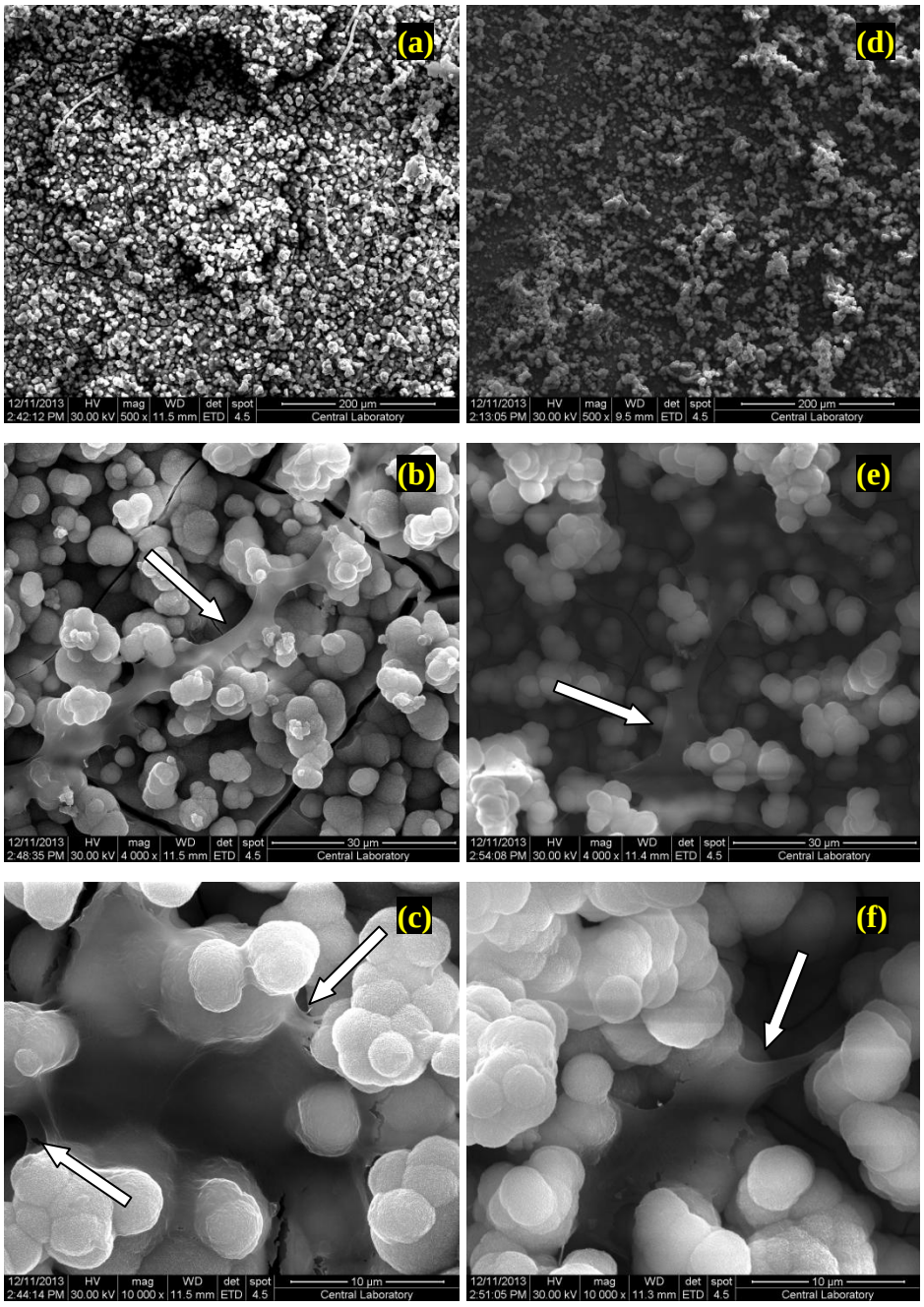

Figure 37 SEM images of co-cultured cells on (a) aged N14 (500×); (b) aged N14 (4000×); (c) aged N14 (10000×); (d) aged S14 (500×); (e) aged S14 (4000×) and (f) aged S14 (arrows indicate cell extensions) (10000×).

It can be said that the cells attached firmly and spread on the coatings following the surface topography in micrometer scale with regard to the SEM images. The migration of the cells on the coated surfaces was demonstrated by the presence of lamellipodia and filopodia on all the materials studied.

It was considered that the cellular response was similar in both of the pure and selenium added HA coatings. However, at a larger scale (100×), it was possible to see the flakes detached from the N14 (data not shown).

3.10. Fluorescent Microscopy Results

The confocal microscopy images of the Saos-2 cells seeded on a cover glass and the coatings obtained by immersing the plates to normal and selenate added 1.5×SBF for 7 days, are given in Figure 38. The nuclei and actin filaments were labeled with PI and FITC-conjugated phalloidin, respectively.

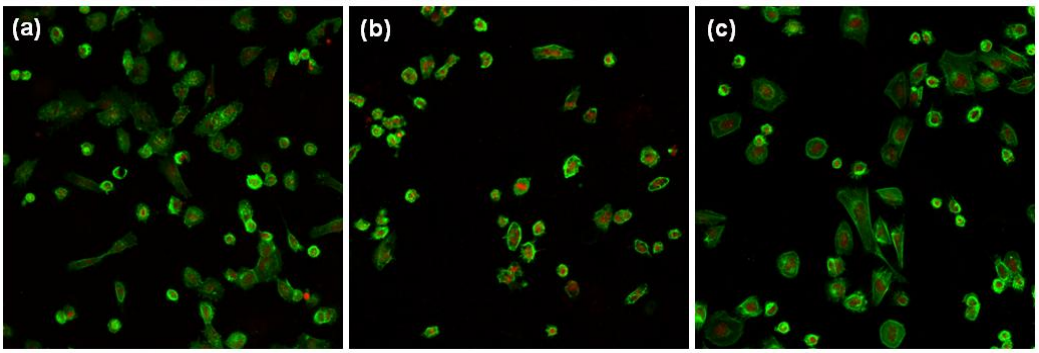

Figure 38 Confocal microscopy images of the FITC-conjugated phalloidin and PI stained Saos-2 cells that were seeded on various substrates and incubated for 1 day. Substrates: (a) N7; (b) S7 and (c) cover glass (control). Image dimensions: 45µm×45µm.

As seen in Figure 38, the nuclei (stained with PI) emit red fluorescence while the actin filaments (stained with FITC-conjugated phalloidin) emit green fluorescence. The cells were attached to the surfaces and some of them showed evidences of cell division. The cover glasses are well-known negative controls that offer a suitable environment on which the cells could attach. There was no visible difference between the cells seeded on the plates and the cover glass in terms of cell density. The confocal microscopy images of the cells seeded on the coatings obtained by immersing the plates to normal and selenate added 1.5×SBF for 14 days, are given in Figure 39. Note that the confocal image of the control group given in Figure 38 (c) is the same as that of in Figure 39 (c).

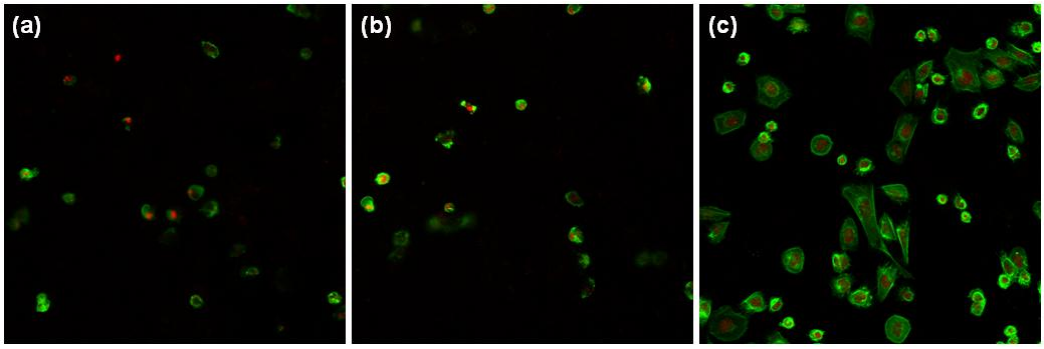

Figure 39 Confocal microscopy images of the FITC and PI stained Saos-2 cells that were seeded on various substrates and incubated for 1 day. Substrates: (a) N14; (b) S14 and (c) cover glass (control). Image dimensions: 45µm×45µm.

It can be stated that unlike the cells seeded on the coatings obtained at the 7th day of immersion (N7 and S7), the cells seeded on the coatings obtained from the normal and selenate added 1.5×SBF after 14 days, were less in number than the cells seeded on the cover glass. The results were in accordance with the cell viability tests performed with the PrestoBlue reagent.

3.11. Bacterial Adherence Tests of Coatings

The media of the cultivated bacteria on pure (N14) and selenium added (S14) HA coatings obtained on the 14th day of biomimetic coating process and pretreated Ti6Al4V plate were analyzed by a spectrophotometer. The optical densities are given in Figure 40.

The optical density of the sterile LB was shown to be around 0.060. As it can be seen from Figure 40, after 3 days of incubation, the supernatant media of all samples contained *S. epidermidis* bacteria. However, the Mann-Whitney U test implied that there was a significant decrease in the number of bacterial cells in the supernatant media of the selenium added HA coating (S14) with respect to LB medium itself and other samples. The media of bacteria seeded on normal HA coating and uncoated Ti alloy yielded higher optical densities than the bacteria cultivated in LB medium, which can be explained by the greater surface area provided by the plates for bacteria to attach.

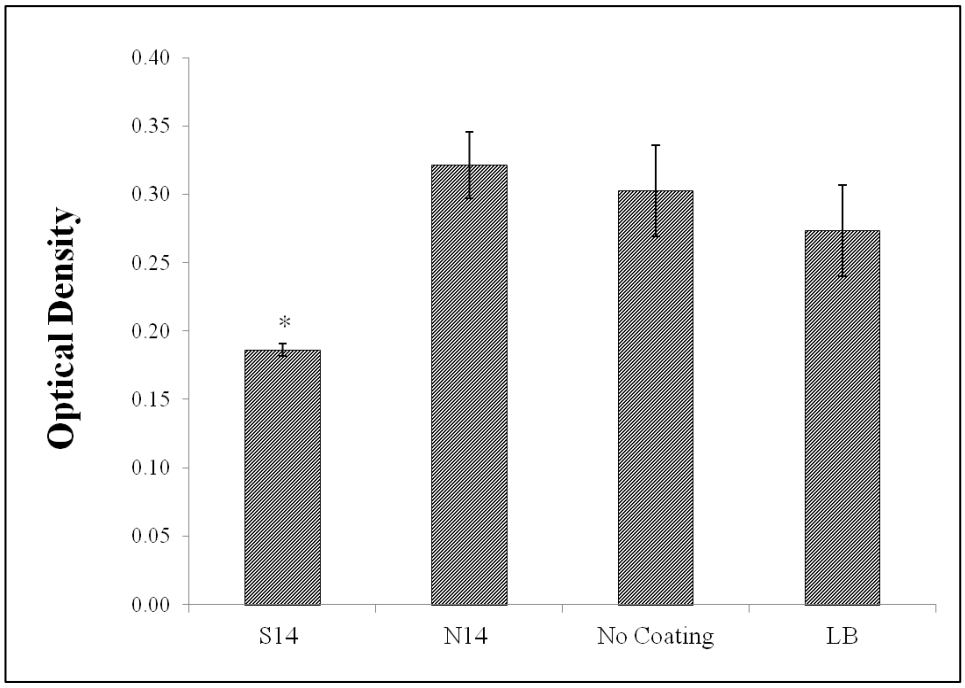

Figure 40 Optical densities of the supernatant media of the coated plates (S14 and N14) and pretreated Ti6Al4V and control (LB medium itself) after 3 days of incubation (n=3). The error bars represent the standard error. Asterisks indicate differences of statistical significance (*$p<0.05$) with respect to control values as determined by the Mann-Whitney U-test.

It is also important to determine the adherent bacterial populations on the surfaces of the samples. Therefore, after vortexing the bacteria inoculated samples to collect the adherent cells; the absorbance of resulting media was measured using a spectrophotometer. In order to distinguish the optical density resulting from the particles disintegrated from the coatings, the bacteria free samples were also vortexed in LB medium. The optical densities are represented in Figure 41.

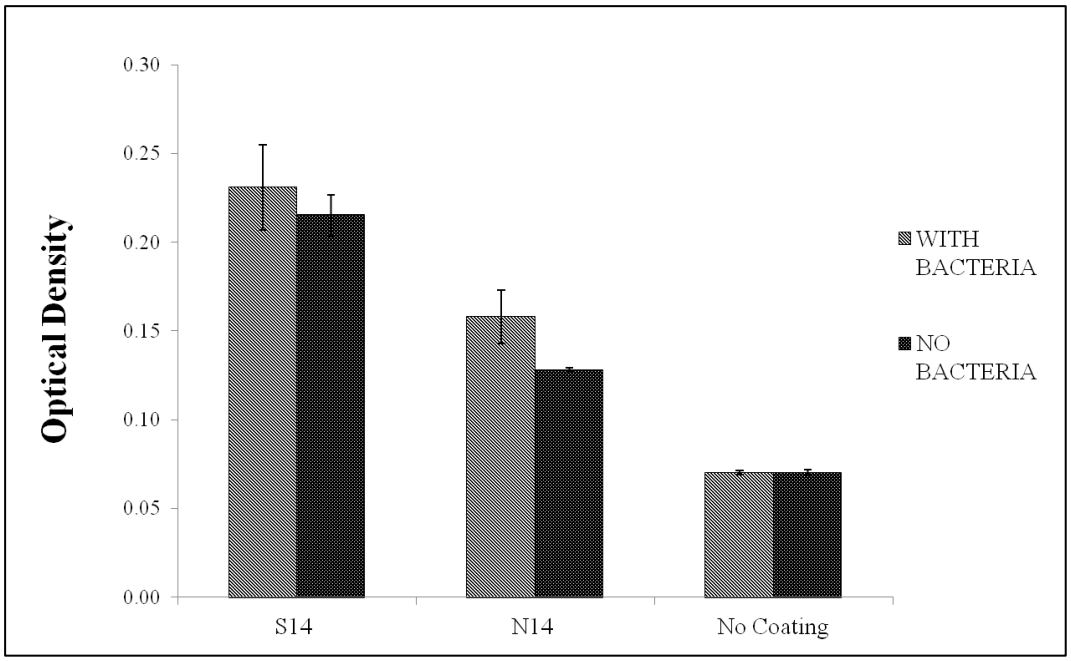

Figure 41 Optical densities of the vortexed media of the coated plates (S14 and N14) and pretreated Ti6Al4V with no bacteria (dark colored bars) and after 3 days of incubation with bacteria (light colored bars).

The bacterial growth on the surfaces of the coated samples was shown to be higher than on the uncoated Ti alloy, as seen in Figure 41. Unlike the supernatant media, the media of the vortexed S14 and N14 samples yielded higher optical densities than the uncoated Ti alloy. It is interesting that the uncoated samples did not exhibit an optical density difference after bacterial inoculation. Thus, it can be said that the bacterial attachment to the uncoated samples was very low.

On the other hand, S14 had higher optical density resulted not only from the bacterial cells but also particles detaching from the coating. However, the difference between the optical density of the substrate with and without bacteria, which is a representation of the optical density of bacterial cells only, was lower than that of the normal coated samples. Therefore, it can be stated that the bacterial attachment on S14 surface was lower than the N14 surface.

In order to observe the bacterial cells on different surfaces, the bacteria inoculated samples were examined under SEM microscopy before and after vortexing. It is known that *S. epidermidis* has spherical shape and forms structures like a bunch of grapes, as implied by its name. The images are given in Figure 42.

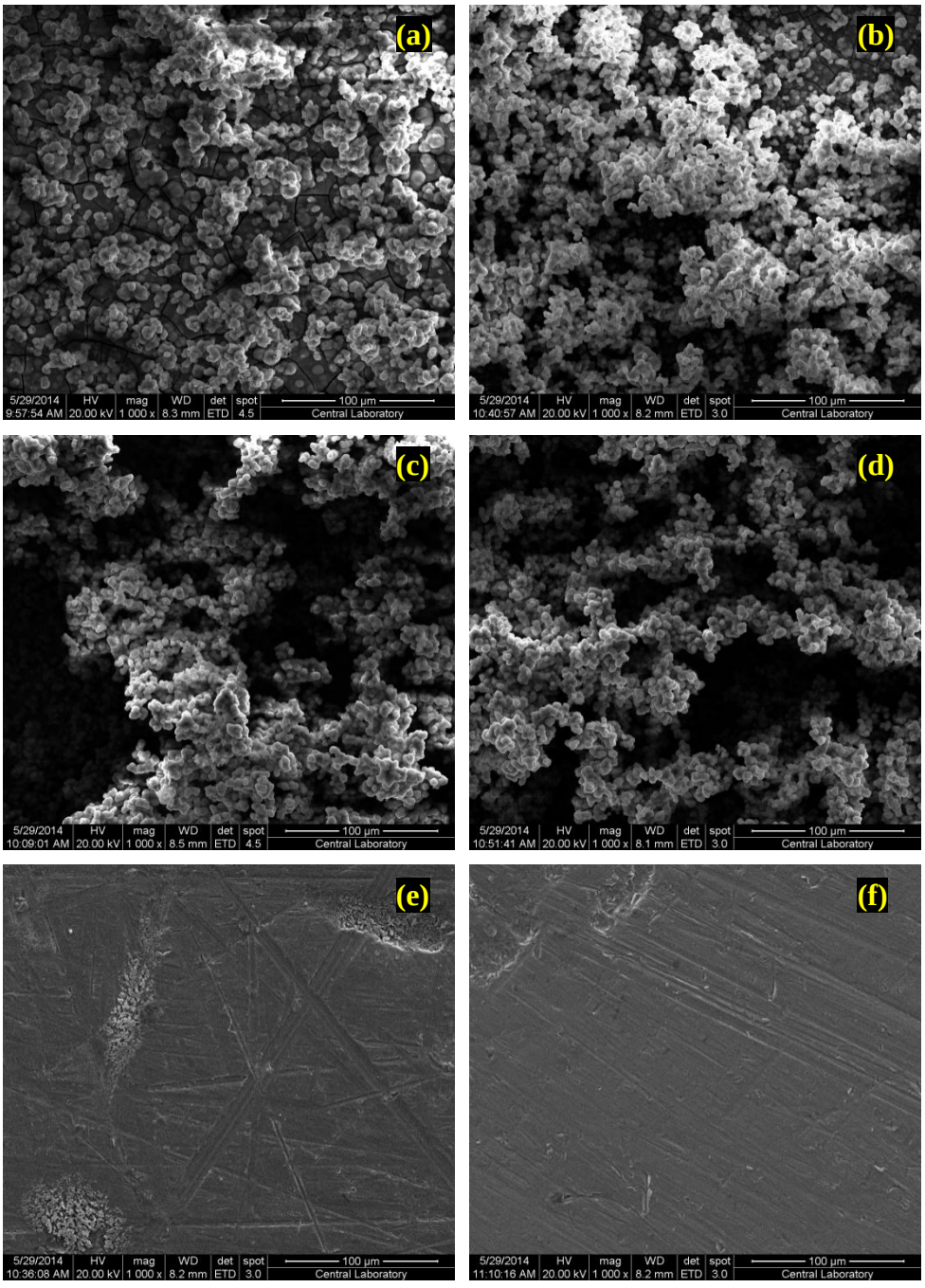

Figure 42 SEM images of various surfaces after 3 days of incubation with *S. epidermidis* (a) S14; (b) S14 after vortexing; (c) N14; (d) N14 after vortexing; (e) pretreated Ti6Al4V and (f) pretreated Ti6Al4V after vortexing (1000×).

As seen in Figure 42, HA deposits had spherical shapes in different sizes. There was no easily distinguishable bacterial colonization on any of the surfaces. The diameter of a single *S. epidermidis* bacterium was about 1 µm. There were also many apatite spheres having the diameter about the same size as a bacterial cell. However, the flake like nano apatite crystals were detectable on the HA spheres at high magnifications providing a discrimination between the apatite crystals and bacteria.

The SEM images of *S. epidermidis* after 3 days of incubation on N14 plate and after vortexing are given in Figure 43.

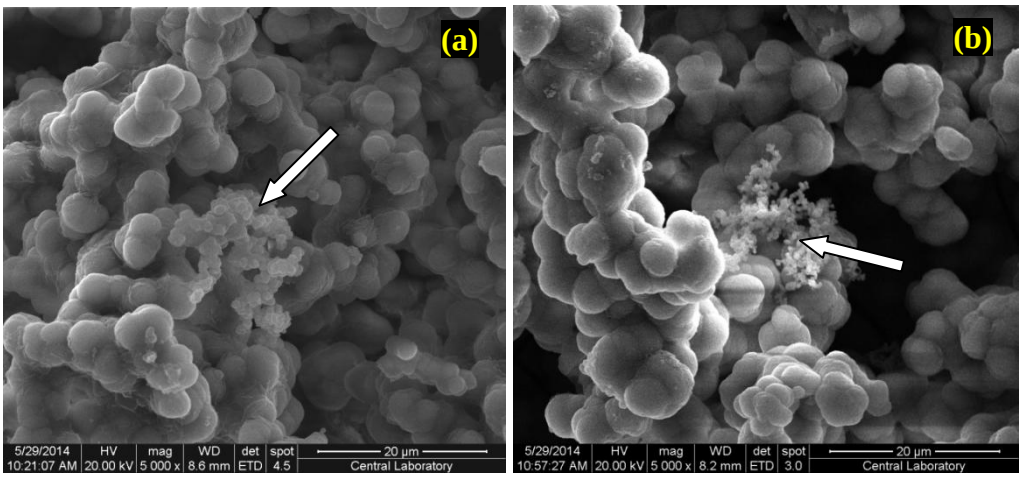

Figure 43 SEM images of *S. epidermidis* (arrows) after 3 days of incubation on (a) N14 and (b) N14 after vortexing (5000×).

From Figure 43, it can be seen that the surfaces of bacteria inoculated normal HA coating before and after vortexing had local bacterial colonization. Similar colonies were also detected on the surface of S14 plates. However, there were no complete bacterial biofilm in any of the coatings.

It was also expected to detect a significant bacterial growth on the uncoated Ti6Al4V plates, especially without vortexing, but there were no colonies detected on these samples having a smoother surface when compared to the HA coated ones. To conclude, SEM images did not provide a clear differentiation between the normal and the selenium added HA coatings or uncoated Ti alloy in terms of *S. epidermidis* attachment.

CHAPTER 4

CONCLUSION

The main purpose of this study was to obtain a selenium doped HA coating on the titanium alloy (Ti6Al4V), and thus to develop a high quality implant material with potential anti-cancer and anti-bacterial properties. It is one of the rare studies on the addition of selenium in the structure of HA in the literature.

For this purpose, both pure and selenium doped HA were coated on Ti6Al4V plates by using normal and selenate containing ionic solutions at physiological pH and temperature with the so called biomimetic method. Selenium doped HA coatings were obtained by soaking the titanium alloy (Ti6Al4V) plates into this solution, which has an ionic concentration of 1.5 times that of the conventional SBF solution and additionally 0.15 mM selenate ion, at 37°C. The resulting coatings were evaluated by several characterization methods and tested *in vitro* in terms of normal and cancerous bone cell responses and bacterial adhesion.

The SEM studies revealed that the nucleation of CaP started on the 4^{th} day of immersion in 1.5×SBF and CaP nucleation increases with the increasing immersion time. It is observed that the surface of the Ti6Al4V plates was entirely covered with numerous and almost spherical granular CaP precipitate after 7 days in 1.5×SBF. The EDS analysis showed that the Ca/P molar ratio of selenate doped coatings increased by the increased immersion time and reached very close to the Ca/P molar ratio of bone. The selenium doped and pure HA coatings showed the typical FTIR spectrum of c-HA regardless of the immersion time. An extra weak band at 764 cm^{-1}, which was attributable to a selenium ion, was observed in the Raman spectra of the S14 plate. However, since the amount of the selenium incorporated into the HA structure was very low, the other bands of selenium ion could not be specified.

The XRD studies also revealed that both types of the biomimetic calcium phosphate coatings exhibited the standard HA (ICDD card No. 1-1008) XRD peaks. The critical lateral force values obtained at the moment of coating failure were found to be above 50 mN for all type of coatings.

The proliferation of the healthy human osteoblasts (hFOB 1.19) and cancerous bone cells (Saos-2) on pure and selenium added HA coatings or in the selenium containing media were assessed by the PrestoBlue cell viability tests. The adherence of these cells onto the coated and aged plates was observed by the SEM technique. The anti-bacterial property of the selenium added HA coating was studied by using *S.epidermidis* bacteria. Briefly, the biological evaluation showed that the selenium is not cytotoxic for the hFOB 1.19 cells at a concentration of 5×10^{-8} g Se/1ml media and it may inhibit cancerous (Saos-2) cell growth. The proliferation of both kinds of cells was observed to be very low on pure and selenium added HA coatings with regard to the PrestoBlue tests. This might result from the loss of the cells due to the detachment of the coatings during the cell culture procedure. This was also confirmed by the SEM micrographs; however it was also possible to see the local firm attachment of cells on both types of the coatings. In order to claim that a material or a surface has the anticancer property; it is needed to assess cytotoxic and anti-tumor activities via both *in vitro* and *in vivo* methods. Although the cell culture studies with hFOB 1.19 and Saos-2 cell lines are informative on the cytotoxicity of the selenium doped HA coatings for both kind of cells, further studies, especially *in vivo* animal studies, are necessary to demonstrate its effectiveness against bone cancer.

Finally, the anti-bacterial property of the selenium added HA coatings obtained from the plate coated in selenate added 1.5×SBF for 14 days (S14) was observed with the supernatant media of *S. epidermidis* bacteria. Although the proliferation of the bacteria on S14 surface was lower than that of N14 surface, the uncoated samples yielded less bacterial attachment.

REFERENCES

1. Williams, D. F. (1987). *Definitions in biomaterials: proceedings of a consensus conference of the European Society for Biomaterials, Chester, England, March 3-5, 1986* (Vol. 4). Elsevier Science Ltd.
2. Williams, D. F. (2009). On the nature of biomaterials. *Biomaterials*, *30*(30), 5897-5909.
3. Ratner, B. D., Hoffman, A. S., Schoen, F. I., & Lemons, J. E. (2013). *Biomaterials science: an introduction to materials in medicine* (3rd ed.) Canada, pp.xxvii
4. Dubok, V. A. (2000). Bioceramics—Yesterday, Today, Tomorrow. *Powder Metallurgy and Metal Ceramics*, 39(7-8), 381-394.
5. Bose, S., & Bandyopadhyay, A. (Eds.) (2013). *Introduction to Biomaterials. Characterization of Biomaterials* (pp. 1-9). Elsevier.
6. Liu, X., Holzwarth, J. M., & Ma, P. X. (2012). Functionalized synthetic biodegradable polymer scaffolds for tissue engineering. *Macromolecular bioscience*, *12*(7), 911-919
7. Ulery, B. D., Nair, L. S., & Laurencin, C. T. (2011). Biomedical applications of biodegradable polymers. *Journal of Polymer Science Part B: Polymer Physics*, *49*(12), 832-864.
8. Angelova, N., & Hunkeler, D. (1999). Rationalizing the design of polymeric biomaterials. *Trends in biotechnology*, *17*(10), 409-421.
9. Hermawan, H. (2012). *Biodegradable Metals: From Concept to Applications*. Springer Berlin Heidelberg.
10. Niinomi, M. (Ed.). (2010). *Metals for biomedical devices*. Elsevier. Preface (p. xv).
11. González-Carrasco, J. L. (2009). Metals as bone repair materials. In J. A. Planell et al. (Eds.), *Bone repair biomaterials* (pp. 154-193). Elsevier.
12. Nakano, T. (2010). Mechanical properties of metallic biomaterials. In M. Niinomi (Ed.), *Metals for biomedical devices* (pp.71-98). Elsevier.

13. Park, J., & Lakes, R. S. (2007). *Biomaterials: an introduction*. Springer.
14. Hanawa, T. (2010). Overview of Metals and Applications. In M. Niinomi (Ed.), *Metals for biomedical devices* (pp.3-24). Elsevier.
15. Hallab, N. J., Urban, R. M., & Jacobs, J. J. (2004). Corrosion and biocompatibility of orthopedic implants. In M.J. Yaszemski et al. (Eds.), *Biomaterials in Orthopedics* (pp.63-92). Marcel Dekker, Inc.
16. Bhabra, G., Sood, A., Fisher, B., Cartwright, L., Saunders, M., Evans, W. H., Surprenant, A., Lopez-Castejon, G., Mann, S., Davis, S. A., Hails, L. A., Ingham, E., Verkade, P., Lane, J., Heesom, K., Newson, R., & Case, C. P. (2009). Nanoparticles can cause DNA damage across a cellular barrier. *Nature Nanotechnology*, *4*(12), 876-883.
17. Yongsheng, W. (2011). Sol–gel derived hydroxyapatite coatings on metallic implants: characterization, *in vitro* and *in vivo* analysis. In S. Zhang (Ed.), *Biological and Biomedical Coatings Handbook: Applications* (pp.1-44). CRC Press.
18. Gu, X. N., & Zheng, Y. F. (2010). A review on magnesium alloys as biodegradable materials. *Frontiers of Materials Science in China*, *4*(2), 111-115.
19. Galeotti, A., Uomo, R., Spagnuolo, G., Paduano, S., Cimino, R., Valletta, R., & D'Antò, V. (2013). Effect of pH on *in vitro* biocompatibility of orthodontic miniscrew implants. *Progress in Orthodontics*, *14*(1), 1-7.
20. Geetha, M., Singh, A. K., Asokamani, R., & Gogia, A. K. (2009). Ti based biomaterials, the ultimate choice for orthopaedic implants–a review. *Progress in Materials Science*, *54*(3), 397-425.
21. Liu, X., Chu, P. K., & Ding, C. (2004). Surface modification of titanium, titanium alloys, and related materials for biomedical applications. *Materials Science and Engineering: R: Reports*, *47*(3), 49-121.
22. Lampman, S. (2012). Titanium and its alloys for biomedical implants. In R. Narayan (Ed.), *ASM Handbook, Volume 23, Materials for Medical Devices*. ASM International.
23. Addison, O., Davenport, A. J., Newport, R. J., Kalra, S., Monir, M., Mosselmans, J. F. W., Proops, D., & Martin, R. A. (2012). Do 'passive'medical titanium surfaces deteriorate in service in the absence of wear? *Journal of The Royal Society Interface*, *9*(76), 3161-3164.

24. Jorge, J. R. P., Barão, V. A., Delben, J. A., Faverani, L. P., Queiroz, T. P., & Assunção, W. G. (2013). Titanium in Dentistry: Historical Development, State of the Art and Future Perspectives. *The Journal of Indian Prosthodontic Society*,*13*(2), 71-77.
25. Patel, N. R., & Gohil, P. P. (2012). A Review on biomaterials: scope, applications & human anatomy significance. *International Journal of Emerging Technology and Advanced Engineering*, *2*(4), 91-101.
26. Arcos, D., & Vallet-Regí, M. (2013). Bioceramics for drug delivery. *Acta Materialia*, *61*(3), 890-911.
27. Dorozhkin, S. V. (2010). Bioceramics of calcium orthophosphates. *Biomaterials*, *31*(7), 1465-1485.
28. Vallet-Regí, M., & Salinas, A. J. (2009). Ceramics as bone repair materials. In J. A. Planell et al. (Eds.), *Bone repair biomaterials* (pp. 194-230). Elsevier.
29. Combes C. & Rey C. (2007). Bioceramics. In. P. Boch, & J. F. Baumard (Eds.), *Ceramic materials: processes, properties and applications* (pp. 493-522). EdISTE Limited., UK.
30. Hench, L. L. (2006). The story of Bioglass®. *Journal of Materials Science: Materials in Medicine*, *17*(11), 967-978.
31. Kokubo, T., Kim, H. M., & Kawashita, M (2003). Ceramics for biomedical applications. In S. Somiya, et al. (Eds.), *Handbook of Advanced Ceramics Vol II Processing and Their Applications* (pp.385-416). Academic Press.
32. Best, S. M., Porter, A. E., Thian, E. S., & Huang, J. (2008). Bioceramics: past, present and for the future. *Journal of the European Ceramic Society*, *28*(7), 1319-1327.
33. Yuan, H. & de Groot, K. (2005). Calcium phosphate biomaterials: an overview. In R.L. Reis & S. Weiner (Eds.) *Learning from nature how to design new implantable biomaterialsis: From biomineralization fundamentals to biomimetic materials and processing routes* (pp. 37-57). Springer Netherlands.
34. Yao, T., & Yabutsuka, T. (2010). Biomimetic fabrication of hydroxyapatite microcapsules by using apatite nuclei. In A. Mukherjee (Ed.), *Biomimetics, learning from nature* (pp.273-288), Intech Croatia.
35. Eichert, D., Salomé, M., Banu, M., Susini, J., & Rey, C. (2005). Preliminary characterization of calcium chemical environment in apatitic and non-apatitic

calcium phosphates of biological interest by X-ray absorption spectroscopy. *Spectrochimica Acta Part B: Atomic Spectroscopy*, *60*(6), 850-858.

36. Dorozhkin, S. V., & Epple, M. (2002). Biological and medical significance of calcium phosphates. *Angewandte Chemie International Edition*, *41*(17), 3130-3146.
37. Suchanek, W., & Yoshimura, M. (1998). Processing and properties of hydroxyapatite-based biomaterials for use as hard tissue replacement implants. *Journal of Materials Research*, *13*(01), 94-117.
38. Saltzman, W. M. (2009). *Biomedical engineering: bridging medicine and technology* (p.540). Cambridge University Press.
39. Tavares, D. S., Resende, C. X., Quitan, M. P., Granjeiro, J. M., & Soares, G. A. (2010). Influence of strontium doping on cytocompatibility of hydroxyapatite: comparison of three *in vitro* assays, The 6th Latin American Congress of Artificial Organs and Biomaterials, Rio Grande Sul, Brazil.
40. Renaudin, G., Laquerriere, P., Filinchuk, Y., Jallot, E., & Nedelec, J. M. (2008). Structural characterization of sol–gel derived Sr-substituted calcium phosphates with anti-osteoporotic and anti-inflammatory properties. *Journal of Materials Chemistry*, *18*(30), 3593-3600.
41. Park, S. S., Lee, H. J., Oh, I. H., & Lee, B. T. (2004). Effects of Ag-doping on microstructure and mechanical properties of hydroxyapatite films. *Key Engineering Materials*, *277*, 113-118.
42. Miao, S., Weng, W., Cheng, K., Du, P., Shen, G., Han, G., & Zhang, S. (2005). Sol–gel preparation of Zn-doped fluoridated hydroxyapatite films. *Surface and Coatings Technology*, *198*(1), 223-226.
43. Mróz, W., Bombalska, A., Burdyńska, S., Jedyński, M., Prokopiuk, A., Budner, B., Ślósarczyk, A., Zima, A., Menaszek, E., Ścisłowska-Czarnecka, A., Niedzielski, K. (2010). Structural studies of magnesium doped hydroxyapatite coatings after osteoblast culture. *Journal of Molecular Structure*, *977*(1), 145-152.
44. LeGeros, R. Z., Coelho, P. G., Holmes, D., Dimaano, F., & LeGeros, J. P. (2011). Orthopedic and dental implant surfaces and coatings. In S. Zhang (Ed.), *Biological and Biomedical Coatings Handbook: Applications* (pp.301-334). CRC Press.

45. Sun, L., Berndt, C. C., Gross, K. A., & Kucuk, A. (2001). Material fundamentals and clinical performance of plasma-sprayed hydroxyapatite coatings: A review. *Journal of Biomedical Materials Research*, *58*(5), 570-592.
46. Yang, Y., Kim, K. H., & Ong, J. L. (2005). A review on calcium phosphate coating produced using a sputtering process-an alternative to plasma spraying. *Biomaterials*. *26*(3), 327-337.
47. Besu, N. (2007). *Silver Doped Hydroxyapatite Coating on Titanium Surfaces and Its Effect on Early Bone Response and Osseointegration* (Master of dental science thesis, The University of Tennessee). Retrieved from http://etd.uthsc.edu/WORLD-ACCESS/Besu/2007-004-Besu.pdf
48. Smith, I. O., & Ma, P. X. (2011). Biomimetic Scaffolds in Tissue Engineering. In Pallua, N., Suscheck, C.V. (Ed.) *Tissue Engineering* (pp. 31-39). Springer Berlin Heidelberg.
49. Habibovic, P., Barrere, F., Blitterswijk, C. A., Groot, K., & Layrolle, P. (2002). Biomimetic hydroxyapatite coating on metal implants. *Journal of the American Ceramic Society*, *85*(3), 517-522.
50. Zhao, C. Y., Fan, H. S., & Zhang, X. D. (2011). Advances in biomimetic apatite coating on metal implants. In A. George (Ed.) *Advances in Biomimetics* (pp. 397-428). InTech Croatia.
51. Bigi, A., Boanini, E., Bracci, B., Facchini, A., Panzavolta, S., Segatti, F., & Sturba, L. (2005). Nanocrystalline hydroxyapatite coatings on titanium: a new fast biomimetic method. *Biomaterials*, *26*(19), 4085-4089.
52. Kokubo, T., & Takadama, H. (2006). How useful is SBF in predicting *in vivo* bone bioactivity? *Biomaterials*, *27*(15), 2907-2915.
53. Cui, X., Kim, H. M., Kawashita, M., Wang, L., Xiong, T., Kokubo, T., & Nakamura, T. (2010). Apatite formation on anodized Ti-6Al-4V alloy in simulated body fluid. *Metals and Materials International*, *16*(3), 407-412.
54. Tas, A. C. (2000). Synthesis of biomimetic Ca-hydroxyapatite powders at 37 C in synthetic body fluids. *Biomaterials*, *21*(14), 1429-1438.
55. Oyane, A., Onuma, K., Ito, A., Kim, H. M., Kokubo, T., & Nakamura, T. (2003). Formation and growth of clusters in conventional and new kinds of simulated body fluids. *Journal of Biomedical Materials Research Part A*, *64*(2), 339-348.

56. Takadama, H., Hashimoto, M., Mizuno, M., & Kokubo, T. (2004). Round-robin test of SBF for *in vitro* measurement of apatite-forming ability of synthetic materials. *Phosphorus Research Bulletin*, *17*(0), 119-125.
57. Kim, H. M., Miyaji, F., Kokubo, T., & Nakamura, T. (1996). Preparation of bioactive Ti and its alloys via simple chemical surface treatment. *Journal of Biomedical Materials Research*, *32*(3), 409-417.
58. Nouri, A., Hodgson, P. D., & Wen, C. E. (2010). Biomimetic porous titanium scaffolds for orthopedic and dental applications. A. Mukherjee (Ed.), *Biomimetics, Learning From Nature* (pp.415-450), Intech Croatia.A.
59. Kokubo, T., Miyaji, F., Kim, H. M., & Nakamura, T. (1996). Spontaneous formation of bonelike apatite layer on chemically treated titanium metals. *Journal of the American Ceramic Society*, *79*(4), 1127-1129.
60. Kokubo, T. (1998). Apatite formation on surfaces of ceramics, metals and polymers in body environment. *Acta Materialia*, *46*(7), 2519-2527.
61. Kokubo, T., Kim, H. M., & Kawashita, M. (2003). Novel bioactive materials with different mechanical properties. *Biomaterials*, *24*(13), 2161-2175.
62. Wei, M., Uchida, M., Kim, H. M., Kokubo, T., & Nakamura, T. (2002). Apatite-forming ability of CaO-containing titania. *Biomaterials*, *23*(1), 167-172.
63. Lu X., & Leng Y. (2004). Theoretical analysis of calcium phosphate precipitation in simulated body fluid. *Biomaterials*, *26*(2005), 1097-1108.
64. Pasinli, A., Yuksel, M., Celik, E., Sener, S., & Tas, A. C. (2010). A new approach in biomimetic synthesis of calcium phosphate coatings using lactic acid–Na lactate buffered body fluid solution. *Acta Biomaterialia*, *6*(6), 2282-2288.
65. Chakraborty J., Daneu N., Recnik A., Chakraborty M., Dasgupta S., Ghosh J., Sengupta S., Mazumdar S., K.Sinha M., & Basu D. (2011). Stepwise formation of crystalline apatite in the biomimetic coating of surgical grade SS 316L substrate: A TEM analysis. *Journal of the Taiwan Institute of Chemical Engineers*, *42*(4), 682-687.
66. Li Y., Li Q., Zhu S., Luo E., Li J., Feng G., Liao Y., & Hu J. (2010). The effect of strontium-substituted hydroxyapatite coating on implant fixation in ovariectomized rats. *Biomaterials*, *31*(34), 9006-9014.

67. Tran, P. A., Sarin, L., Hurt, R. H., & Webster, T. J. (2009). Opportunities for nanotechnology-enabled bioactive bone implants. *Journal of Materials Chemistry*, *19*(18), 2653-2659.
68. Reznikov, N., Shahar, R., & Weiner, S. (2014). Bone hierarchical structure in three dimensions. *Acta Biomaterialia*, *10*(9), 3815-3826.
69. Lakes, R. (1993). Materials with structural hierarchy. *Nature*, *361*(6412), 511-515.
70. Tran, P. A., Sarin, L., Hurt, R. H., & Webster, T. J. (2010). Titanium surfaces with adherent selenium nanoclusters as a novel anticancer orthopedic material.*Journal of Biomedical Materials Research Part A*, *93*(4), 1417-1428.
71. Cecen, E., & Bolaman, Z. (2010). İkincil kanserler, *Uluslararası Hematoloji Onkoloji Dergisi*, *20*(3), 190-200.
72. American Cancer Society. (2014). Cancer Facts & Figures 2014. Atlanta: American Cancer Society. Retrieved from http://www.cancer.org/acs/groups/content/@research/documents/webcontent/acspc-042151.pdf
73. Chowdhry, M., Cockshott, S., & Jeys, L. (2009). Secondary malignant tumours of bone. *Surgery (Oxford)*, *27*(2), 86-89.
74. Tran, P. A., Taylor, E., Sarin, L., Hurt, R. H., & Webster, T. J. (2009, January). Novel anti-cancer, anti-bacterial coatings for biomaterial applications: selenium nanoclusters. In *MRS Proceedings* (Vol. 1209, No. 1). Cambridge University Press.
75. Yalniz, E., Çiftdemir, M., & Memişoğlu, S., Tümör rezeksiyon protezi uygulanan kemik tümörlü olgularda fonksiyonel sonuçlar. *Acta Orthopaedica et Traumatologica Turcica*, *42*(4), 238-245.
76. Keel, S. B., Jaffe, K. A., Nielsen, G. P., & Rosenberg, A. E. (2001). Orthopaedic implant-related sarcoma: a study of twelve cases. *Modern Pathology*, *14*(10), 969-977.
77. Gupta, R., & Kumar, A. (2008). Bioactive materials for biomedical applications using sol–gel technology. *Biomedical Materials*, *3*(3), 034005.
78. Teterycz, D., Ferry, T., Lew, D., Stern, R., Assal, M., Hoffmeyer, P., Bernard, L., & Uçkay, I. (2010). Outcome of orthopedic implant infections due to different staphylococci. *International Journal of Infectious Diseases*, *14*(10), e913-e918.

79. Gristina, A. (2004). Biomaterial-Centered Infection. Clinical Orthopaedics & Related Research: October 2004, Volume 427, pp. 4-12.
80. Montdargent, B., & Letourneur, D. (2000). Toward new biomaterials. *Infection Control and Hospital Epidemiology*, *21*(6), 404-410.
81. Xi, L., Yi, L., Jun, W., Huigang, L., & Songsheng, Q. (2002). Microcalorimetric study of *Staphylococcus Aureus* growth affected by selenium compounds. *Thermochimica Acta*, *387*(1), 57-61.
82. Moriarty, T. F., Schlegel, U., Perren, S., & Richards, R. G. (2010). Infection in fracture fixation: can we influence infection rates through implant design? *Journal of Materials Science: Materials in Medicine*, *21*(3), 1031-1035.
83. Letavayová, L., Vlčková, V., & Brozmanová, J. (2006). Selenium: from cancer prevention to DNA damage. *Toxicology*, *227*(1), 1-14.
84. Navarro-Alarcon, M., & Cabrera-Vique, C. (2008). Selenium in food and the human body: a review. *Science of the Total Environment*, *400*(1), 115-141.
85. Combs, G.F. (2001). Selenium in global food system, *British Journal of Nutrition*, 85, 517-547.
86. McDowell, L. R. (2003). Minerals in animal and human nutrition (pp. 397-448) (No. Ed. 2). Elsevier Science BV.
87. Yang, J., Huang, K., Qin, S., Wu, X., Zhao, Z., & Chen, F. (2009). Antibacterial action of selenium-enriched probiotics against pathogenic *Escherichia coli*. *Digestive Diseases and Sciences*, *54*(2), 246-254.
88. Hiraoka, K., Komiya, S., Hamada, T., Zenmyo, M., & Inoue, A. (2001). Osteosarcoma cell apoptosis induced by selenium. *Journal of Orthopaedic Research*, *19*(5), 809-814.
89. Jiang, X-R., Macey, M. G., Lin, H-X., & Newland, A. C. (1992). The antileukaemic effects and the mechanism of sodium selenite, *Leukemia Research*, *16*, 347–352.
90. Lanfear, J., Fleming, J., Wu, L., Webster, G., & Harrison, P. R. (1994). The selenium metabolite selenodiglutathione induces p53 and apoptosis: relevance to the chemopreventive effects of selenium? *Carcinogenesis*, *15*(7), 1387-1392.
91. Zeng, H., Cao, J. J., & Combs, G. F. (2013). Selenium in bone health: roles in antioxidant protection and cell proliferation. *Nutrients*, *5*(1), 97-110.

92. Rayman, M. P. (2005). Selenium in cancer prevention: a review of the evidence and mechanism of action. *Proceedings of the Nutrition Society*, *64*(04), 527-542.
93. Chen, Y. C., Sosnoski, D. M., Gandhi, U. H., Novinger, L. J., Prabhu, K. S., & Mastro, A. M. (2009). Selenium modifies the osteoblast inflammatory stress response to bone metastatic breast cancer. *Carcinogenesis*, *30*(11), 1941-1948.
94. Rocha, A. S. S. D., Ramos-Perez, F. M. D. M., Bóscolo, F. N., Manzi, F. R., Cchicarelo, M., & Almeida, S. M. (2009). Effect of sodium selenite on bone repair in tibiae of irradiated rats. *Brazilian Dental Journal*, *20*(3), 186-190.
95. Wang, Y., Lv, P., Ma, Z., & Zhang, J. (2013). Enhanced Healing of Rat Calvarial Critical Size Defect with Selenium-Doped Lamellar Biocomposites. *Biological Trace Element Research*, *155*(1), 72-81.
96. Turan, B., Can, B., & Delilbasi, E. (2003). Selenium combined with vitamin E and vitamin C restores structural alterations of bones in heparin-induced osteoporosis. *Clinical Rheumatology*, *22*(6), 432-436.
97. Liu, H., Bian, W., Liu, S., & Huang, K. (2012). Selenium protects bone marrow stromal cells against hydrogen peroxide-induced inhibition of osteoblastic differentiation by suppressing oxidative stress and ERK signaling pathway. Biological trace element research, 150(1-3), 441-450.
98. Tran, P. A., Sarin, L., Hurt, R. H., & Webster, T. J. (2010). Differential effects of nanoselenium doping on healthy and cancerous osteoblasts in coculture on titanium. *International Journal of Nanomedicine*, *5*, 351–358.
99. Perla, V., & Webster, T. J. (2005). Better osteoblast adhesion on nanoparticulate selenium—A promising orthopedic implant material. *Journal of Biomedical Materials Research Part A*, *75*(2), 356-364.
100. Tran, P.A., & Webster, T. J. (2008). Enhanced osteoblast adhesion on nanostructured selenium compacts for anti-cancer orthopedic applications. *International Journal of Nanomedicine*, *3*(3), 391–396.
101. Rodríguez-Valencia, C., López-Álvarez, M., Cochón-Cores, B., Pereiro, I., Serra, J., & Gonzalez, P. (2013). Novel selenium-doped hydroxyapatite coatings for biomedical applications. *Journal of Biomedical Materials Research Part A*, *101*(3), 853-861.

102. Bigi, A., Boanini, E., Panzavolta, S., & Roveri, N. (2000). Biomimetic growth of hydroxyapatite on gelatin films doped with sodium polyacrylate. *Biomacromolecules*, *1*(4), 752-756.
103. Pittrof, A., Bauer, S., & Schmuki, P. (2011). Micropatterned TiO_2 nanotube surfaces for site-selective nucleation of hydroxyapatite from simulated body fluid. *Acta Biomaterialia*, *7*(1), 424-431.
104. Invitrogen Product Manuals, Life Technologies http://tools.lifetechnologies.com/content/sfs/manuals/PrestoBlueFAQ.pdf (Accessed on: 6 November 2014).
105. Invitrogen Product Manuals, Life Technologies http://tools.lifetechnologies.com/content/sfs/manuals/mp01304.pdf (Accessed on: 6 November 2014).
106. Rupp, M. E., & Fey, P. D. (2010). Staphylococcus epidermidis and other coagulase negative staphylococci. In G.L. Mandell, J. E. Bennett, Dolin R. (Ed.), *Mandell, Douglas, and Bennett's Principles and Practice of Infectious Diseases*, (pp.2579-2589), Elsevier.
107. Wang, X.-X., Hayakawa, S., Tsuru, K. & Osaka, A. (2000). Improvement of Bioactivity of H_2O_2/$TaCl_5$-Treated Titanium after Subsequent Heat Treatments. *Journal of Biomedical Materials Research*, *52*(1), 171–176.
108. Kim, H. M., Miyaji, F., & Kokubo, T. (1997). Effect of heat treatment on apatite forming ability of ti metal induced by alkali treatment. *Journal of Materials Science: Materials in Medicine, 8*(6), 341–347.
109. Jalota, S., Bhaduri, S. B., & Tas, A. C. (2006). Effect of carbonate content and buffer type on calcium phosphate formation in SBF solutions. *Journal of Materials Science: Materials in Medicine*, *17*(8), 697-707.
110. Fujibayashi, S., Nakamura, T., Nishiguchi, S., Tamura, J., Uchida, M., Kim, H. M., & Kokubo, T. (2001). Bioactive titanium: Effect of sodium removal on the bone-bonding ability of bioactive titanium prepared by alkali and heat treatment.*Journal of Biomedical Materials Research*, *56*(4), 562-570.
111. Dorozhkin, S.V., & Epple, M. (2002). Biological and medical significance of calcium phosphates. *Angewandte Chemie International Edition*, *41*(17), 3130–3146.

112. Dorozhkin, E.I., Dorozhkin, S.V. (2003). Structure and properties of the precipitates formed from condensed solutions of the revised simulated body fluid, *Journal of Biomedical Materials Research Part A*, 67(2), 578–581.
113. Gualtieri, M.L., Prudenziati, M., & Gualtieri, A.F. (2006). Quantitative determination of the amorphous phase in plasma sprayed alumina coatings using the Rietveld method, *Surface and Coatings Technology*, *201*(6), 2984–2989.
114. Lee, Y.J. (2010). Spectroscopic investigation of arsenate and selenate incorporation into hydroxylapatite, *Current Applied Physics*, *10*(1), 158–163.
115. Zhang, W., Chai, Y., Cao, N., & Wang, Y. (2014). Synthesis and characterization of selenium substituted hydroxyapatite via a hydrothermal procedure. *Materials Letters*, *134*, 123-125.
116. Kolmas, J., Oledzka, E., Sobczak, M., & Nałęcz-Jawecki, G. (2014). Nanocrystalline hydroxyapatite doped with selenium oxyanions: A new material for potential biomedical applications. *Materials Science and Engineering: C*, *39*, 134-142.
117. Morejón-Alonso, L., Carrodeguas, R. G., García-Menocal, J. A. D., Pérez, J. A. A., & Manent, M. S. (2007). Effect of sterilization on the properties of CDHA-OCP-β-TCP biomaterial. *Materials Research*, *10*(1), 15–20.
118. Santos, C., Gomes, P. S., Duarte, J. A., Franke, R. P., Almeida, M. M., Costa, M. E. V., & Fernandes, M. H. (2012). Relevance of the sterilization-induced effects on the properties of different hydroxyapatite nanoparticles and assessment of the osteoblastic cell response, *Journal of Royal Society Interface*, *9*(77), 3397–3410.
119. Ma, J., Wang, Y., Zhou, L., & Zhang, S. (2013). Preparation and characterization of selenite substituted hydroxyapatite. *Materials Science and Engineering: C*, *33*(1), 440-445.
120. Silva, C.C., Pinheiro, A.G., Miranda, M.A.R., Góes, J.C., & Sombra, A.S.B. (2003). Structural properties of hydroxyapatite obtained by mechanosynthesis, *Solid State Sciences*, *5*(4), 553–558.
121. Suchaneka, W.L., Shuk, P., Byrappa, K., Riman, R.E., TenHuisen, K.S., & Janas, V.F. (2002). Mechanochemical–hydrothermal synthesis of carbonated apatite powders at room temperature, *Biomaterials*, *23*(3), 699-710.

122. Wang, Y., Ma, J., Zhou, L., Chen, J., Liu, Y., Qiu, Z., & Zhang, S. (2012). Dual functional selenium-substituted hydroxyapatite. *Interface Focus*, rsfs20120002.
123. Kazanci, M., Fratzl, P., Klaushofer, K., & Paschalis, E. P. (2006). Complementary information on *in vitro* conversion of amorphous (precursor) calcium phosphate to hydroxyapatite from Raman microspectroscopy and wide-angle X-ray scattering. *Calcified Tissue International*, *79*(5), 354-359.
124. Frost, R.L., Weier, M.L., Reddy, B., & Cejka, J. (2006). A Raman spectroscopic study of the uranyl selenite mineral haynesite, *Journal of Raman Spectroscopy*, *37*(8), 816-821.
125. Wijnja, H., & Schulthess, C.P. (2000). Vibrational spectroscopy study of selenate and sulfate adsorption mechanisms on Fe and Al (hydr)oxide surfaces. *Journal of Colloid and Interface Science*, *229*(1), 286-297.
126. Frost, R. L., & Keeffe, E. C. (2008). Raman spectroscopic study of the schmiederite Pb_2Cu_2 [(OH) $_4$| SeO_3| SeO_4]. *Journal of Raman Spectroscopy*, *39*(10), 1408-1412.
127. Wang, J., Layrolle, P., Stigter, M., & De Groot, K. (2004). Biomimetic and electrolytic calcium phosphate coatings on titanium alloy: physicochemical characteristics and cell attachment. *Biomaterials*, *25*(4), 583-592.
128. Forsgren, J., Svahn, F., Jarmar, T., & Engqvist, H. (2007). Formation and adhesion of biomimetic hydroxyapatite deposited on titanium substrates. *Acta Biomaterialia*, *3*(6), 980-984.
129. Stewart, M. S., Spallholz, J. E., Neldner, K. H., & Pence, B. C. (1999). Selenium compounds have disparate abilities to impose oxidative stress and induce apoptosis. *Free Radical Biology and Medicine*, *26*(1), 42-48.
130. Zhong, W., & Oberley, T. D. (2001). Redox-mediated effects of selenium on apoptosis and cell cycle in the LNCaP human prostate cancer cell line. *Cancer research*, *61*(19),7071-7078.
131. Mauro, M. O., Sartori, D., Oliveira, R. J., Ishii, P. L., Mantovani, M. S., & Ribeiro, L. R. (2011). Activity of selenium on cell proliferation, cytotoxicity, and apoptosis and on the expression of CASP9, BCL-XL and APC in intestinal adenocarcinoma cells. *Mutation Research/Fundamental and Molecular Mechanisms of Mutagenesis*, *715*(1), 7-12.

CURRICULUM VITAE

PERSONAL INFORMATION

Surname, Name: Yılmaz, Bengi

Date of Birth: 26/08/1984

Tel.: +90-312-210-4149

e-mail: ybengi@metu.edu.tr

Address: Research Coordination Office, Presidency 6th Floor

Middle East Technical University, 06800, Ankara/Turkey

EDUCATION

Degree	Instutition	Year of Graduation
A.S.	Anadolu University, Healthcare Management	2009
M.S.	Boğaziçi University, Biomedical Engineering	2008
B.S.	METU, Chemical Engineering	2006

WORK EXPERIENCE

Year	Place	Enrollment
01.2009 – Now	METU, Research Coordination Office	Research Assistant
12.2011 – 12.2013	TÜBİTAK Project No 111M262	Project Assistant
07.2007 – 08.2007	Taksim İlkyardım Hospital	Intern Student
06.2005 – 07.2005	PETKİM	Intern Student
08.2004 – 09.2004	BARUTSAN	Intern Student

PUBLICATIONS

1. **Yilmaz, B.**, & Evis, Z. (2014). Raman spectroscopy investigation of nano hydroxyapatite doped with yttrium and fluoride ions. *Spectroscopy Letters*, *47*(1), 24-29.

2. Kutbay, I., **Yilmaz, B.**, Evis, Z., & Usta, M. (2014). Effect of calcium fluoride on mechanical behavior and sinterability of nano hydroxyapatite and titania composites. *Ceramics International*, *40*(9), 14817–14826.
3. **Yilmaz, B.**, Evis, Z., & Guldiken, M. (2014). Biomimetic calcium phosphate coating of titanium alloy. *Journal of the Faculty of Engineering and Architecture of Gazi University*, *29*(1), 105-109 (Article in Turkish).
4. Evis, Z., **Yilmaz, B.**, Usta, M., & Levent Aktug, S. (2013). X-Ray investigation of sintered cadmium doped hydroxyapatites. *Ceramics International*, *39*(3), 2359-2363.

CONFERENCES PARTICIPATED

1. **Yilmaz, B.**, Tezcaner, A., Banerjee, S. & Evis, Z.*, Selenium incorporated hydroxyapatite coating on Ti alloy. Presented at: AMPT 2014 – Advances in Materials & Processing Technology Conference, 2014 Nov 17-20; Dubai, UAE.
2. **Yilmaz, B.***, & Evis, Z., Biomimetic calcium phosphate coating of Ti alloy in SBF and 1.5×SBF. Presented at: ISITES 2014 – 2nd International Symposium on Innovative Technologies in Engineering and Science, 2014 Jun 18-20; Karabük, Turkey.
3. **Yilmaz, B.***, & Evis, Z., Biomimetic selenium doped hydroxyapatite coating on titanium alloy. Poster Presented at: ESB 2013 – 25th European Conference on Biomaterials, 2013 Sep 8-12; Madrid, Spain.
4. **Yilmaz, B.***, & Evis, Z., Selenium doped hydroxyapatite coating by biomimetic method on titanium alloy. Poster Presented at: SSB 2013 – 19th Swiss Conference on Biomaterials, 2013 Jun 25-26, Davos, Switzerland.
5. Kalyoncuoglu, U. T.*****, Gungor S., **Yilmaz, B.**, Evis, Z., & Kansu G., Influence of chitosan coating to titanium on HGF-1 cells attachment and proliferation *in vitro*, Presented at: FDI 2013 Annual World Dental Congress, 2013 Aug 28-31; Istanbul, Turkey.
6. **Yilmaz, B.**, & Evis, Z.*****, Coating of Ti alloy with selenium doped hydroxyapatite. Presented at: VIII. Ceramic Congress with International Participation, 2012 Nov 22-24; Afyonkarahisar, Turkey.

7. **Yilmaz, B.***, Aksoy, E., Bindal, C., Usta, M., & Ucisik, H., The effect of dialysis environment and reprocessing procedure on the mechanical and structural stability of high flux polysulfone membrane. Poster Presented at: World Congress of Nephrology, 2009 May 22-26; Milan, Italy.

RESEARCH INTERESTS

- Biomaterials: bioceramics, orthopedic and dental implants and their coatings
- Artificial Organs: hemodialysis membranes

LABORATORY SKILLS

- Synthesis of Bioceramics: Precipitation and Biomimetic Methods
- Material Characterization Experience: SEM, FTIR, XRD, EDS, ICP-MS, AFM, Raman Spectroscopy, Mechanical Tests (Scratch test and Vickers hardness test)
- Cell Culture: (Saos-2, hFOB 1.19, NHOst) cell subculturing, proliferation and viability tests, confocal microscopy staining, protein expression tests, fixation and SEM observations, freezing for storage
- Bacterial Culture: (*S. epidermidis*, *S.aureus*) cell subculturing proliferation, adhesion and viability testing, fixation and SEM observations, freezing for storage

LANGUAGE SKILLS

- English – good command in reading and writing, fluent in speaking

COMPUTER SKILLS

- Basic knowledge of SPSS, Xpert, Matlab
- Working knowledge of MS Office Applications (Word, Excel, Powerpoint)

HOBBIES

- Classical guitar playing
- Japanese culture and fine arts